

PROBABILISTIC-NUMERICAL MODELING OF STABILITY OF A ROCK  
SLOPE IN AMASYA TURKEY

A THESIS SUBMITTED TO  
THE GRADUATE SCHOOL OF NATURAL AND APPLIED SCIENCES  
OF  
MIDDLE EAST TECHNICAL UNIVERSITY

BY

SOHRAB GHEIBIE

IN PARTIAL FULFILLMENT OF THE REQUIREMENTS  
FOR  
THE DEGREE OF MASTER OF SCIENCE  
IN  
MINING ENGINEERING

FEBRUARY 2012

Approval of the thesis:

**PROBABILISTIC-NUMERICAL MODELING OF STABILITY OF A ROCK  
SLOPE IN AMASYA TURKEY**

Submitted by **SOHRAB GHEIBIE** in partial fulfillment of the requirements for the degree of **Master of Science in Mining Engineering Department, Middle East Technical University** by;

Prof. Dr. Canan Özgen \_\_\_\_\_  
Dean, Graduate School of **Natural and Applied Sciences**

Prof Dr. Ali İhsan Arol \_\_\_\_\_  
Head of Department, **Mining Engineering**

Prof Dr. H.Şebnem Düzgün \_\_\_\_\_  
Supervisor, **Mining Engineering Dept., METU**

Assist. Prof. Dr. Aykut Akgün \_\_\_\_\_  
Co-supervisor, **Geological Engineering Dept., KTU**

**Examining Committee Members:**

Prof. Dr. Candan Gökceoğlu \_\_\_\_\_  
Geological Engineering Dept., Hacettepe University

Prof. Dr. H.Şebnem Düzgün \_\_\_\_\_  
Mining Engineering Dept., METU

Prof. Dr. Haluk Akgün \_\_\_\_\_  
Geological Engineering Dept., METU

Assoc. Prof. Dr. H. Aydın Bilgin \_\_\_\_\_  
Mining Engineering Dept., METU

Assist. Prof. Dr. Aykut Akgün \_\_\_\_\_  
Geological Engineering Dept., KTU

**Date:** **10/02/2012**

**I hereby declare that all information in this document has been obtained and presented in accordance with academic rules and ethical conduct. I also declare that, as required by these rules and conduct, I have fully cited and referenced all material and results that are not original to this work.**

Name, Last name: Sohrab Gheibie

Signature:

## **ABSTRACT**

### **PROBABILISTIC-NUMERICAL MODELING OF STABILITY OF A ROCK SLOPE IN AMASYA-TURKEY**

Gheibie, Sohrab

M.Sc., Department of Mining Engineering

Supervisor: Prof. Dr. H.Şebnem Düzgün

Co-supervisor: Assist. Prof. Dr. Aykut Akgün

February 2012, 179 pages

Rock slope stability is considered as one of the most important fields in rock engineering. Developments of computation facilities and increase in application of sophisticated mathematical concepts in engineering problems have also affected the methods of slope stability analysis. In recent years, the numerical modeling methods have extensively applied instead of limit equilibrium methods. Also, the probabilistic methods are considered in rock slope designs to quantify the uncertainties of input effecting variables.

In this research, a probabilistic-numerical approach was developed by integration of three dimensional Distinct Element Method (DEM) and probabilistic approach to analyze the stability of discontinuous rock slopes. Barton models have been used to model the behavior of rock discontinuities and the shear strain was considered as failure indicator of discontinuities.

The proposed methodology was applied to a rock slope in Amasya, Turkey where the Joint Roughness Coefficient (JRC) was considered as the main random variable. The effect of basic friction angle and cohesion of joints infilling material and its strength reduction due to weathering were included in the analysis. In the slope the shearing behavior of fourteen discontinuities and the failure probability of each block were investigated, and the corresponding Reliability Index ( $\beta$ ) was derived for each of the discontinuities.

Keywords: Discontinuity, Joint Shear Stiffness, Probabilistic-Numerical Approach, 3DEC, Reliability Index ( $\beta$ )

## ÖZ

### AMASYA-TÜRKİYE'DEKİ BİR KAYA ŞEVİNİN DURAYLILIĞININ OLASILIK-SAYISAL MODELLEMESİ

Gheibie, Sohrab

Yüksek Lisans, Maden Mühendisliği Bölümü

Tez Yöneticisi : Prof. Dr. H. Şebnem Düzgün

Ortak Tez Yöneticisi : Yrd. Doç. Dr. Aykut Akgün

Şubat2012, 179 sayfa

Kaya şev duraylılığı, kaya mühendisliğindeki en önemli alanlardan birisidir. Mühendislik problemlerinde modern matematiksel kavramların uygulamasındaki artış ve hesaplama imkanlarının gelişimi aynı zamanda şev duraylılık analizi yöntemlerini de etkilemiştir. Son yıllarda, limit denge yöntemlerinden çok sayısal modelleme yöntemleri geniş biçimde uygulanmaktadır. Ayrıca, değişkenleri etkileyen girdi parametrelerinin belirsizliğini sayısal olarak ifade etmek için kaya şevi tasarımında olasılıksal yöntemler de kullanılmaktadır.

Bu çalışmada, süreksizlik içeren bir kaya şevinin duraylılığını analiz etmek için üç boyutlu Farklı Elemanlar Yöntemi (DEM) ve olasılık yöntemi'nin birleştirilmesi ile bir olasılıksal-sayısal yaklaşım geliştirilmiştir. Barton modelleri kaya süreksizliklerinin davranışını modellemek için kullanılmış

ve kesme dayanımı süreksizliklerin yenilme göstergeleri olarak dikkate alınmıştır.

Önerilen yöntem, Amasya (Türkiye)'da bir kaya şevine uygulanmış, burada Süreksizlik Pürüzlülük Katsayısı (JRC) çalışmanın ana rastgele değişkeni olarak dikkate alınmış, bununla birlikte süreksizlik dolgu malzemesinin kohezyon ve temel içsel sürtünme açısının etkisi ve bozunmadan dolayı bu dolgu malzemesinin dayanım azalımı analize dahil edilmiştir. Şevde, on dört süreksizliğin kesme davranışı ve her bir bloğun yenilme olasılığı araştırılmış ve buna karşılık gelen Güvenilirlik İndeksi ( $\beta$ ) süreksizliklerin her biri için elde edilmiştir.

Anahtar Kelimeler: Süreksizlik, Süreksizlik Kesme stifnesi, Olasılıksal-Sayısal Yaklaşım, 3DEC, Güvenilirlik İndeksi ( $\beta$ )

To My Parents and love

## **ACKNOWLEDGEMENT**

I wish to express my sincerest gratitude to Prof. Dr. H. Şebnem Düzgün for her kind supervision, invaluable support, friendship and help during my study.

Moreover, I would like to express my appreciation to Assist. Prof. Dr. Aykut Akgün for his, valuable comments and suggestions throughout the study.

A special gratitude goes to my friend Sami Kilic who has always found in assistance to me.

I also express my gratitude to Sanam Dehghan, Alvand Mehrabzadeh and Shahin Takht Firouz for their helps during my study.

My special thanks also go to Onur Golbasi, I. Ferid Oge, Hakan Uysal, Tahsin Işıksal for their continual friendship and help throughout the study.

I am grateful to all members of my great family: my mother Nazanin, my father Jaber, my brothers Abulfazl, Mahammad, Bahman, my sister Fatima, my niece Samira, my nephews Armin and Mahammad Husein, my uncles Habil, Saleh, Valeh for their continual encouragement and support in every stage of the entire of my life.

I would like to thank the Scientific and Technical Research Council of Turkey (TUBITAK) and Middle East Technical University for providing financial support for carrying out this research.

Finally, I am deeply thankful to my love, Tarlan, for her continual love and support. It would not be possible for me to achieve this goal without her patience, understanding and unconditional support.

# TABLE OF CONTENTS

ABSTRACT.....	iv
ÖZ.....	vi
ACKNOWLEDGEMENT .....	ix
TABLE OF CONTENTS.....	xi
LIST OF TABLES.....	xiii
LIST OF FIGURES .....	xvi
LIST OF SYMBOLS .....	xxiii
CHAPTERS	
1. INTRODUCTION .....	1
2. BASIC MECHANICS OF ROCK DISCONTINUITY.....	9
2.1 Introduction .....	9
2.2 Shear Strength of Discontinuities.....	9
2.3 Rock discontinuity deformation .....	20
3. NUMERICAL AND PROBABILISTIC METHODS IN ROCK SLOPE STABILITY ANALYSIS .....	24
3.2 Reliability Index Methods .....	29
3.2.1 The Performance Function.....	31
3.2.2 Linear Performance Functions.....	34
3.2.3 Non-Linear Performance Functions .....	36
3.2.4 Equivalent Normal Distributions .....	38

4. THE DEVELOPED NUMERICAL-PROBABILISTIC APPROACH.....	41
4.1 Methodology .....	41
5. IMPLEMENTATION OF PROPOSED PROBABILISTIC-NUMERICAL METHODOLOGY.....	50
5.1 General information about the study region .....	50
5.2 Field and laboratory studies.....	51
5.3 Rock Slope Modeling.....	68
5.3.1 Model construction.....	70
5.3.2 Choice of Block and Joint Constitutive Models and Material Properties .....	73
5.3.3 Different realization of random variables .....	74
5.4 Results.....	76
5.5 Discussion of the Results.....	106
6. CONCLUSIONS AND RECOMMENDATIONS.....	109
REFERENCES .....	113
APPENDICES	
A: FIELD DATA AND LABORATORIAL TESTS RESULTS.....	118
B: DISTRIBUTIONS OF SHEAR DISPLACEMENT .....	133
C: WRITTEN CODES IN 3DEC .....	140

## LIST OF TABLES

### TABLES

TABLE 5. 1 RECORDED DATA OF ROCK DISCONTINUITY FROM SCANLINE FOR SECTION 1 .....	56
TABLE 5. 2 RECORDED DATA OF ROCK DISCONTINUITY FROM SCANLINE FOR SECTION 2 .....	58
TABLE 5. 3 RECORDED DATA OF ROCK DISCONTINUITY FROM SCANLINE FOR TOE OF SECTION 3.....	59
TABLE 5. 4 STATISTICALANALYSISDATA FOR JRC .....	60
TABLE 5. 5 STATISTICAL DATA ANALYSIS FOR SCHMIDT HAMMER .....	61
TABLE 5. 6 JOINTS GEOMETRY USED IN MODELING THE KING'S GRAVE	71
TABLE 5. 7 SHEAR DEFORMATION, PEAK SHEAR DEFORMATION OF BARTON MODEL FOR FRICTION= 33, COH.=0.05 MPA, DIFFERENT JCS, JRC AND KS.....	86
TABLE 5. 8 SHEAR DEFORMATION, PEAK SHEAR DEFORMATION OF BARTON MODEL FOR FRICTION= 33, COHESION=0.15 MPA, JCS=70 MPA AND DIFFERENT JRC VALUES AND JOINT SHEAR STIFFNESS FOR EACH DISCONTINUITY.....	89
TABLE 5. 9 SHEAR DEFORMATION, PEAK SHEAR DEFORMATION OF BARTON MODEL FOR FRICTION= 33, COHESION=0.2 MPA, JCS =70	

AND DIFFERENT JRC VALUES AND JOINT SHEAR STIFFNESS FOR EACH DISCONTINUITY .....	91
TABLE 5. 10 SHEAR DEFORMATION, PEAK SHEAR DEFORMATION OF BARTON MODEL FOR FRICTION= 33, COHESION=0.3 MPA, JCS=70 MPA, JRC=2 VALUES AND JOINT SHEAR STIFFNESS FOR EACH DISCONTINUITY .....	93
TABLE 5. 11 SHEAR DEFORMATION, PEAK SHEAR DEFORMATION OF BARTON MODEL FOR FRICTION= 33, COHESION=0.5 MPA, JCS=70 MPA, JRC=2 AND 5 VALUES AND JOINT SHEAR STIFFNESS FOR EACH DISCONTINUITY .....	94
TABLE 5. 12 SHEAR DEFORMATION, ALLOWABLE PEAK SHEAR DEFORMATION FOR COHESION=0.05 MPA, JCS=70 AND DIFFERENT JRC VALUES AND JOINT SHEAR STIFFNESS FOR EACH DISCONTINUITY .....	96
TABLE 5. 13 SHEAR DEFORMATION, ALLOWABLE PEAK SHEAR DEFORMATION FOR COHESION=0.1 MPA, FRICTION ANGLE=30, JRC=70 MPA, DIFFERENT JRC VALUES AND JOINT SHEAR STIFFNESS FOR EACH DISCONTINUITY .....	99
TABLE 5. 14 SHEAR DEFORMATION, ALLOWABLE PEAK SHEAR DEFORMATION FOR COHESION=0.15 MPA, JCS=70 MPA, JRC=9.5 AND JOINT SHEAR STIFFNESS FOR EACH DISCONTINUITY .....	100
TABLE 5. 15 SHEAR DEFORMATION, ALLOWABLE PEAK SHEAR DEFORMATION FOR COHESION=0.2 MPA, FRICTION ANGLE=30, JCS=70 MPA AND DIFFERENT JRC AND JOINT SHEAR STIFFNESS FOR EACH DISCONTINUITY .....	102

TABLE 5. 16 SHEAR DEFORMATION, ALLOWABLE PEAK SHEAR DEFORMATION FOR COHESION=0.3 MPA, FRICTION ANGLE=30, JCS=70 MPA AND DIFFERENT JRC AND JOINT SHEAR STIFFNESS FOR EACH DISCONTINUITY.....	104
TABLE 5. 17 SHEAR DEFORMATION, ALLOWABLE PEAK SHEAR DEFORMATION FOR COHESION=0.5 MPA, JCS=70 MPA, JRC=2 AND JOINT SHEAR STIFFNESS FOR EACH DISCONTINUITY .....	105
TABLE 5. 18 FAILURE PROBABILITY AND CORRESPONDING RELIABILITY INDEX ( $\beta$ ) FOR AVERAGE, MINIMUM AND MAXIMUM VALUE OF $\delta_{PEAK}$ FOR EACH DISCONTINUITY.....	108

## LIST OF FIGURES

### FIGURES

FIGURE 2. 1 RELATION BETWEEN RESIDUAL FRICTION ANGLE WITH SCHMIDT REBOUND VALUE (RICHARDS, 1975, IN BARTON AND CHOUBEY, 1977).....	12
FIGURE 2. 2 MECHANISM OF RESIDUAL TILT TEST (BANDIS ET AL., 1983) .....	13
FIGURE 2. 3 LABORATORY SCALED JOINT ROUGHNESS PROFILES (BARTON AND CHOUBEY, 1977).....	15
FIGURE 2. 4 MEASUREMENT OF ASPERITY AMPLITUDE FOR DETERMINING JOINT ROUGHNESS (BARTON AND BANDIS (1982), IN HOEK (2007)).....	16
FIGURE 2. 5 CHART FOR DETERMINING JOINT ROUGHNESS COEFFICIENT FROM ASPERITY AMPLITUDE AND PROFILE LENGTH (BARTON AND BANDIS (1982), IN HOEK (2007)).....	17
FIGURE 2. 6 GROUPS OF DISCONTINUITY TYPES ACCORDING TO THEIR ROUGHNESS (BANDIS ET AL., 1981) .....	19
FIGURE 4. 1 THE PROCESS OF DEVELOPMENT OF PROPOSED PROBABILISTIC NUMERICAL APPROACH .....	42
FIGURE 4. 2 BARTON MODEL AND THE INSTANTANEOUS COHESION AND FRICTION CONCEPTS.....	44

FIGURE 5. 1 LOCATION OF AMASYA.....	51
FIGURE 5. 2 STUDIED FIELD AD FAILED STRUCTURES AND FAILURE POTENTIAL.....	52
FIGURE 5. 3 BEDDING JOINTS OF SEC_1 ON STERONET (064 <sup>0</sup> /42 <sup>0</sup> ) .....	53
FIGURE 5. 4 JOINTS IN SEC_1 REGION IN AMASYA 175 <sup>0</sup> /75 <sup>0</sup> AND 237 <sup>0</sup> /66 <sup>0</sup> .....	54
FIGURE 5. 5 JOINTS IN SEC_2 REGION IN AMASYA 180 <sup>0</sup> /73 <sup>0</sup> , 094 <sup>0</sup> /81 <sup>0</sup> AND 030 <sup>0</sup> /45 <sup>0</sup> .....	54
FIGURE 5. 6 JOINTS IN TOE OF SEC_3 REGION IN AMASYA 146 <sup>0</sup> /74 <sup>0</sup> , 213 <sup>0</sup> /46 <sup>0</sup> AND 028 <sup>0</sup> /35 <sup>0</sup> .....	55
FIGURE 5. 7 LOGNORMAL DISTRIBUTION OF JOINT ROUGHNESS COEFFICIENT (JRC).....	60
FIGURE 5. 8 RELATION BETWEEN THE SCHMIDT HARDNESS AND JOINT WALL STRENGTH .....	63
FIGURE 5. 9 SHEAR STRESS/DISPLACEMENT CURVES FOR JOINT SAMPLE NAMED AS S_2 FOR DIFFERENT NORMAL STRESS VALUES .....	64
FIGURE 5. 10 RELATION OF SHEAR AND NORMAL STRESSES ACTED ON JOINT OF S_2 TO OBTAIN THE BASIC FRICTION ANGLE OF JOINT SURFACE WHICH IS 32.092 <sup>0</sup> .....	65
FIGURE 5. 11 DEPENDENCY OF JOINT SHEAR STIFFNESS (KS) TO NORMAL STRESS IN SMOOTH JOINT PLANE (S_2).....	65
FIGURE 5. 12 SHEAR STRESS/DISPLACEMENT CURVES FOR JOINT SAMPLE N_1 FOR DIFFERENT NORMAL STRESS VALUES .....	66
FIGURE 5. 13 RELATION OF SHEAR AND NORMAL STRESSES ACTED ON JOINT OF N_1.....	67

FIGURE 5. 14 DEPENDENCY OF JOINT SHEAR STIFFNESS (KS) TO NORMAL STRESS IN ROUGH JOINT PLANE (N_1) .....	67
FIGURE 5. 15 STRESS-STRAIN CURVE OF SAMPLE I.....	68
FIGURE 5. 16 KING'S ROCK GRAVE, AMASYA, TURKEY .....	69
FIGURE 5. 17 FALLEN BLOCKS, BIG FAILURE AND HANGING BLOCKS ON THE GRAVE STRUCTURE .....	70
FIGURE 5. 18 CONSTRUCTED MODEL OF THE KING'S GRAVE.....	71
FIGURE 5. 19 FINAL MODEL OF THE GRAVE TO BE ANALYZED BY 3DEC	72
FIGURE 5. 20 MATERIAL NUMBER OF FOURTEEN DISCONTINUITIES TO BE ANALYZED .....	74
FIGURE 5. 21 STATE F THE STRUCTURE FOR JRC=18, JCS=70 MPA, $\Phi =$ $33^{\circ}$ AND NO INFILLING MATERIAL.....	77
FIGURE 5. 22 SHEAR DISPLACEMENT OF DISCONTINUITY 1, FOR JCS=70, C=50 KPA, $\Phi=33^{\circ}$ AND JRC=10 .....	79
FIGURE 5. 23 SHEAR DISPLACEMENT OF DISCONTINUITY 2, FOR JCS=70 MPA, C=50 KPA, $\Phi=33^{\circ}$ AND JRC=10.....	79
FIGURE 5. 24 SHEAR DISPLACEMENT OF DISCONTINUITY 3, FOR JCS=70 MPA, C=50 KPA, $\Phi=33^{\circ}$ AND JRC=10.....	80
FIGURE 5. 25 SHEAR DISPLACEMENT OF DISCONTINUITY 4, FOR JCS=70 MPA, C=50 KPA, $\Phi=33^{\circ}$ AND JRC=10.....	80
FIGURE 5. 26 SHEAR DISPLACEMENT OF DISCONTINUITY 5, FOR JCS=70 MPA, C=50 KPA, $\Phi=33^{\circ}$ AND JRC=10.....	81
FIGURE 5. 27 SHEAR DISPLACEMENT OF DISCONTINUITY 6, FOR JCS=70 MPA, C=50 KPA, $\Phi=33^{\circ}$ AND JRC=10.....	81
FIGURE 5. 28 SHEAR DISPLACEMENT OF DISCONTINUITY 7, FOR JCS=70 MPA, C=50 KPA, $\Phi=33^{\circ}$ AND JRC=10.....	82

FIGURE 5. 29 SHEAR DISPLACEMENT OF DISCONTINUITY 8, FOR JCS=70 MPA, C=50 KPA, $\Phi=33^{\circ}$ AND JRC=10.....	82
FIGURE 5. 30 SHEAR DISPLACEMENT OF DISCONTINUITY 9, FOR JCS=70 MPA, C=50 KPA, $\Phi=33^{\circ}$ AND JRC=10.....	83
FIGURE 5. 31 SHEAR DISPLACEMENT OF DISCONTINUITY 10, FOR JCS=70 MPA, C=50 KPA, $\Phi=33^{\circ}$ AND JRC=10.....	83
FIGURE 5. 32 SHEAR DISPLACEMENT OF DISCONTINUITY 11, FOR JCS=70 MPA, C=50 KPA, $\Phi=33^{\circ}$ AND JRC=10.....	84
FIGURE 5. 33 SHEAR DISPLACEMENT OF DISCONTINUITY 12, FOR JCS=70 MPA, C=50 KPA, $\Phi=33^{\circ}$ AND JRC=10.....	84
FIGURE 5. 34 SHEAR DISPLACEMENT OF DISCONTINUITY 13, FOR JCS=70 MPA, C=50 KPA, $\Phi=33^{\circ}$ AND JRC=10.....	85
FIGURE 5. 35 RELATION OF COHESION AND FAILURE PROBABILITY OF DISCONTINUITIES .....	106
FIGURE 5.36 BETA DISTRIBUTION OF SHEAR DISPLACEMENT OF DISCONTINUITY NO. 1.....	107
FIGURE A.1 SHEAR STRESS/DISPLACEMENT CURVES FOR JOINT SAMPLE NAMED AS S_3 FOR DIFFERENT NORMAL STRESS VALUES .....	125
FIGURE A.2 RELATION OF SHEAR AND NORMAL STRESSES ACTED ON JOINT OF S_3 TO OBTAIN THE BASIC FRICTION ANGLE OF JOINT SURFACE WHICH IS 32.23 .....	125
FIGURE A.3 DEPENDENCY OF JOINT SHEAR STIFFNESS (KS) TO NORMAL STRESS IN SMOOTH JOINT PLANE (S_3).....	126

FIGURE A.4 SHEAR STRESS/DISPLACEMENT CURVES FOR JOINT SAMPLE NAMED AS S_4 FOR DIFFERENT NORMAL STRESS VALUES .....	126
FIGURE A.5 RELATION OF SHEAR AND NORMAL STRESSES ACTED ON JOINT OF S_4 TO OBTAIN THE BASIC FRICTION ANGLE OF JOINT SURFACE WHICH IS 29.16 .....	127
FIGURE A.6 DEPENDENCY OF JOINT SHEAR STIFFNESS (KS) TO NORMAL STRESS IN SMOOTH JOINT PLANE (S_4).....	127
FIGURE A.7 SHEAR STRESS/DISPLACEMENT CURVES FOR JOINT SAMPLE NAMED AS S_5 FOR DIFFERENT NORMAL STRESS VALUES .....	128
FIGURE A.8 RELATION OF SHEAR AND NORMAL STRESSES ACTED ON JOINT OF S_5 TO OBTAIN THE BASIC FRICTION ANGLE OF JOINT SURFACE WHICH IS 33.48 .....	128
FIGURE A.9 DEPENDENCY OF JOINT SHEAR STIFFNESS (KS) TO NORMAL STRESS IN SMOOTH JOINT PLANE (S_5).....	129
FIGURE A.10 SHEAR STRESS/DISPLACEMENT CURVES FOR JOINT SAMPLE NAMED AS S_5 FOR DIFFERENT NORMAL STRESS VALUES .....	129
FIGURE A.11 RELATION OF SHEAR AND NORMAL STRESSES ACTED ON JOINT OF S_5 TO OBTAIN THE BASIC FRICTION ANGLE OF JOINT SURFACE WHICH IS 29 .....	130
FIGURE A.12 DEPENDENCY OF JOINT SHEAR STIFFNESS (KS) TO NORMAL STRESS IN SMOOTH JOINT PLANE (S_5).....	130

FIGURE A.13 SHEAR STRESS/DISPLACEMENT CURVES FOR JOINT SAMPLE NAMED AS N_2 FOR DIFFERENT NORMAL STRESS VALUES .....	131
FIGURE A.14 RELATION OF SHEAR AND NORMAL STRESSES ACTED ON JOINT OF N_2.....	131
FIGURE A.15 DEPENDENCY OF JOINT SHEAR STIFFNESS (KS) TO NORMAL STRESS IN ROUGH JOINT PLANE (N_2).....	132
FIGURE A.16 STRESS-STRAIN CURVE OF SAMPLE II.....	132
FIGURE B.1 BETA DISTRIBUTION OF SHEAR DISPLACEMENT OF DISCONTINUITY NO. 2.....	133
FIGURE B.2 STUDENT'S DISTRIBUTION OF SHEAR DISPLACEMENT OF DISCONTINUITY NO. 3.....	134
FIGURE B.3 STUDENT'S DISTRIBUTION OF SHEAR DISPLACEMENT OF DISCONTINUITY NO. 4.....	134
FIGURE B.4 STUDENT'S DISTRIBUTION OF SHEAR DISPLACEMENT OF DISCONTINUITY NO. 5.....	135
FIGURE B.5 TRIANGULAR DISTRIBUTION OF SHEAR DISPLACEMENT OF DISCONTINUITY NO. 6.....	135
FIGURE B.6 STUDENT'S DISTRIBUTION OF SHEAR DISPLACEMENT OF DISCONTINUITY NO. 7.....	136
FIGURE B.7 STUDENT'S DISTRIBUTION OF SHEAR DISPLACEMENT OF DISCONTINUITY NO. 8.....	136
FIGURE B.8 TRIANGULAR DISTRIBUTION OF SHEAR DISPLACEMENT OF DISCONTINUITY NO. 9.....	137
FIGURE B.9 STUDENT'S DISTRIBUTION OF SHEAR DISPLACEMENT OF DISCONTINUITY NO. 10.....	137

FIGURE B.10 STUDENT'S DISTRIBUTION OF SHEAR DISPLACEMENT OF DISCONTINUITY NO. 11.....	138
FIGURE B.11 STUDENT'S DISTRIBUTION OF SHEAR DISPLACEMENT OF DISCONTINUITY NO. 12.....	138
FIGURE B.12 LOGNORMAL DISTRIBUTION OF SHEAR DISPLACEMENT OF DISCONTINUITY NO. 13.....	139
FIGURE B.13 NORMAL DISTRIBUTION OF SHEAR DISPLACEMENT OF DISCONTINUITY NO. 14.....	139

## LIST OF SYMBOLS

$\tau_{\text{peak}}$  = peak shear strength

$\tau_{\text{residual}}$  = residual shear strength

$\tau_{\text{ult}}$  = ultimate shear strength

$\tau_{\text{m}}$  = bounding shear stress

$c$  = cohesion

$\sigma_{\text{n}}$  = normal stress

$\sigma_{\text{nmax}}$  = maximum normal stress

$\sigma_{\text{c}}$  = uniaxial compressive strength

$\sigma_{\text{i}}$  = initial normal stress

$\phi_{\text{p}}$  = peak friction angle of the discontinuity

$\phi_{\text{r}}$  = residual friction angle of the discontinuity

$\phi_{\text{b}}$  = basic friction angle of the discontinuity

$\phi_{\text{p}}'$  = peak drained friction angle of the discontinuity

$\text{JRC}_{\text{o}}$  = lab scale joint roughness coefficient

$\text{JRC}_{\text{n}}$  = insitu size joint roughness coefficient

$\text{JRC}_{\text{mob}}$  = mobilized joint roughness coefficient

$\text{JCS}_{\text{o}}$  = lab scale joint wall compressive strength

$\text{JCS}_{\text{n}}$  = insitu size joint wall compressive strength

$r$  = Schmidt rebound on weathered rock surface

$R$  = Schmidt rebound on unweathered rock surface

$d_{\text{peak}}$  = peak dilation angle

$\alpha$  = tilt angle

$\gamma$  = rock density

$K$  = bulk modulus

$G$  = shear modulus

$\bar{\delta}$  = shear displacement

$\bar{\delta}_{\text{peak}}$  = peak shear displacement

$L_o$  = lab scale block length

$L_n$  = insitu block length

$K_n$  = joint normal stiffness

$K_{ni}$  = initial joint normal stiffness

$K_s$  = joint shear stiffness

$n_j$  = shear stiffness exponent

$\Delta V$  = normal displacement

$V_m$  = Maximum joint closure

$a_j$  = mechanical joint aperture

$K_j$  = shear stiffness number

$R_f$  = failure ratio

$A_c$  = Area of joint face

$F^n$  = normal force

$\Delta F^n$  = normal force increment

$F^s$  = shear force

$\Delta F^s$  = shear force increment

$\Delta V^i$  = normal displacement increment

$\Delta \bar{\delta}$  = shear displacement increment

$\Delta \bar{\delta}^p$  = plastic shear displacement increment

$F$  = tangent modulus factor (3DEC continuously yielding joint model)

$a_n$  = joint normal stiffness (3DEC continuously yielding joint model)

$a_s$  = joint shear stiffness (3DEC continuously yielding joint model)

$e_n$  = joint normal stiffness exponent (3DEC continuously yielding joint model)

# CHAPTER I

## INTRODUCTION

### 1.1 Problem statement

Rock slope stability is one of the most important concerns in rock engineering. Loss of lives of people living on hills near to mountain area, falling of blocks to the roads and loss of minerals in open pit mines have enhanced the necessity of using and developing much reliable methods to analyze the stability of those structures.

Generally, rock slope stability analysis methods can be divided into two: Namely deterministic and probabilistic approaches. In deterministic approaches the input variables are assumed to have certain values. Depending on the judgment of engineer, minimum, maximum, average of a parameter is selected and used in the calculations. However, in probabilistic approaches the variables are considered to be random with associated probability distribution.

Generally, the deterministic approach itself is divided into two as limit equilibrium and numerical methods. Commonly, in industrial design the limit equilibrium methods are applied for design of rock slopes. Hoek and Bray (1981) have formulated the rock slope instability problems in four distinct categories as planar, wedge, toppling and circular failures. However, limit equilibrium methods have been formulated based on some

assumptions. Such assumptions usually include elastic behavior, homogeneous, isotropic material, time independent behavior, quasi-static loading, etc. Geomaterials such as soils and rock masses display non-linear behavior, either because this is inherent to the material or because it has been externally induced (e.g., past stress history). Rocks and soils may not be isotropic or homogeneous, and the loading may not be static, or the geometry of the problem may be complex (Bobet 2010). According to Krahn (2003) the fundamental shortcoming of limit equilibrium methods which only satisfy statics equation is that they do not consider strain and displacement compatibility.

To solve the shortcomings of limit equilibrium methods, different numerical methods have been developed and applied extensively in rock mechanics. In Krahn's (2003) opinion, this shortcoming can be overcome by using Finite Element Method (FEM) computed stresses inside conventional limit equilibrium framework. From the finite element stresses both the total shear resistance and the total mobilized shear stress on a slip surface can be computed and used to determine the factor of safety.

Numerical methods have been extensively used in the past several decades due to advances in computing power. Generally, numerical methods can be classified into continuum and discontinuum methods (Jing and Hudson 2002, Jing 2003). There are quite a large number of numerical methods that have been used in the literature to estimate the behavior of geomaterials. The most important or at least the most used methods are: Continuum, Finite Difference Method (FDM), Finite Element Method (FEM) and Boundary Element Method (BEM); Discontinuum, Distinct Element Method (DEM), Discontinuous Deformation Analysis (DDA), and Bonded Particle Model (BPM). There are two other methods which do not follow this classification: Meshless Methods (MM) and Artificial Neural Networks (Bobet 2010). Jing and Hudson (2002) and

Bobet (2010) have discussed the different numerical methods applied in rock mechanics.

However, rock mass parameters are always containing uncertainty, the utilization of probabilistic methods in rock engineering, permits a rational treatment of various uncertainties that significantly influence the safety of a rock slope. Moreover, probabilistic approaches offer a systematic way of treating uncertainties and quantifying the reliability of a design (Kirsten, 1983). Düzgün (1994) and Düzgün et al. (1995) have applied advanced First Order Second Moment method (AFOSM) to a non-linear performance function with non-normal correlated variables to analyze the planer stability of a rock slope based on Mohr-Coulomb criterion. Düzgün et al. (2003) have proposed a methodology for reliability based design of rock slopes. In this study, a model is developed within the framework first-order second-moment approach to analyze the uncertainties underlying the in situ shear strength properties of rock discontinuities. Düzgün and Özdemir (2006) have applied AFOSM and risk assessment to a planar failure of a rock mass in Konya to manage the risk by decision analytical procedure. Jimenez-Rodriguez et al. (2006) considered a sliding mass on an inclined plane with two blocks separated by a vertical tension crack. Two cases were defined, in which the two blocks may have interaction or not. The models were formulated by Limit Equilibrium Method for each case. It was assumed that when Safety Factor (SF) is lower than one a block will fail. Düzgün and Bhasin (2009) used first order reliability method (FORM) to model a plane failure of a slope with 734 m-height using the Barton-Bandis (1982) shear strength criterion for modeling the limit state function. The slope was consisting of three big blocks laying on each. They have defined possible failure scenarios and by using conditional probability theory the failure probability was calculated.

Low (1997) calculated the safety factor for a wedge slope utilizing AFOSM. In addition, utilizing Excel spreadsheet he calculated the

reliability index and probability of failure for the slope. Low (1997) used Coulomb linear failure criterion and he assumed that all the parameters are normally distributed. Park and West (2001) have worked on probabilistic modeling of rock wedge failure in their work. First they have modeled the probability of kinematic instability in which planes dip and dip direction were considered as random variables, then probability of kinetic instability was modeled to provide a proper, combined evaluation for failure probability by Monte Carlo Simulation. Joint orientation, geometric parameters, such as length and spacing, shear strength parameters and pore water pressure in the discontinuity were considered to be probabilistic parameters.

Also, Jimenez-Rodriguez and Sitar (2007) have modeled the stability of the wedge using a disjoint cut-set formulation, in which disjoint parallel sub-systems were used to represent the different failure modes of the slope, and the used random variables were strength parameters of joint planes and the geometry of wedge, they have concluded that the reliability results were found to be highly sensitive to variations in the geometry of the wedge and to variations in water level conditions, whereas variations in the unit weight of the slope were found to have almost no influence on the probability of failure.

Fadlelmula (2007) in his study presents the results of probabilistic modeling of plane and wedge types of slope failures, based on the "Advance First Order Second Moment (AFOSM)" reliability method. In both of those failure types, two different failure criteria namely, Coulomb linear and Barton-Bandis non-linear failure criteria were utilized in the development of the probabilistic models.

Moreover, Li et al. (2009) has developed a probabilistic fault tree to model the system reliability of the rock wedges. The N-dimensional equivalent method was used to perform the system reliability analysis due

to its accuracy and efficiency. The proposed approach has the ability to quantify the relative importance of each failure mode which enables the designer to establish priorities and decision making for rock slope.

Scavia et al. (1990) have developed a probabilistic model using 2-D limit equilibrium analysis of block toppling failure in rock, resting on a stepped failure surface was carried out including both Monte Carlo simulation procedure and Markov Chains theory.

Tatone and Grasselli (2010) also have developed a new probabilistic method for analyzing the stability of rock slopes according to the limit equilibrium method developed by Goodman and Bray (1976) and introduced a Monte Carlo simulation procedure for the probabilistic analysis of block-toppling and described its implementation into a spreadsheet-based program (ROCKTOPPLE). The analysis procedure considers both kinematic and kinetic probabilities of failure. These probabilities are evaluated separately and multiplied to give the total probability of block toppling.

All of the above mentioned works have used Limit Equilibrium Method to model the performance function, because by that method it is easy to formulate the performance of a rock mass.

To consider the effects of uncertainties in numerical modeling the Stochastic Finite Element was proposed for continuum media and there are some works such as Wong (1985), Griffiths et al. (2005), Tan and Wang (2009) for soil slope. Also Hammah et al. (2009) applied stochastic finite element in analyzing the stability of a rock slope in which uncertainties were related to strength parameters and joint network geometry. In their work they used both Monte Carlo and Point Estimate Method (PEM) to calculate statistical moments. Furthermore, Wang et al. (2000) have used FLAC software which is based on Finite Difference

Method to assess the stability of a coal mine slope, in this study the stability of a coal mine slope was analyzed using numerical analysis considering reliability engineering concepts.

However, none of these methods can be applied in rock slope stabilities which are discontinuous. To solve this lack Moarefvand and Verdel (2008) tried to contribute the probabilistic methods in Distinct Element Method in UDEC software and they named it as PUDEC. It was the first time that probabilistic numerical method was used in a discontinuous media in rock mechanics. In this method the statistical moments are given to software and the software solves the model by considering these uncertainties and simulation outputs are in statistical form. However, the performance of this method relies on a wrong assumption by which the plastic flow starts when  $E(\tau) > E(\tau_{max})$ , where  $E(\tau)$  is the mean of shear stress and  $E(\tau_{max})$  is the mean of shear strength. Also, in this research, reliability engineering concepts such as reliability index, probability of failure are not taken into account.

## **1.2 Objectives and scope of the research**

Considering these features of all the previous studies done in reliability engineering related to rock slope stability, this thesis proposes a probabilistic numerical approach for stability assessment of rock slopes. The proposed approach uses the capabilities of numerical modeling method and simultaneously it considers the randomness of the rock slope stability parameters. For this purpose the probabilistic modeling approach is integrated with 3D distinct element method in 3DEC software by developing codes in FISH language of 3DEC.

Generally, the failure mechanism in discontinuous rock slopes is controlled by existing rock discontinuities. Therefore, the shear behavior of the rock discontinuities plays a vital role in stability or instability of a

rock slope. Commonly, the linear Coulomb criterion is used in analyzing the stability of rock slopes either in limit equilibrium or numerical methods. However, it is clear that the Coulomb parameters do not have the sufficient ability to model the shear and normal behavior of the rock discontinuities. Therefore, it is much realistic to apply a series of models known as Barton models. In contrast to Coulomb, Barton models consider the surface conditions such as roughness, strength of joint walls and basic friction angle of the rock discontinuities and their dependency on stress level in its calculations. Hence nonlinear Barton models are used rather than linear Coulomb function. Since the distinct element code used in this thesis was 3DEC and it does not include the Barton model in contrast to UDEC (2D distinct element code), the approach is applied by developing codes in 3DEC.

One of the drawbacks of limit equilibrium methods is not considering the strain of in their calculations. Therefore, the probabilistic approaches that use the limit equilibrium method do not consider the strain as a possible failure criterion. Instead, they work with the safety factor concept. Based on this concept, the structure fails when the stress applied is greater than the strength. However, in some circumstances, the deformation of a structure can be called as failure and the structure uses its applicability although the safety factor claiming a safe state.

For this reason in this thesis strain is considered to be the indicator of failure as well as simultaneously taking the randomness of the rock mechanical parameters into account. Based on a definite strain value the failure or survival of the rock discontinuities is determined and the failure probability and the corresponding reliability index are obtained. Because of the importance of historical places in Turkey, a rock slope containing a historical grave in Amasya, Turkey was selected to implement the proposed methodology. Akgun and Kockar (2004) studied the stability of a sandy limestone rock slope under a historical castle in Turkey.

The present study is divided into six chapters. Chapter I covers a brief introduction of the thesis subject and previous works and scope of the thesis. In Chapter II the basic mechanics of rock discontinuity is discussed. The Distinct Element Method (DEM) and Probabilistic Method are reviewed in Chapter III. In Chapter IV the Proposed Numerical-Probabilistic Approach is explained. Chapter V includes the implementation of the proposed approach in Amasya, Turkey and its results and discussions. At the end, the conclusions and the recommendation are presented at Chapter VI.

## CHAPTER II

### BASIC MECHANICS OF ROCK DISCONTINUITY

#### 2.1 Introduction

Generally, rock masses contain discontinuities such as bedding planes, joints, shear zones and faults. At shallow depth, where stresses are low, the behavior of the rock mass is controlled by the discontinuities rather than rock mass itself. In order to analyze the stability of this system of individual rock blocks, it is necessary to understand the factors that control the shear strength of the discontinuities which separate the blocks (Hoek, 2007). In this Chapter, it is intended to overview the basic mechanics of discontinuities under normal and shear stresses.

#### 2.2 Shear Strength of Discontinuities

A discontinuity is generally referred to all structural breaks in rocks which usually have zero to low tensile strength. Normally, joints, bedding, shear zones, contacts, veins, and faults are called as discontinuities.

Shear behavior of rock discontinuities always plays important role in rock engineering. There are several discontinuity shear failure criterion developed for the past decade. The most common one is the linear Coulomb relation in which the peak shear ( $\tau$ ) strength is expressed in terms of the effective normal stress ( $\sigma_n$ ), cohesion ( $c$ ) and angle of friction ( $\Phi$ ). The Mohr-Coulomb relation is given as;

$$\tau_{\text{peak}} = c + \sigma_n \tan \Phi \quad (2.1)$$

This shear strength equation was developed by assuming that the discontinuity surface is planar. If a smooth planar surface is sheared at a constant normal stress, the surface will behave elastically, and the shear stress acting on the discontinuity surface increases rapidly till the peak shear strength is reached. After that the shear strength drops and becomes constant at the level which is called as residual shear strength. Equation (2.1) can be expressed to give the residual shear strength as;

$$\tau_{\text{residual}} = \sigma_n \tan \Phi_r \quad (2.2)$$

Where, the residual friction angle ( $\Phi_r$ ) is approximately equal to the basic friction angle ( $\Phi_b$ ), which is usually measured with sawn rock surfaces. However, a natural rock discontinuity may probably have some asperities that directly affect the shear strength of the discontinuity. As the discontinuity is under shear loading, the shear displacement will be on these asperities that causes the block move upward on the inclined surfaces of the asperities (dilation). For this reason the roughness component (i) should be added to the basic friction angle ( $\Phi_b$ ), ( $\Phi_b + i$ ), where 'i' is the angle of the inclined surface of the asperities.

Sliding along the wavy faces of discontinuity can occur only under very low normal stress. If the normal stress is increased, then the asperities may break or wear out and in such cases the discontinuity wall strength becomes important.

Barton-Bandis (1982) failure criterion includes discontinuity surface properties besides the effective normal stress and friction angle of the

discontinuity. Barton (1973) derived an empirical relationship for determining the shear strength of discontinuities. It is written as follows:

$$\tau = \sigma_n \tan \left[ \text{JRC} \times \log_{10} \left( \frac{\text{JCS}}{\sigma_n} \right) + \Phi_b \right] \quad (2.3)$$

Where;

$\sigma_n$  = effective normal stress

JRC = joint roughness coefficient

JCS = joint wall compressive strength

$\Phi_b$  = basic friction angle (obtain from residual shear tests on flat unweathered rock surfaces)

The joint wall compressive strength (JCS) generally reduces with water saturation compared to the dry state (Barton, 2007). This is because of the effect of moisture on the uniaxial compressive strength ( $\sigma_c$ ). The value of is obtained from Schmidt hammer tests (ISRM, 1978).

Another major component of the shear strength is the basic friction angle ( $\Phi_b$ ) of unweathered artificial, planar, dry rock surfaces and the residual friction angle ( $\Phi_r$ ) applying to flat, non-dilatant, saturated, well sheared surfaces, i.e.  $\Phi_r \leq \Phi_b$ . The friction angles obtained from flat unweathered rock surfaces, which are most frequently prepared by diamond saw, will not be applicable to weathered rock discontinuities unless the effective normal stress is high enough for the thin layers of weathered rock to be worn away (Richards, 1975, in Barton and Choubey, 1977). Low levels of effective normal stress and the thin layers of weathered material, perhaps less than 1 mm in thickness, may continue to control the shear strength, post peak strength and even for displacements up to residual strength. Richards' (1975) tests on weathered sandstone joints showed strong correlation between residual friction angles ( $\Phi_r$ ) and Schmidt rebound value (Figure 2.1).

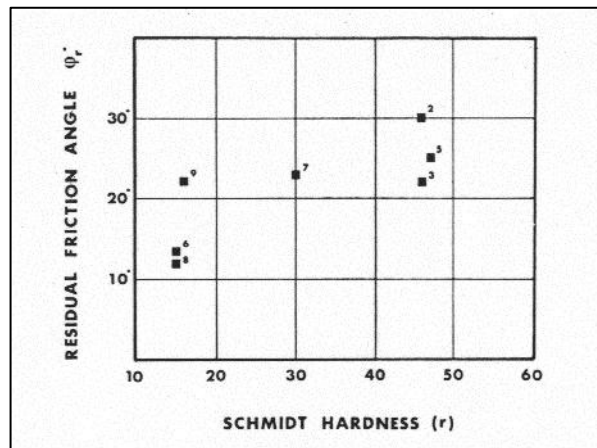


Figure 2. 1 Relation between residual friction angle with Schmidt rebound value (Richards, 1975, in Barton and Choubey, 1977)

Richards' (1975) looked for a simple method of estimating  $\Phi_r$  from Schmidt hammer rebound values. The first empirical relationship tried was as follows:

$$\Phi_r = 10^\circ + (r/R) (\Phi_b - 10^\circ) \quad (2.4)$$

Where;

$r$  = Schmidt rebound on weathered discontinuity surface

$R$  = Schmidt rebound on unweathered discontinuity surface

Therefore the Eq. 2.3 for the general case of weathered and unweathered discontinuities was rewritten as (Barton and Choubey (1977) :

$$\tau_{\text{peak}} = \sigma_n \tan \left[ \text{JRC} \log_{10} \left( \frac{\text{JCS}}{\sigma_n} \right) + \Phi_r \right] \quad (2.5)$$

In the work of Barton and Choubey (1977), eight different rock types with total of 136 individual discontinuities were studied. The specimens were sawn from larger blocks containing through going discontinuities.

Following this study another methodology for determining  $\Phi_r$  by residual tilt test was introduced, which is basically a shear test under very low normal stress (Figure 2.2). In this test, pair of flat and sawn surfaces was mated, and the pair of blocks tilted until sliding occurred.

An empirical equation was obtained from residual tilt tests that enable to relate  $\Phi_r$  to  $\Phi_b$ ;

$$\Phi_r = (\Phi_b - 20^\circ) + 20(r/R) \quad (2.6)$$

Where;

$\Phi_b$  = basic friction angle estimated from residual tilt tests on dry unweathered sawn surfaces

$r$  = Schmidt hammer rebound value on the saturated joint wall,

$R$  = Schmidt hammer rebound value on the dry, artificially cut rock surfaces

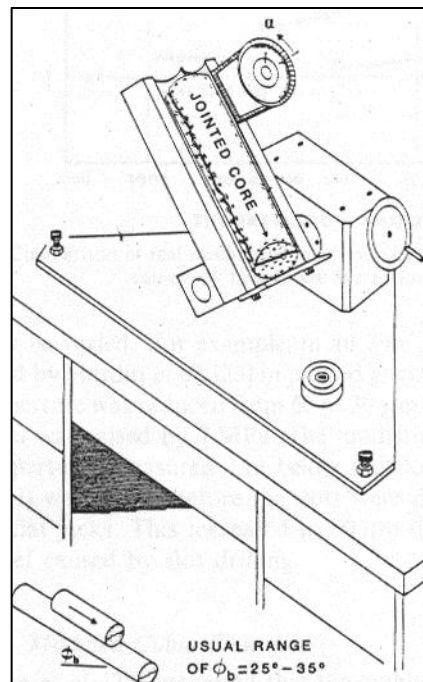


Figure 2. 2 Mechanism of residual tilt test (Bandis et al., 1983)

Eq. 2.6 is preferred since it allows for a range of  $\Phi_r$  values even when the discontinuity is highly weathered. Eq. 2.3 tends to discount mineralogical differences since  $\Phi_r$  tends to a single minimum value of  $10^\circ$  when  $r$  value is zero.

The strength measured along individual discontinuities by direct shear methods is strongly dependent on the roughness of the discontinuity surfaces (Barton, 1973). The roughness parameter represents an index of the unevenness and waviness of the adjacent discontinuity rock wall (Giani, 1992). Barton (1973) defined the term joint roughness coefficient (JRC), which varies from 0 to 20. Unlike the JCS parameter, the JRC parameter is not significantly affected by the dry or wet condition, since it essentially represents geometry (Barton, 2007). Figure 2.3 presents the laboratory-scale joint roughness profiles with their measured JRC values defined by Barton and Choubey (1977).

Besides the joint roughness profiles, simple residual tilt test may help to obtain JRC indirectly. In a tilt test on a rough joint, the angle ( $\alpha$ ) at which sliding occurs may be  $40^\circ$  or  $50^\circ$  more than  $\Phi_b$  (higher than compared to  $\Phi_r$ ) (Barton and Choubey, 1977). This additional shear strength is a result of discontinuity surface roughness.

The maximum dilation angle ( $d_o$ ) when sliding occurs is probably given by the following simple relationship derived by Barton and Choubey, 1977).

$$d_o = \alpha - \Phi_r \quad (2.7)$$

The tilt angle ( $\alpha$ ) is a function of shear stress and normal stress acting on the joint is given as:

$$\Phi = \arctan\left(\frac{\tau}{\sigma_n}\right) \quad (2.8)$$

The effective normal stress generated by the gravitational force acting on the upper half of the block is given as:

$$\sigma_n = \gamma \cdot h \cdot \cos \alpha \quad (2.9)$$

Where;

$h$  = thickness of the top block (m)

$\gamma$  = rock density ( $\text{kN/m}^3$ )

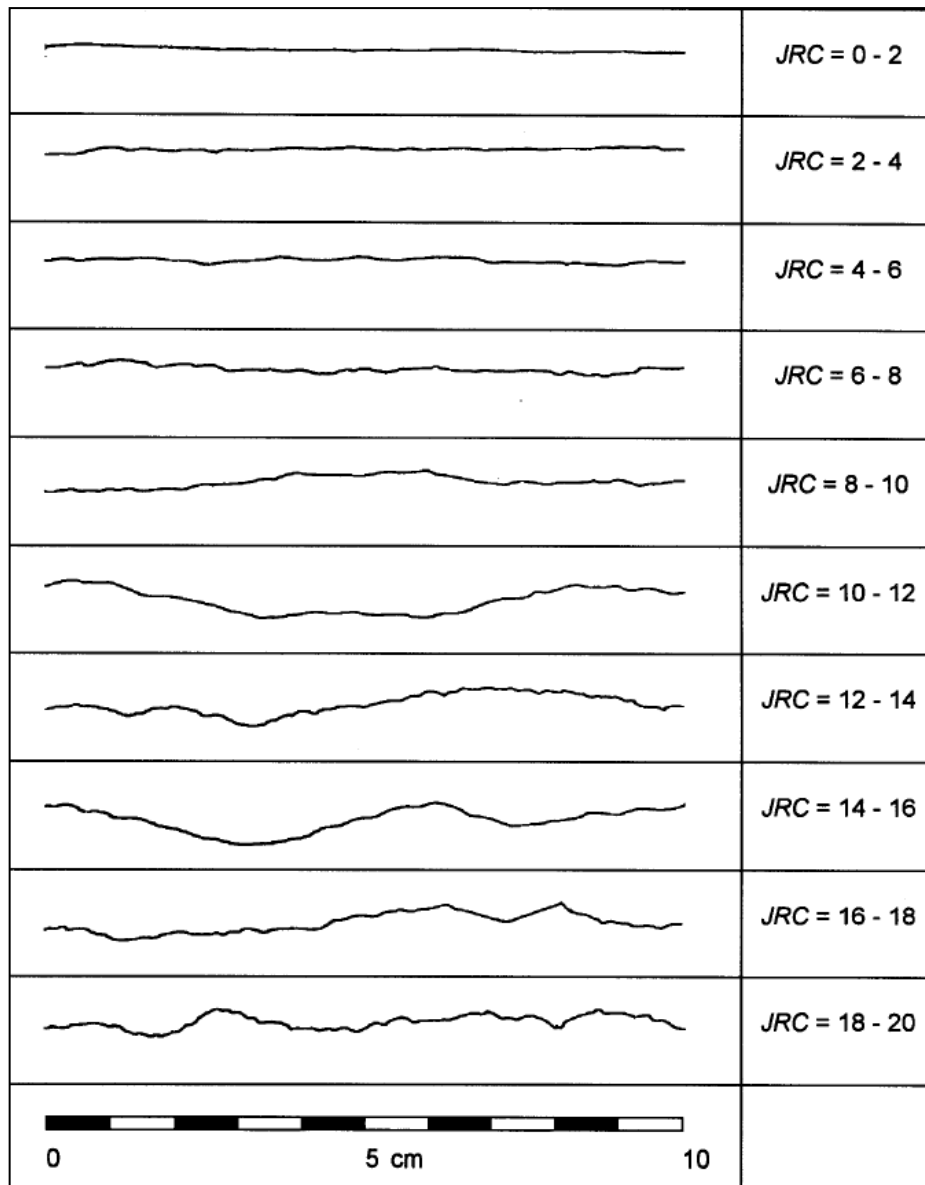


Figure 2. 3 Laboratory scaled joint roughness profiles (Barton and Choubey, 1977)

The JRC value is estimated from tilt tests using Eq. 2.5, by substituting  $\alpha$  and  $\sigma_n$  results in:

$$JRC = \frac{\alpha - \Phi_r}{\log_{10} \left( \frac{JCS}{\sigma_n} \right)} \quad (2.10)$$

Barton and Choubey (1977) recommended “push” or “pull” tests in order to determine the JRC values of rougher discontinuities. In “push” or “pull” test the top block is pushed or pulled parallel to the discontinuity plane. First applying a dry tilt test then a dry push or pull test, it was found to be possible to test whole spectrum of joint roughness (0-20). However, they mentioned the fact that, discontinuous joints and discontinuities with cross jointing cannot be tested by such methods.

Another method for determining JRC was presented by Barton and Bandis (1982) by considering the amplitudes of the asperities of the discontinuity surface as shown in Figure 2.4.

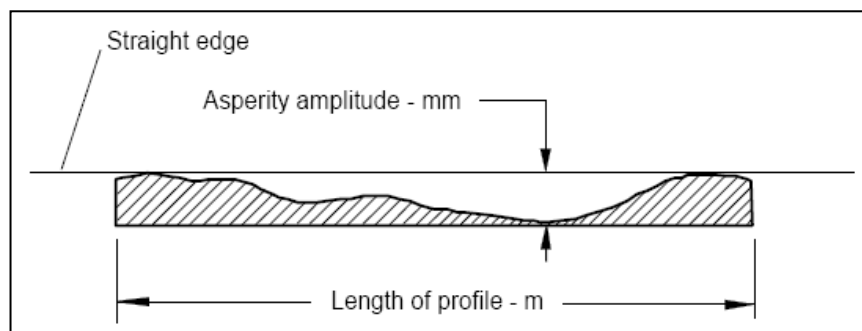


Figure 2. 4 Measurement of asperity amplitude for determining joint roughness (Barton and Bandis (1982), in Hoek (2007))

After determining the asperity amplitude and the sample length the chart which is shown in Figure 2.5 can be used to determine JRC.

The chart of Barton and Bandis (1982) is a useful tool for determining joint roughness coefficient. From the chart the relation between asperity height, discontinuity length and joint roughness coefficient can be summarized as;

$$\text{Asperity height} = 2 \times \text{JRC} \times \text{Discontinuity length} \quad (2.11)$$

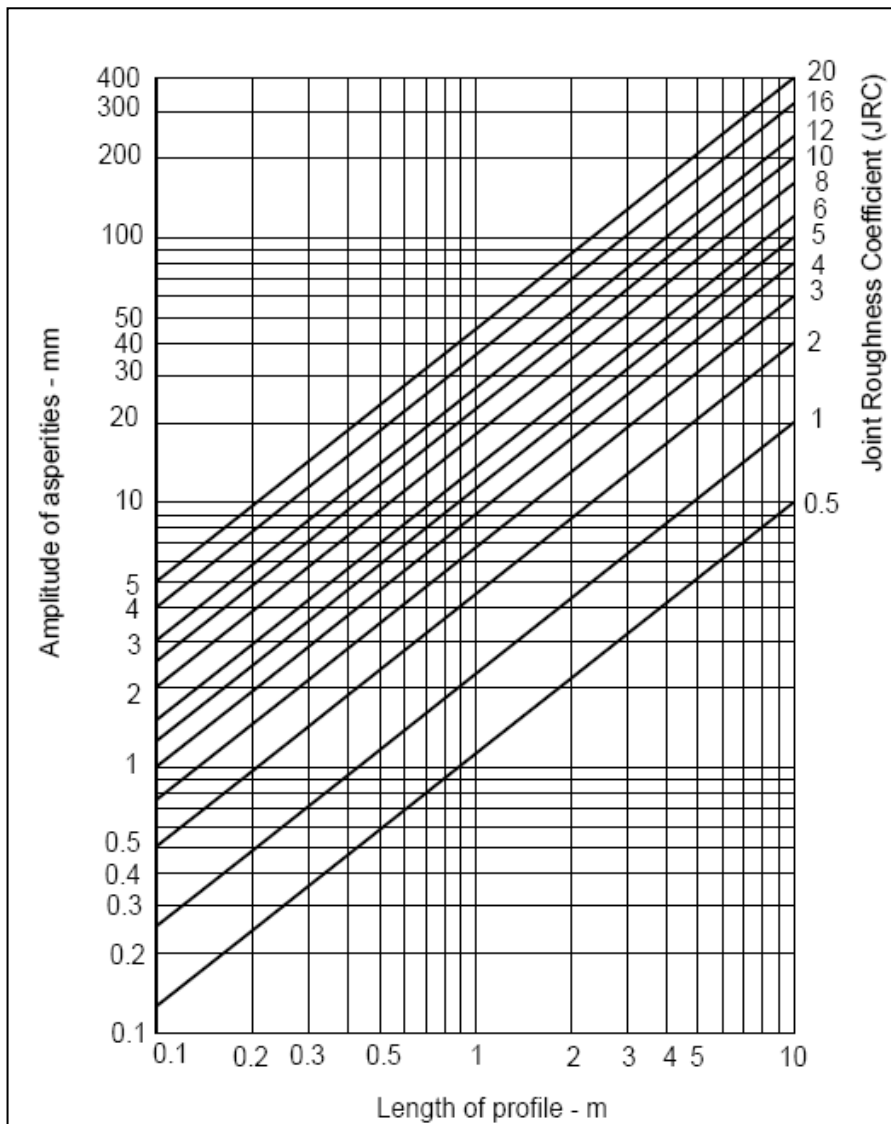


Figure 2. 5 Chart for determining joint roughness coefficient from asperity amplitude and profile length (Barton and Bandis (1982), in Hoek (2007))

If the shearing of a non-planar discontinuity occurs, the asperities on either side of the discontinuity slide over each other and cause an increase in aperture which is called dilation. This process requires a finite displacement to get started, and occurs at an increasing rate as peak strength is approached (Barton et al., 1985). The peak dilation angle,  $d_{\text{peak}}$ , is the maximum dilation angle which occurs more or less at the same time with peak shear resistance (Barton and Choubey, 1977) and it is defined as:

$$d_{\text{peak}} = 1/2 \times \text{JRC} \times \log_{10} \left( \frac{\text{JCS}}{\sigma_n} \right) \quad (2.12)$$

The choice of an appropriate discontinuity size during a shear strength investigation is generally based on both economic and technical considerations (Bandis et al., 1981).

Pratt et al. (1974) (in Bandis et al. (1981)) studied the effect of scale on shear strength and concluded that the reduction in peak shear strength was due to the decrease in actual contact area. Their prediction was that, the scale effect would be negligible if the discontinuities are unweathered, perfectly mating under high normal stresses. Barton (1976) also interpreted similar results of scale effect on joint wall compressive strength (JCS). The study of Barton and Choubey (1977) showed that different lengths of discontinuities affect joint roughness coefficient (JRC) and thus the shear strength of the discontinuity.

Bandis et al. (1981) studied the scale effect on the shear strength of discontinuities with eleven types of discontinuities, of which was divided into four groups according to their roughness (Figure 2.6).

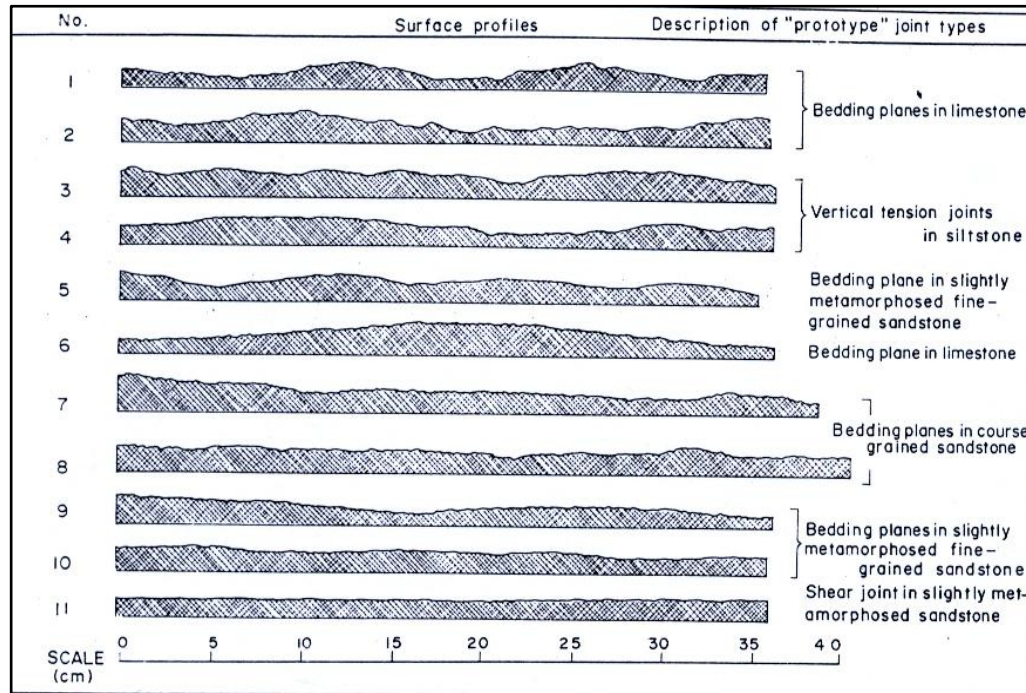


Figure 2. 6 Groups of discontinuity types according to their roughness (Bandis et al., 1981)

Barton and Bandis (1982) suggested some empirical relations for the scale effects on the joint wall compressive strength; joint roughness coefficient and peak shear displacement. They developed some empirical relations for predicting the large scale joint wall compressive strength ( $JCS_n$ ), joint roughness coefficient ( $JRC_o$ ) from lab scale values ( $JCS_o$ ,  $JRC_o$ ) and the peak shear displacement ( $\delta_{peak}$ ) of the discontinuity.

The effects of scale on the dry or saturated state of the discontinuities are expressed below; Large-scale joint wall compressive strength (Barton and Bandis (1982), in Barton et al. (1985)) is:

$$JCS_n = JCS_o \times \left(\frac{L_n}{L_o}\right)^{-0.03JRC_o} \quad (2.13)$$

Large-scale joint roughness (Barton and Bandis (1982), in Barton et al. (1985)) is:

$$JRC_n = JRC_o \times \left(\frac{L_n}{L_o}\right)^{-0.02JRC_o} \quad (2.14)$$

Displacement at the peak strength (Barton and Bandis (1982), in Barton et al. (1985)) is:

$$\bar{\delta}_{peak} = \frac{L_n}{500} \times \left(\frac{JRC_n}{L_n}\right)^{\frac{1}{3}} \quad (2.15)$$

### 2.3 Rock discontinuity deformation

Discontinuity deformation is a principal component of the behavior of the discontinuous rock mass (Bandis et al., 1983). The terms of joint normal stiffness and joint shear stiffness were defined in order to analyze the deformation characteristics of the joints.

Normal stiffness ( $K_n$ ) is defined as the normal stress increment required for a small closure of a joint or fracture, at a given level of effective stress. Similarly the shear stiffness ( $K_s$ ) is taken as the average slope up to the shear strength-peak shear displacement curve. The units of joint stiffness values are stress/displacement (e.g. MPa/mm, MPa/m etc.). Therefore it is usually expected that  $K_n$  values are larger than the shear stiffness  $K_s$  values (Barton, 2007). While the stress level is low the normal deformation of the discontinuities are not discussed in this study.

The non-linear stress - shear displacement behavior of sheared discontinuities in the pre-peak range were frequently expressed by hyperbolic functions (Bandis et al., 1983). Kulhaway (1975, in Bandis et al., 1983) refers to the relation;

$$T = \frac{\bar{\delta}}{m+n\bar{\delta}} \quad (2.16)$$

Where  $\delta$  is the shear displacement at a given shear stress level and  $m$  and  $n$  are constants of the hyperbola. Constant  $m$  is the reciprocal of the initial shear stiffness and constant  $n$  is the reciprocal of the horizontal asymptote  $\tau_{ult}$  to the hyperbolic  $\tau$ - $\delta$  curve. Development of Eq. 2.16 results with the following relation for shear stiffness;

$$K_s = K_j (\sigma_n)^{n_j} \left(1 - \frac{\tau R_f}{\tau_p}\right)^2 \quad (2.17)$$

Where;

$K_j$  = stiffness number,

$n_j$  = stiffness exponent,

$R_f$  = failure ratio =  $T/T_{ult}$ ,

$\tau_p$  = peak shear strength.

The indices  $R_f$ ,  $n_j$  and  $K_j$  describes the non-linearity in discontinuity shear behavior. The stiffness exponent  $n_j$  is the slope of log-log relation between initial shear stiffness  $K_{si}$  and  $\sigma_n$  with a unit of  $(\text{MPa})^2/\text{mm}$ . Also the experimental studies Bandis et al. (1983) showed that stiffness number  $K_j$  (intercept of the log-log relation between initial shear stiffness  $K_{si}$  and  $\sigma_n$ ) can be written empirically as;

$$K_j = -17.19 + 3.86 \text{ JRC} \quad (2.18)$$

With  $R = 0,835$  for  $\text{JRC} > 4, 5$ .

However, for calculation of the value of joint shear stiffness ( $K_s$ ) the Eq. 2.17 is dependent on the current shear stress acting on the joint plane, from other side, in this research, the analysis are done based on distinct element method, therefore, the unbalanced forces in the model will cause instability in shear stress then the joint shear stiffness derived

from the Eq. 2.17 will not be reliable. To overcome this problem, it is possible to calculate the  $K_s$  from relation between shear displacement  $\bar{\delta}$  (peak) and the peak shear strength. According to Barton and Choubey (1976) the shear displacement  $\bar{\delta}$  (peak) required to reach the peak shear strength determines the stiffness of joints in shear. As Barton and Choubey (1976) admitted that joint shear stiffness is extremely important input data in finite element analyses of joints, since joints are very deformable in shear compared to normal direction and compared to intact rock (Barton 1972).

Since the reliable method of estimating shear strength was developed for any given values of JCS, JRC,  $\Phi_r$  and  $\sigma_n$ , it only remains to estimate the  $\bar{\delta}$  (peak) for an estimate of  $K_s$  to be obtained (Barton and Choubey, 1976). Barton and Choubey (1976) assumed  $\bar{\delta}$  (peak) as 1% of joint length (L) and estimated the  $K_s$  based on following relations:

$$K_s = \tau / \bar{\delta}_{peak} \quad (2.19)$$

$$K_s = \frac{100}{L} \sigma_n \tan \left[ JRC \log_{10} \left( \frac{JCS}{\sigma_n} \right) + \Sigma_r \right] \quad (2.20)$$

In Eq. 2.20 Barton and Choubey (1976) assumed that a joint reaches to its peak shear strength after about 1% of its length (L).  $K_s$  is strongly dependent on scale. A review of laboratory and insitu shear tests (Barton 1972) indicated that shear stiffness was indeed inversely proportional to joint length. However, it seems clear that  $\bar{\delta}$  (peak) will eventually reduce to less than 1% L as the joint length increases to several meters (Barton and Choubey 1976). Later, Barton et al. (1985) suggested Eq. 2.21 estimate the  $\bar{\delta}$  (peak) value as:

$$\bar{\delta}_{peak} = \frac{L_n}{500} \times \left( \frac{JRC_n}{L_n} \right)^{\frac{1}{3}} \quad (2.21)$$

Therefore, it is possible to estimate the  $\delta$  (peak) and then  $K_s$  value by substitution of Eq. 2.21 into Eq. 2.19.

## CHAPTER III

# NUMERICAL AND PROBABILISTIC METHODS IN ROCK SLOPE STABILITY ANALYSIS

### 3.1 The Distinct Element Method

The Distinct Element Method (DEM) was introduced by Cundall (1971) as a model to simulate large movements in blocky rock masses, and then used for soils which were modeled as discs (Cundall and Strack 1979). Later, the method has been applied to spherical and polyhedral blocks (Pande et al. 1990, Cundall 1988 and Potyondy and Cundall 2004) for both soils and rocks.

The DEM belongs to the family of Discrete Element Methods, which Cundall and Hart (1998) define as those that: (1) allow finite displacements and rotations of discrete bodies, including detachment; and (2) automatically recognize new contacts between bodies during calculations. Discrete Element Methods need to address three key issues: (1) representation of contacts; (2) representation of solid material; and (3) detection and revision of contacts during execution. An in-depth discussion of these issues is provided by Cundall and Hart (1998).

The distinct element technique was originally developed by Cundall (1971) and has resulted in formulation and development of three

dimensional distinct element code (3DEC) and it progressed over a period of 35 years (Anon, 2007).

3DEC is three-dimensional numerical software based on the distinct element method for modeling discontinuous medium subjected to static or dynamic loading. A discontinuous medium is distinguished from a continuous medium by the existence of contacts between the discrete bodies that comprise the system (Anon, 2007).

3DEC is based on a dynamic (time-domain) algorithm that solves the equations of motion of the block system by an explicit finite difference method. At each time step, the law of motion and the constitutive equations are applied. For both rigid and deformable blocks, sub-contact force-displacement relations are prescribed. The integration of the law of motion provides the new block positions, and therefore the contact displacement increments (or velocities). The sub-contact force-displacement law is then used to obtain the new sub-contact forces, which are to be applied to the blocks in the next time step. The cycle of mechanical calculations is illustrated in Figure 3.1 (Anon, 2007).

3DEC also has a built in programming language called FISH which can be used for user specific purposes.

3DEC has two constitutive models for analyzing discontinuity behavior. The first one is the generalization of Coulomb friction law. This law works similarly for sub-contacts between both rigid and deformable blocks. Both shear and tensile failure is considered. In elastic range the model behavior is governed by discontinuity normal stiffness and discontinuity shear stiffness.

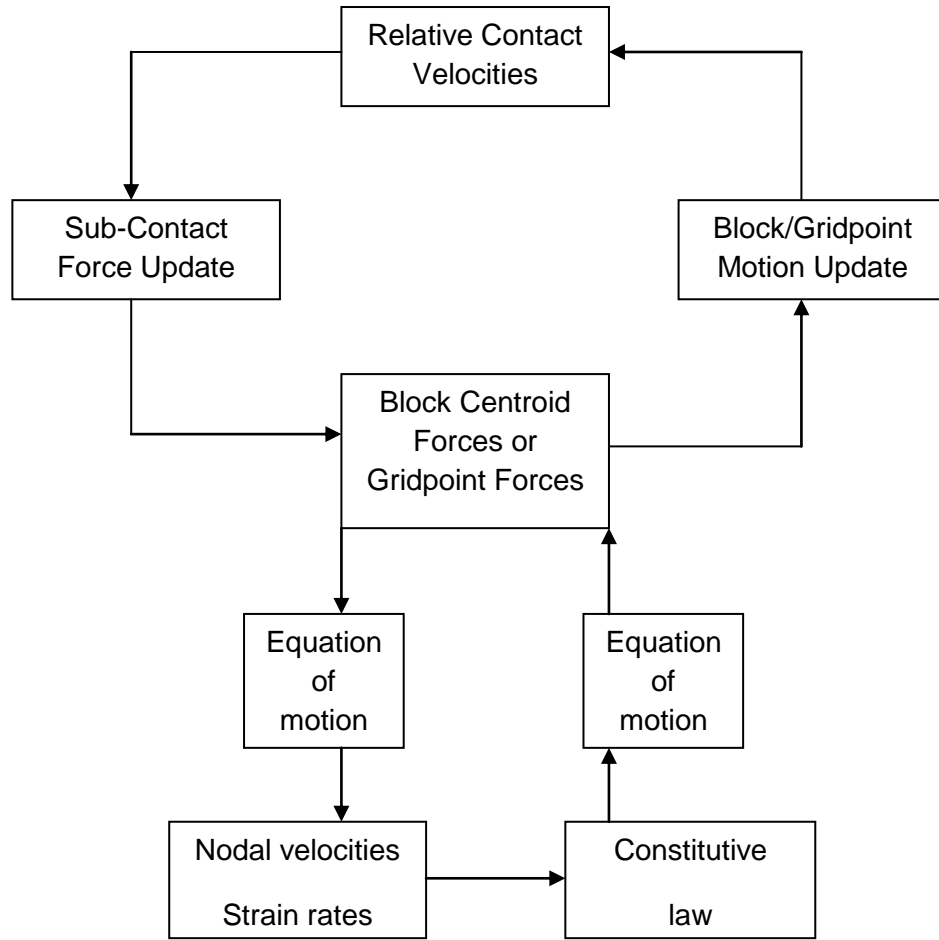


Figure 3.1 The calculation cycle of 3DEC program (Anon, 2007)

The force increments are found by using displacement increment and the input discontinuity stiffness. The normal force increment  $\Delta F^n$  is found as;

$$\Delta F^n = -K_n \Delta V^i A_c \quad (3.1)$$

And the shear force increment is found as;

$$\Delta F^s = -K_s \Delta \delta A_c \quad (3.2)$$

Where;

$\Delta V^i$  = Normal displacement increment

$A_c$  = Area of contact

$\Delta\delta$  = Shear displacement increment

The total normal and shear forces,  $F^n$  and  $F^s$  are then updated for the next cycle as;

$$F^n = F^n + \Delta F^n \quad (3.3)$$

And,

$$F^s = F^s + \Delta F^s \quad (3.4)$$

For tensile failure;

$$F^n < T_{\max}, \text{ then } F^n = T_{\text{residual}} \quad (3.5)$$

Where;

$$T_{\max} = -T A_c \quad (3.6)$$

$$T_{\text{residual}} = -T_{\text{residual}} A_c \quad (3.7)$$

$T_{\max}$  = Peak tensile strength

$T_{\text{residual}}$  = Residual tensile strength

For shear failure;

$$F^s < F_{\max}^s, \text{ then } F^s = F^s \left( \frac{F_{\max}^s}{F^s} \right) \quad (3.8)$$

Where;

$$F_{\max}^s = c A_c + F^n \tan \phi \quad (3.9)$$

Shear displacement leads to a dilation that is;

$$\Delta V(\text{dil}) = \Delta\delta \tan(d) \quad (3.10)$$

Where  $d$  is the dilation angle specified.

Then the normal force is corrected to consider the effect of dilation as;

$$F^n = F^n + K_n A_c \Delta \delta \tan(d) \quad (3.11)$$

The second constitutive model of 3DEC for discontinuities is the continuously yielding joint model. The model attempts to account for some nonlinear behavior observed in physical tests. The model generates the discontinuity shearing damage, normal stiffness dependence and decrease in dilation angle with plastic shear displacement.

The normal stress is found incrementally as;

$$\Delta \sigma_n = K_n \Delta V^i \quad (3.12)$$

Where the normal stiffness  $K_n$  is given by;

$$K_n = a_n \sigma_n^{e_n} \quad (3.13)$$

Where  $a_n$  and  $e_n$  are model input parameters

For shear loading, the shear stress increments calculated as;

$$\Delta \tau = F k_s \Delta \delta \quad (3.14)$$

Where the shear stiffness  $K_s$  is given by;

$$K_s = a_s \sigma_n^{e_s} \quad (3.15)$$

And where  $e_s$  and  $a_s$  are model input parameters and  $F$  is the tangent modulus factor which depends on the distance from the actual stress curve to the target or bounding strength;

$$F = \frac{(1 - T/T_m)}{1 - r} \quad (3.16)$$

Where;

$r$  is the stress ratio at the last reversal and it is limited to 0.75 in order to avoid numerical noise.

$\tau_m$  is the bounding strength and found as;

$$\tau_m = \sigma_n \tan \phi_m \Delta \delta \quad (3.17)$$

$\phi_m$  is the friction angle at which the discontinuity is dilating at the maximum dilation angle and it is continuously reduced according to the equation;

$$\Delta \phi_m = -\frac{1}{R} (\phi_m - \phi) \Delta \delta^p \quad (3.18)$$

$R$  is the model input parameter defines the surface roughness,

The plastic increment  $\Delta \delta^p$  is found as;

$$\Delta \delta^p = (1-F) |\Delta \delta| \quad (3.19)$$

Studies related to 3DEC were mostly conducted by Coulomb slip model rather than continuously yielding joint model (Kulatilake et al. 1993, Konietzky et al. 2001, Hutri and Antikainen 2002, Corkum and Martin 2004). The main reason is the easiness of the parameter determination. Only the discontinuity cohesion and discontinuity friction angle should be determined for the Coulomb slip model.

### 3.2 Reliability Index Methods

In these methods the safety of a slope is measured by a reliability index, rather than the classical safety factor. Engineering reliability problems can generally be reduced to comparison of demand and supply in meeting a specified performance requirement. For example, the safety of a structure depends on the strength of the structure, (supply) and the applied load (demand) (Düzgün et al. 2003). The calculation of probability of survival or

failure, requires the knowledge of the distribution of supply, denoted by  $f_X(x)$ , and demand, denoted by  $f_Y(y)$  or their joint distribution  $f_{XY}(x,y)$ , if  $X$  and  $Y$  are correlated. In practice, however, it is difficult to assess these distributions due to insufficient data. Moreover, even if the required distributions are available, the exact evaluation of probabilities is impractical due to the numerical integrations involved (Düzgün and Özdemir 2006).

Frequently, the available information and data are sufficient only to calculate the first and second moments, in other words the means, the variances and the covariances of the respective random variables. In such cases, practical measure of safety or reliability is limited to functions of these first two moments (Düzgün and Özdemir 2006).

Two similar procedures are used for the computation of the reliability index. These are the first-order second-moment (FOSM) and advanced first-order second-moment (AFOSM) methods. In both methods, random variables are described only by their first and second statistical moments (i.e. mean, variance and correlation characteristics).

Although these two methods have been proposed long time ago, their application to rock slope stability is quite recent. Genske and Walz (1991), Kimmance and Howe (1991), Muralha (1991), Trunk (1993) applied FOSM method to rock slopes. Slope stability studies using AFOSM method in rock engineering are very few. However, the more recent probabilistic slope stability studies prefer this method (Düzgün et al., 1994, Düzgün et al., 1995, Quek and Leung, 1995, Chen et al., 1998) since it is free from some of the disadvantages of previously mentioned methods (Ang and Tang, 1984).

The formulation of a performance function (failure function) or a limit state equation is the first step in both methods, and is explained in the following section.

### 3.2.1 The Performance Function

The reliability assessment of an engineering structure usually involves the consideration of many variables. In particular, the supply and demand generally depend on several other variables. In FOSM approach, the reliability index,  $P$ , is similar to the safety factor used in the deterministic analysis. It gives the mean safety margin in multiples of the standard deviation of the safety margin. The mean safety margin is the mean difference between the mean capacity and the mean demand. The higher this difference, the higher is the value indicating a higher safety. It is to be noted that this difference is normalized with respect to the standard deviation of the safety margin. Accordingly, the uncertainties in demand and capacity are also reflected in the reliability index (Duzgun et al. 1995).

For the purpose of generalized formulation, it is necessary to define a performance function or a state function as shown below:

$$g(x) = g(x_1, x_2, x_3, \dots, x_n) \quad (3.20)$$

Where,  $\{X\} = \{X_1, X_2, X_3, \dots, X_n\}$  is the vector of basic variables which are involved in the physical problem such as strength, load and geometrical parameters. The function  $g(x)$  determines the performance or state of the structure. Accordingly, the limiting performance is defined as  $g(x) = 0$  which is the "limit-state" of the system. As a result it follows that:

$g(x) > 0$     The "safe state"

$g(x) < 0$     The "failure state"

Geometrically, the limit state equation,  $g(x) = 0$ , forms an  $n$ -dimensional surface which is called as the "failure surface ". One side of the failure surface is called the safe state,  $g(x) > 0$ ; while the other side  $g(x) < 0$  is

the failure state. Figure 3.2 illustrates the safe and failure states for the two-dimensional case.

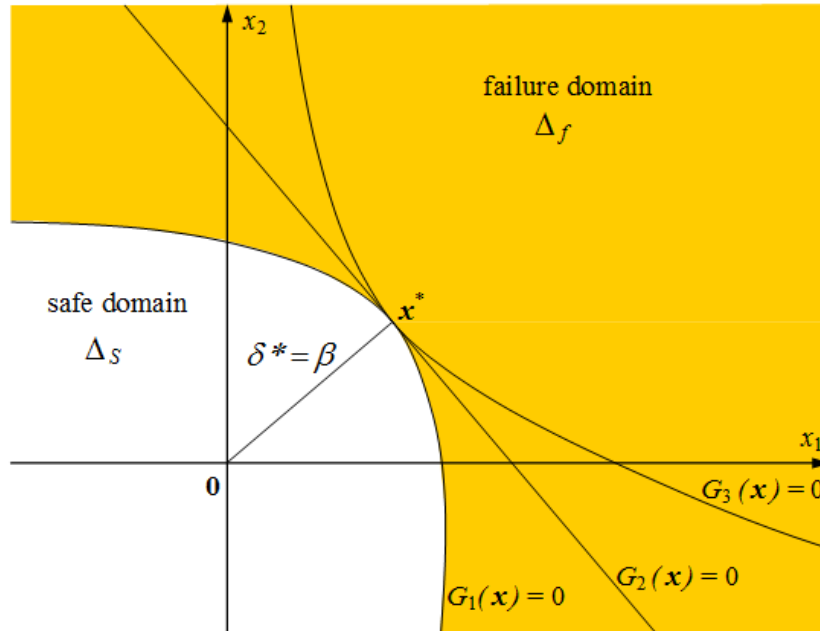


Figure 3.2 Safe and failure states for the variables  $x_1$  and  $x_2$

If the joint p.d.f. of the basic variables,  $X_1, X_2, X_3, \dots, X_n$  is  $f_{X_1, X_2, X_3, \dots, X_n}(X_1, X_2, X_3, \dots, X_n)$  the probability of safe state is

$$P_s = \iiint \dots \int_{g(x) > 0} f_{X_1, X_2, X_3, \dots, X_n}(X_1, X_2, X_3, \dots, X_n) dx_1 \dots dx_n \quad (3.21)$$

The above equation is simply the volume integral of  $f_x(x)$  over the safe region  $g(x) > 0$ . On the other hand, the failure state probability or  $p$  is the corresponding volume integral over the failure region  $g(x) < 0$ :

$$P_f = \iiint \dots \int_{g(x) < 0} f_{X_1, X_2, X_3, \dots, X_n}(X_1, X_2, X_3, \dots, X_n) dx_1 \dots dx_n \quad (3.22)$$

In FOSM modeling, mean and standard deviation of the limit state or performance function is found for any continuous mathematical form of the limit state equations. If the function is non-linear, the approximate first and second moments of the limit state function are obtained by Taylor series expansion of the function around the mean values of the basic variables ( $\mu$ ). This approximation is called as "mean point expansion method" and proposed by Cornell (1969). The linearized failure function is given as

$$z \approx g(\mu_1, \mu_2, \dots, \mu_n) + \sum_{i=1}^n (X_i - \mu_i) \left( \frac{\partial g}{\partial X_i} \right)_{\mu_i} \quad (3.23)$$

Where the vector  $\mu_i = (\mu_1, \mu_2, \mu_3, \dots, \mu_n)$  is the linearizing point. The reliability analysis is carried out according to the function  $z$ . The mean ( $\mu_z$ ) and standard deviation ( $\sigma_z$ ) of  $z$  is approximated by (Düzgün and Özdemir 2006):

$$\mu_z = g(\mu_1, \mu_2, \dots, \mu_n) \quad (3.24)$$

$$\sigma_z = \sqrt{\sum_{i=1}^n \left( \frac{\partial g}{\partial X_i} \right)_{\mu_i}^2} \sigma_i \quad (3.25)$$

The accuracy of the approximation depends on the degree of non-linearity, effect of neglecting higher order terms in failure function  $z$  and the magnitudes of coefficients of variation of  $x_i$ 's. It is obvious that if the function  $g(X_1, X_2, X_3, \dots, X_n)$  is linear then the approximation of the mean and the standard deviation of  $z$  is exact. In the FOSM method the reliability index  $\beta$  as defined by Cornell (1969) is  $\beta = \frac{\mu_z}{\sigma_z}$

The FOSM method which is based on the mean point expansion using Taylor series approximation has two basic shortcomings. First, the

performance (unction is linearized at the mean values of the basic variables. When performance junction is non-linear, significant errors may arise at increasing distances from the linearizing point by neglecting the higher order terms. Second, the Taylor series expansion around the mean values fails to be invariant under different but mechanically equivalent formulations of the same problem (Hasofer and Lind, 1974). In other words, it lacks the desirable property of being failure function invariant. Due to these shortcomings of the FOSM formulation, the AFOSM method proposed by Hasofer and Lind (1974) became the most widely used method of reliability determination. In the following sections the principles of AFOSM is explained in detail

### 3. 2. 2 Linear Performance Functions

The performance function may be a linear function. A linear performance function can be represented as

$$g(X) = a_0 + \sum_{i=1}^n a_i X_i \quad (3.26)$$

Where  $a_0$  and  $a_i$  are constants.

Here the variables are assumed to be uncorrelated and have a normal distribution. The reduced (standardized) variables are defined as follows:

$$a_0 + \sum_{i=1}^n a_i X_i = 0 \quad (3.27)$$

Here the variables are assumed to be uncorrected and have a normal distribution. The reduced (standardized) variables are defined as follows

$$X'_i = \frac{X_i - \mu_i}{\sigma_i} \quad (3.28)$$

Then

$$X_i = X'_i \sigma_i + \mu_i \quad (3.29)$$

$$a_0 + \sum_{i=1}^n a_i (X'_i \sigma_{X_i} + \mu_{X_i}) = 0 \quad (3.30)$$

For instance, for three dimensions the minimum distance of origin of reduced variates  $X'_i$  is:

$$\beta = \frac{a_0 + \sum_{i=1}^n a_i \mu_{X_i}}{\sqrt{\sum_{i=1}^n (a_i \sigma_{X_i})^2}} \quad (3.31)$$

Then, the following generalization can be made. If the random variables  $X_1, \dots, X_n$  are uncorrelated normal variate, the probability of being in the safe state is:

$$P_s = P\left(a_0 + \sum_{i=1}^n a_i (X'_i \sigma_{X_i} + \mu_{X_i}) > 0\right) \quad (3.32)$$

$$P_s = 1 - \Phi\left(\frac{-\left(a_0 + \sum_{i=1}^n a_i \mu_{X_i}\right)}{\sqrt{\sum_{i=1}^n (a_i \sigma_{X_i})^2}}\right) \quad (3.33)$$

$$= \Phi \left( \frac{a_0 + \sum_{i=1}^n a_i \mu_{X_i}}{\sqrt{\sum_{i=1}^n (a_i \sigma_{X_i})^2}} \right) \quad (3.34)$$

Where  $\Phi ( )$  is the cumulative distribution function (c.d.f.) of the standard normal variate. As observed the probability  $P_s$  is a function of the distance from the failure plane  $g(x) = 0$  to the origin of the reduced variates. Hence, in the general case of  $n$  uncorrelated normal variates the probability of being in the safe state  $P_s = \Phi (\beta)$  and the probability of failure is  $P_f = 1 - \Phi (\beta)$ .

### 3.2.3 Non-Linear Performance Functions

Generally, the performance functions are non-linear. Accordingly, the limit state equation  $g (X) = 0$  will also be non-linear. Unlike the linear case, there is no unique distance from the failure surface to the origin of the reduced variates. However, Shinozuka (1983) identified the point  $(X_1^*, \dots, X_n^*)$  on the failure surface with minimum distance to the origin of the reduced variates as the most probable failure point. Hence, the tangent plane to the failure surface at  $(X_1^*, \dots, X_n^*)$  can be used to approximate the actual failure surface and to evaluate the reliability index. The tangent plane at  $(X_1^*, \dots, X_n^*)$  is

$$\sum (X_i' - X_i^*) \left( \frac{\partial g}{\partial X_i'} \right)^* = 0 \quad (3.35)$$

In which the partial derivatives  $\left( \frac{\partial g}{\partial X_i'} \right)^*$ .

Thus, the minimum distance from the tangent plane to the origin of the reduced variates is taken as the reliability index  $\beta$ . This is illustrated in Figure 4.1 for the two-variable case. This minimum distance to tangent plane on the failure surface can be determined through the Lagrange multiplier method as explained by Tang (1984). The following summarizes this numerical procedure, which is an iterative algorithm for calculating the reliability index  $\beta$ , (Ang and Tang, 1984):

- i. Define the appropriate limit-state function.
- ii. Make an initial guess of the reliability index  $\beta$ .
- iii. Set the initial checking point values  $x_i^* = \mu_i$  for all  $i = 1, \dots, n$ .
- iv. Compute the mean and the standard deviation of the equivalent normal distributions for those variables that are non-normal
- v. Obtain reduced variates as  $X_i^* = \frac{X_i^* - \mu_i}{\sigma_{X_i}}$ .
- vi. Evaluate  $\left(\frac{\partial g}{\partial X_i}\right)^*$  at  $X_i^*$ .
- vii. Compute the direction cosines  $\alpha_i$  as

$$\alpha_i = \frac{\left(\frac{\partial g}{\partial X_i}\right)^*}{\sqrt{\sum_{i=1}^n \left(\frac{\partial g}{\partial X_i}\right)^{*2}}} \quad (3.36)$$

- viii. Calculate new values of  $X_i^*$  from  $X_i^* = \mu_i - \alpha_i \beta \sigma_i'$
- ix. ix. Substitute above  $X_i^*$  in  $g(X_1^*, \dots, X_n^*) = 0$  and solve for  $\beta$
- x. Using  $\beta$  obtained in step ix, re-evaluate  $X_i^* = -\alpha_i \beta$
- xi. Repeat step v through x until convergence is reached.

### 3.2.4 Equivalent Normal Distributions

If the probability distributions of the random variables  $X_1, \dots, X_n$  are not normal, the probability  $P_f$  and  $P_s$  can also be calculated. The equivalent normal distribution for a non-normal variate can be obtained in such a way that the cumulative probability as well as the probability density ordinate of the equivalent normal distribution are equal to those of the corresponding non-normal distribution at the design point  $X_i^*$  (Ang and Tang, 1984). Accordingly the following can be obtained:

$$\Phi\left(\frac{X_i^* - \mu_{X_i}^N}{\sigma_{X_i}^N}\right) = F_{X_i}(X_i^*) \quad (3.37)$$

Where;

$\mu_{X_i}^N, \sigma_{X_i}^N$  = The mean value and the standard deviation, respectively, of the equivalent normal distribution of  $X_i$ .

$F_{X_i}(X_i^*)$  = The original cumulative density function (c.d.f) of  $X_i$ , evaluated at  $X_i^*$ .

$\Phi(\cdot)$  = The c.d.f. of the standard normal distribution

From Eq. 3.37 it is obtained:

$$\mu_{X_i}^* = X_i^* - \sigma_{X_i}^N \Phi^{-1}\left[F_{X_i}(X_i^*)\right] \quad (3.38)$$

On the other hand, equating the corresponding probability density functions at  $X_i^*$  yields to:

$$\frac{1}{\sigma_{X_i}^N} \phi\left(\frac{X_i^* - \mu_{X_i}^N}{\sigma_{X_i}^N}\right) = f_{X_i}(X_i^*) \quad (3.39)$$

Where,  $\phi(\ )$  is the probability density function (p d f.) of the standard normal variable. From this it can be obtained

$$\sigma_{X_i}^N = \frac{\phi\{\Phi^{-1}(F_{X_i}(X_i^*))\}}{f_{X_i}(X_i^*)} \quad (3.40)$$

For a linear performance function, the appropriate point on the failure surface can be given in terms of direction cosines,  $\alpha_i$ , and safety index,  $\beta$ , in the following way:

$$\alpha_i = \frac{a_0}{\sqrt{\sum_{i=1}^n (a_i)^2}} \quad (3.41)$$

$$\beta = \frac{a_0 + \sum_{i=1}^n a_i \mu_{X_i}^N}{\sqrt{\sum_{i=1}^n (a_i \sigma_{X_i}^N)^2}} \quad (3.42)$$

Where the superscript N denotes the statistics for the equivalent normal distribution.

Accordingly, the design point is:

$$X_i^* = \sigma_{X_i}^N \alpha_i \beta + \mu_{X_i}^N = \alpha_i \beta \sigma_{X_i}^N + \mu_{X_i}^N \quad (3.43)$$

It is obvious that replacing the actual distribution with an equivalent normal distribution requires replacing the actual mean and the standard deviation with those of the equivalent normal distribution. The safety index  $\beta$  and the probabilities  $P_s$  and  $P_f$  are then calculated in terms of the mean and standard deviation of the equivalent normal distribution.

## CHAPTER IV

### THE DEVELOPED NUMERICAL-PROBABILISTIC APPROACH

#### 4.1 Methodology

In probabilistic modeling of rock slopes, the performance function is constructed based on the ratio of strength to the stress acting over rock discontinuity. Therefore, for calculating the Reliability Index ( $\beta$ ) and consequently the failure probability, the procedure discussed in section 3.2 of Chapter III is used.

However, the displacement of the structure is an important parameter that controls the stability of the structures. Limit equilibrium methods does not have the capability to obtain the displacement of rock mass; therefore, the numerical methods are required.

For analyzing the stability of rock slopes, different numerical methods are applied, however, the commonly acceptable method for discontinuous rock slopes is Distinct Element Method. The main output of the DEM is the displacement of blocks. Hence, the shear strain or shear displacement of rock discontinuities is considered as the failure indicator in this study. The flowchart in Figure 4.1 indicates the process for development of the proposed probabilistic numerical approach for analyzing of rock slope stability.

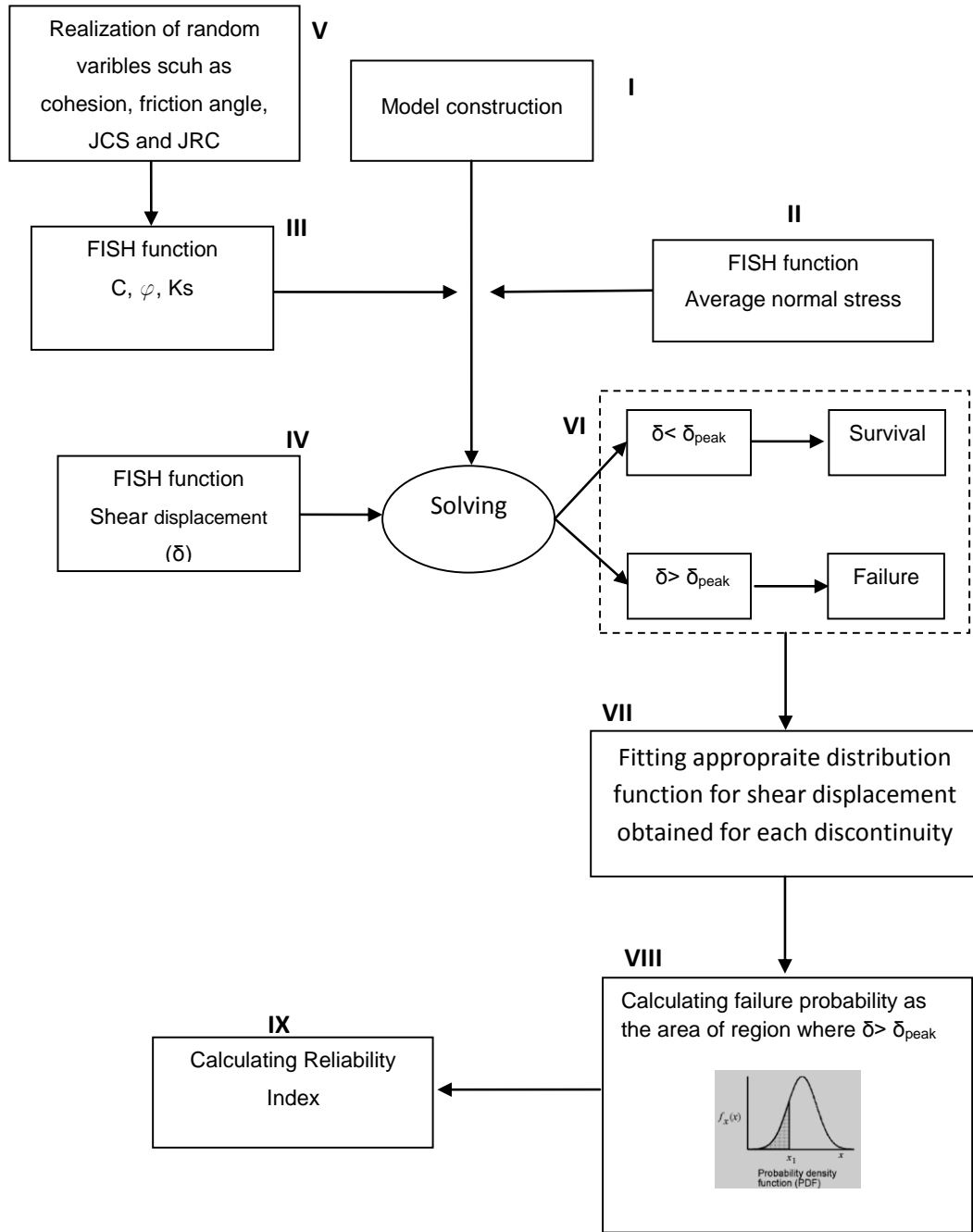


Figure 4.1 The process of development of proposed probabilistic numerical approach

As seen in Figure 4.1, there are different stages that should be followed in application of the proposed approach for a rock slope. The stages are described in detail as below:

- **Model construction (I)**

As indicated in Figure 4.1, the first step is to construct the geometry of slope in 3DEC. For this purpose, the shape of the slope is surveyed then constructed in the software and the rock discontinuities are added. The constructed shape must be meshed by using different zoning commands available in the software. The other step is to define the boundary condition which is dependent on geometry of the rock slope. In discontinuous media, the model has two separate components which are blocks and the contact face between blocks. Both of these components are given material properties based on the obtained data in the laboratory and the field. In most of the cases when the stress level is low the failure occurs in discontinuities rather than intact rock body. Therefore, the intact rock is modeled elastically for the sake of simplicity. However, the rock discontinuities are modeled plastically. To calculate and assign the material properties of the rock discontinuities the stage II and III are followed.

- **Discontinuity material properties calculations and their assignment (II and III)**

As indicated in Figure 4.1, in stages II and III FISH functions were written to calculate the rock discontinuity material properties and to assign to the model. In the proposed methodology, the Barton models discussed in Chapter II are used to model the rock discontinuities. The Barton model does not include as material model in 3DEC library; therefore, the Barton model should be applied indirectly to the model. Barton suggested instantaneous cohesion and friction angle concepts by which the nonlinear behavior of normal and shear stress ( $\tau$ - $\sigma_n$ ) relation can be equalized by drawing tangents to the  $\tau$ - $\sigma_n$  curve for defined  $\sigma_n$  values. Figure 4.2 shows the concept of instantaneous cohesion and friction

angle. The instantaneous cohesion and friction angle are obtained from Eqs. 4.1 to 4.3:

$$\frac{\partial \tau}{\partial \sigma_n} = \tan \left( JRC \log_{10} \frac{JCS}{\sigma_n} + \phi_b \right) - \frac{\pi JRC}{180 \ln 10} \left[ \tan^2 \left( JRC \log_{10} \frac{JCS}{\sigma_n} + \phi_b \right) + 1 \right] \quad (4.1)$$

$$\phi_i = \arctan \left( \frac{\partial \tau}{\partial \sigma_n} \right) \quad (4.2)$$

$$c_i = \tau - \sigma_n \tan \phi_i \quad (4.3)$$

By applying Eqs. 4.1, 4.2 and 4.3 the relevant cohesion and friction angle for a definite stress level and consequently for any discontinuity are calculated. Therefore, the calculated values for cohesion and friction angle are applied by using Coulomb slip model. The joint material parameters required to apply Coulomb slip are Joint Normal Stiffness (kn), Joint Shear Stiffness (ks), Friction Angle (Jfriction), Cohesion (Jcohesion), Joint Tensile Strength (Jten) and Dilatancy Angle (dil).

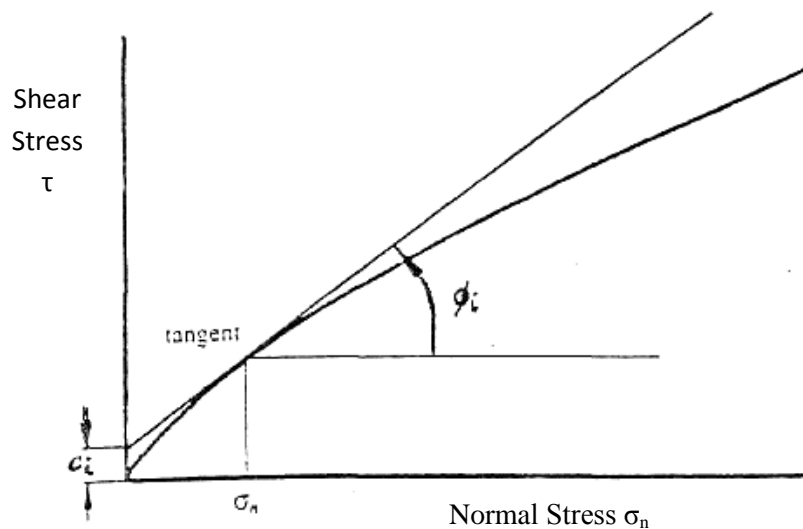


Figure 4.2 Barton model and the instantaneous cohesion and friction concepts

According to Eqs. 4.2 and 4.3, both the cohesion and friction angle are function of normal stress applied on discontinuity surface. Therefore, a FISH function was written to calculate the average normal stress on each plane. It is to be noted that the FISH is a programming language embedded within 3DEC that enables the user to define new variables and functions. These functions may be used to extend 3DEC's usefulness or add user defined features. An example of the FISH function written is as below for one discontinuity:

```

Def av_str1
  whilestepping
    nstav1 = 0
    Are1=0
    ic1 = c_near(x1, y1, z1)
    icsub1 = c_cx(ic1)
    Loop while icsub1 # 0
      ncono1 = ncono1 + 1
      Are1=Are1 + cx_area(icsub1)
      nstav1 = nstav1 +cx_nforce (icsub1)
      icsub1 = cx_next(icsub1)
    Endloop
    If ncono1 # 0
      nstav1 = nstav1 / Are1
    Endif
end

```

In this function, for any discontinuity, the normal force and the area (Are<sub>1</sub>) of contact and the average normal stress (nstav<sub>1</sub>) are calculated and saved to be used in calculation of cohesion and friction angle. The ic<sub>1</sub>, icsub1 and (x<sub>1</sub>, y<sub>1</sub>, z<sub>1</sub>) are related to the ID and the coordinate of location of discontinuity in 3DEC.

The failure criterion in this methodology is shear displacement; and the Joint Shear Stiffness ( $k_s$ ) is one of the most important factors that directly controls the shear displacement. According to the Eq. 2.17 the  $K_s$  is dependent on normal stress, length, JRC, JCS and basic friction angle of any discontinuity. As discussed in Chapter II, the Eq. 2.17 is not a suitable formula to calculate the  $K_s$  for analysis being done by 3DEC. For this purpose, Eq. 2.19 is used which is the ratio of Eq. 2.3, the Barton's empirical shear strength formula, to Eq. 2.21, the estimated peak shear displacement value.

In 3DEC the joint parameters must be assigned to relevant location or discontinuity. Commonly, the models are complex and the material properties should be assigned by FISH coding. One sample of written FISH for calculating and assigning the joint parameters is as below:

Def prop<sub>1</sub>

Fi (basic friction angle)

L<sub>1</sub> (discontinuity length)

JCS (Joint Compressive Strength)

JRC (Joint Roughness Coefficient)

$$\text{fric\_1} = \text{abs}((180/\pi) * \text{atan}(\text{abs}(\tan(\text{degrad} * (\text{JRC} * \log(\text{abs}(\text{jcs}/\text{nstav}_1)) + \text{Fi})))) * \text{degrad} * \text{JRC} * (1/\ln(10)) * ((\tan(\text{degrad} * (\text{JRC} * \log(\text{abs}(\text{jcs}/\text{nstav}_1)) + \text{Fi}))^2 + 1)))$$

$$\text{coh\_1} = \text{nstav}_1 * \text{abs}(\tan(\text{degrad} * (\text{JRC} * \log(\text{abs}(\text{jcs}/\text{nstav}_1)) + \text{Fi}))) * \text{nstav}_1 * \text{abs}(\tan(\text{degrad} * \text{fric\_1}))$$

$$\text{d\_peak1} = (\text{L1} * (\text{JRC}/\text{L1})^{0.33}) / 500$$

$$\text{J\_ks\_1} = ((\text{coh\_14}) + \text{abs}(\text{NS11} * \tan(\text{degrad} * \text{fric\_14}))) / (\text{L1} * (\text{JRC}/\text{L1})^{0.33})$$

```
ic1=c_near(34.43,57.22,80.4)
End
```

```
Hide dip 87 dd 180 org 0 61 20 below
Hide dip 75 dd 288 org 14.8 46.9 40 above
Hide range z 0 65
Change jmat=1
```

- **Recording the shear displacement (IV)**

As indicated in Figure 4.1, the fourth stage in this methodology is to record the history of displacement of discontinuities during shearing which is the failure indicator in the proposed methodology. For this purpose, another FISH function was written to obtain the shear displacement of the discontinuity as below:

```
whilestepping
  ncono1= 0
  xsd1=0
  ysd1=0
  zsd1=0
  ic1= c_near(x1,y1, z1)
  icsub1 = c_cx(ic1)
  Loop while icsub1 # 0
    ncono1= ncono1 + 1
    ssdisp1 = cx_sdis(icsub1)
  xsd1= xsd2+ xcomp(ssdisp1)
    ysd1= ysd2+ ycomp(ssdisp1)
    zsd1= zsd2+ zcomp(ssdisp1)
    icsub1 = cx_next(icsub1)
  Endloop
  If ncono1 # 0
Sheardisp1 = sqrt((xsd1)^2+(ysd1)^2+(zsd1)^2) / ncono1
```

Endif

In this function, the `ssdisp1` is the shear displacement vector and the `xsd1`, `ysd1` and `zsd1` are its components and the `Sheardisp1` is the final shear displacement scalar. From the beginning up to the end of the solution, the shear displacement of a discontinuity with ID of `ic1` is recorded and can be plotted if necessary. After, the model is executed and the equilibrium state is reached the final shear displacement of the discontinuity is obtained.

- **Stages V, VI, VII, VIII and IX**

As indicated in Figure 4.1, the processes of stages from I to IV should be followed to prepare the model to be executed. In stage V, the realization of random variables are selected from their distribution and input to the model. These variables are transformed to rock discontinuity properties using FISH function discussed in stage II and III of the methodology in Figure 4.1, such as instantaneous cohesion and friction angle,  $K_s$  and etc. Then the model is executed and the shear displacement ( $\delta$ ) of each discontinuity is recorded as described in stage IV. According to Figure 4.1, in stage VI, the shear displacement obtained in stage IV is compared to the peak shear displacement estimated by Eq. 2.21. In the proposed methodology, it is assumed that if the shear displacement is greater than the estimated peak shear displacement ( $\delta_{peak}$ ) it is called as failure. The boundary of the failure and survival is called the limit state condition in the proposed approach. For example, if for certain realization of cohesion, JCS and friction angle for  $JRC=10$  the shear displacement ( $\delta$ ) is greater than the estimated peak shear displacement ( $\delta_{peak}$ ) and for  $JRC=11$  the  $\delta$  is lower than  $\delta_{peak}$ , the  $10 < JRC < 11$  is considered as limit state condition depending on the opinion of the user.

This methodology was developed for one or more random variables. For one random variable like JRC, suppose that the limit state is  $JRC=10$ , and the discontinuity fails for  $JRC<10$ . Therefore, the probability of failure equals to the area of region less than 10 in density function of distribution of JRC.

However, when the number of random variables is more than one, for different realization of random variables the model is run and the shear displacement of each discontinuity is recorded and according to stage VI the failure state is obtained. Then an appropriate distribution function is fitted to the shear displacement. Then, area for which  $\delta > \delta_{peak}$  is the failure probability and the corresponding Reliability Index is obtained from  $P_f=1-\Phi(\beta)$ , Where  $\Phi()$  is the cumulative distribution function of the standard normal variate. (Stages VIII and IX).

## CHAPTER V

### IMPLEMENTATION OF PROPOSED PROBABILISTIC- NUMERICAL METHODOLOGY

#### 5.1 General information about the study region

The case study is selected as the Kings Rock Grave in Amasya, Turkey, which was carved on a rock mass containing bedding planes and joints and generally discontinuities. The host rock is limestone and discontinuities cut the Grave, and simply the rock grave can be considered as a rock slope. Figure 5.1 is shows the location of Amasya in map of Turkey.

Amasya is located between  $41^{\circ} 04' 54''$  - $40^{\circ} 16' 16''$  North Latitude and  $34^{\circ} 57' 06''$ - $36^{\circ} 31' 53''$  East Longitude in the Yesilirmak Valley of the Central Black Sea Region . The surface area of Amasya is  $5,701 \text{ km}^2$  and the population is 133,000, of which 74,000 live in the city and in surrounding towns and villages. The average altitude is 592 m. Amasya was a fortified city high on the cliffs above the river. It has a long history as provincial capital, a wealthy city producing kings and princes, artists, scientists, poets and thinkers, from the kings of Pontus, through Strabo the geographer, to many generations of the Ottoman imperial dynasty, and up to being the location of an important moment in the life of Ataturk. With its Ottoman period wooden houses and the tombs of the Pontus kings carved into the cliffs overhead, Amasya is attractive to visitors.

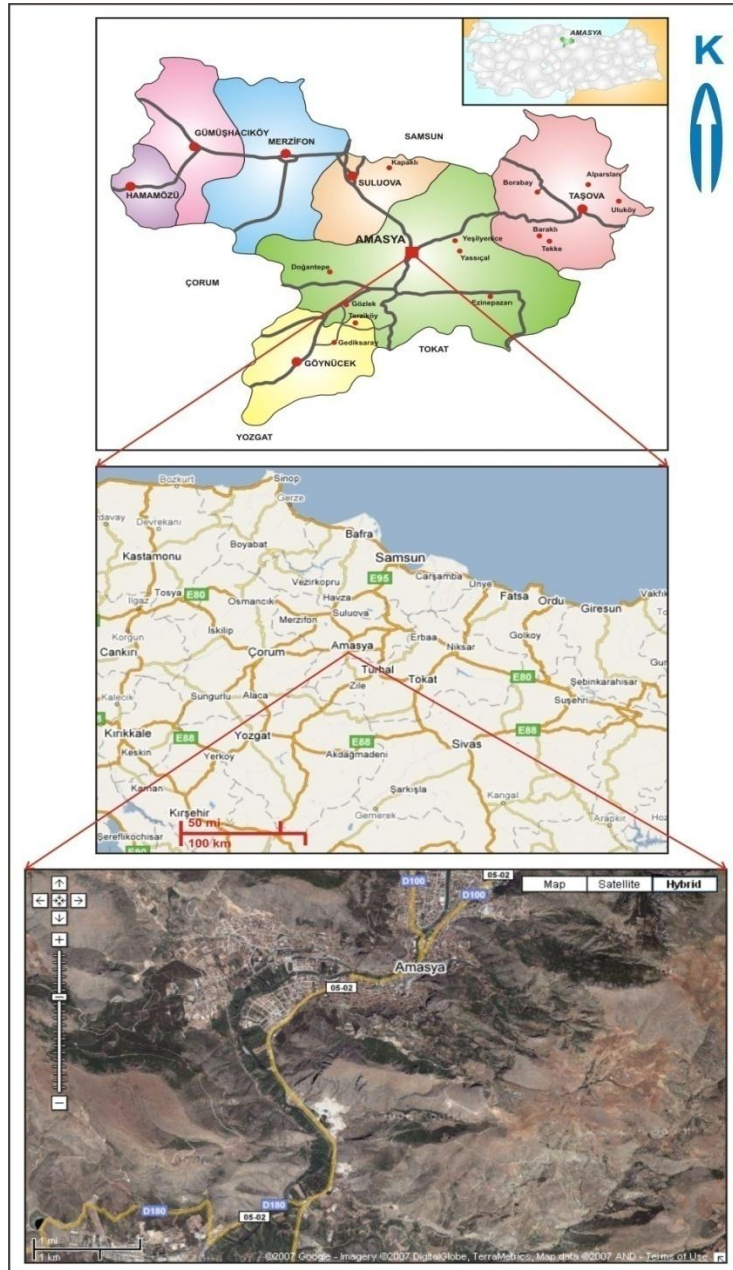


Figure 5.1 Location of Amasya

## 5.2 Field and laboratory studies

The Harsena Mountain was surveyed to understand the problem in the region. There are sliding, and rock fall problems in Harsena region. Figure 5.2 indicates the potential locations suffering from rock slope problem.

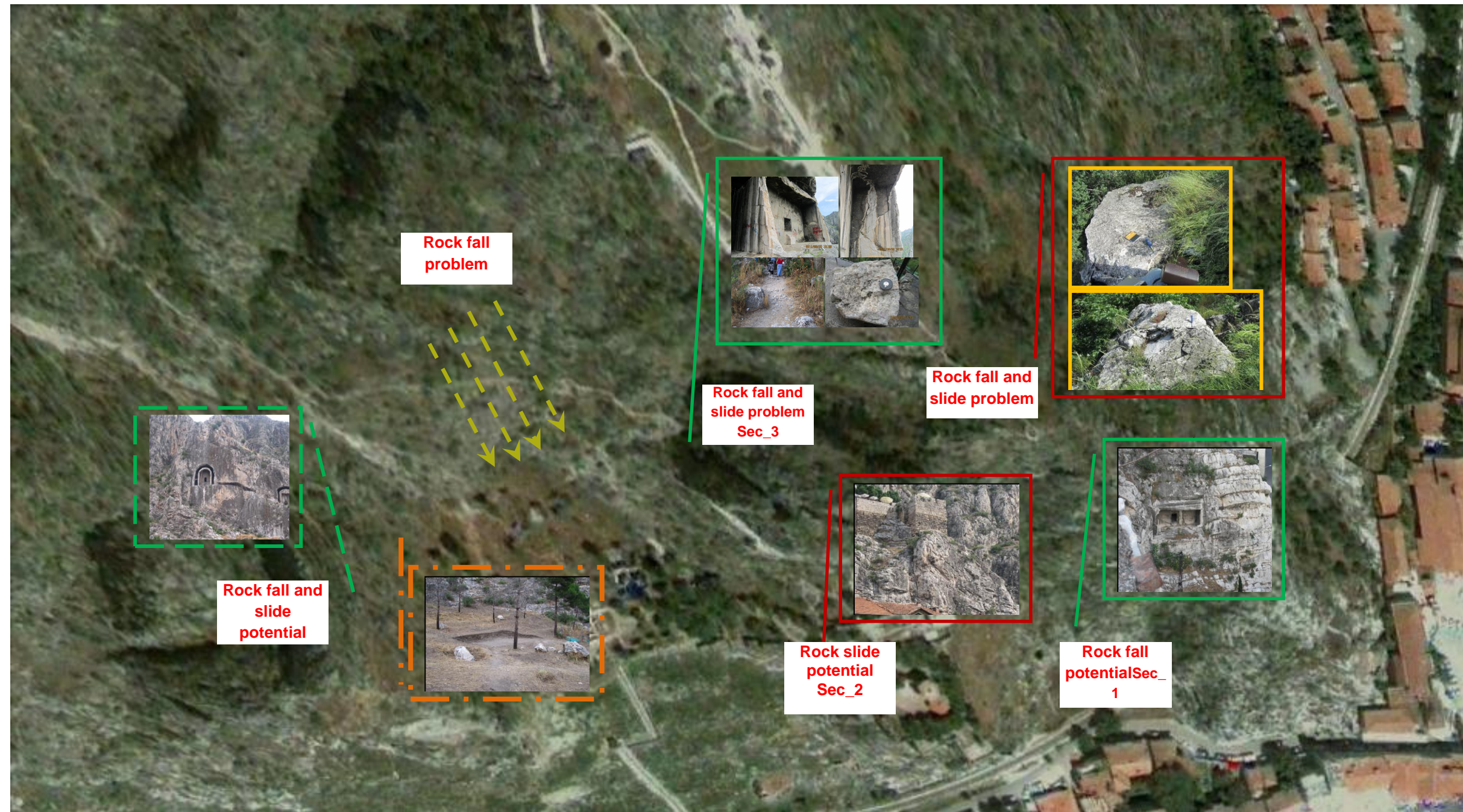


Figure 5.2 studied field ad failed structures and failure potential

The rock discontinuities were recorded by a compass either individually or massively by scan line. In joint mapping operation, geometrical parameters like, dip, dip direction, spacing and location of the joint and the mechanical parameters such as Joint Roughness Coefficient (JRC), Joint Wall Compressive Strength (JCS) for each joint were recorded. Tables 5.1 to 5.3 indicate the scanline data recorded in the field for different study regions. Figures 5.3to 5.6 indicate the rock joint distribution in the studied regions.

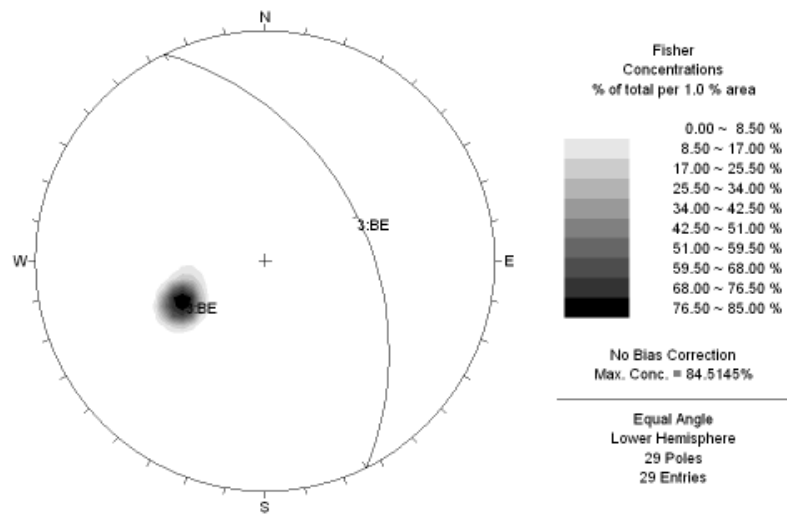


Figure 5.3 Bedding joints of sec\_1 on stereonet (064<sup>0</sup>/42<sup>0</sup>)

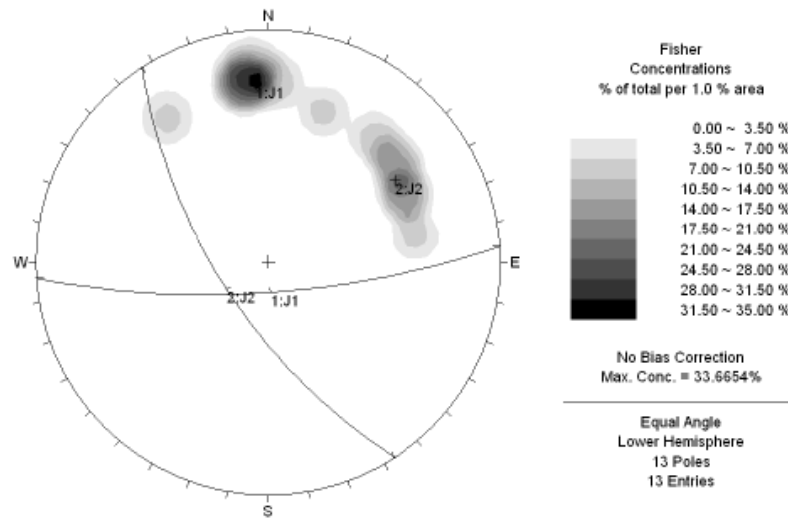


Figure 5.4 Joints in sec\_1 region in Amasya  $175^{\circ}/75^{\circ}$  and  $237^{\circ}/66^{\circ}$

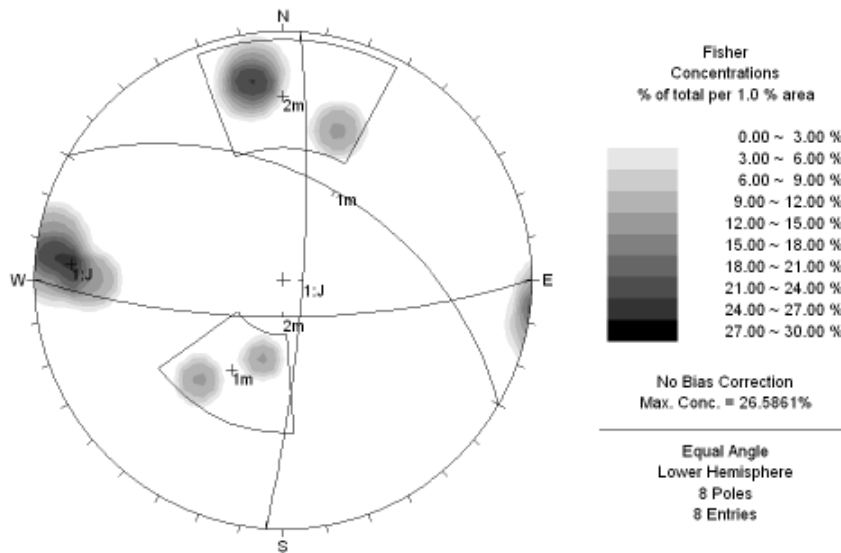


Figure 5.5 Joints in sec\_2 region in Amasya  $180^{\circ}/73^{\circ}$ ,  $094^{\circ}/81^{\circ}$  and  $030^{\circ}/45^{\circ}$

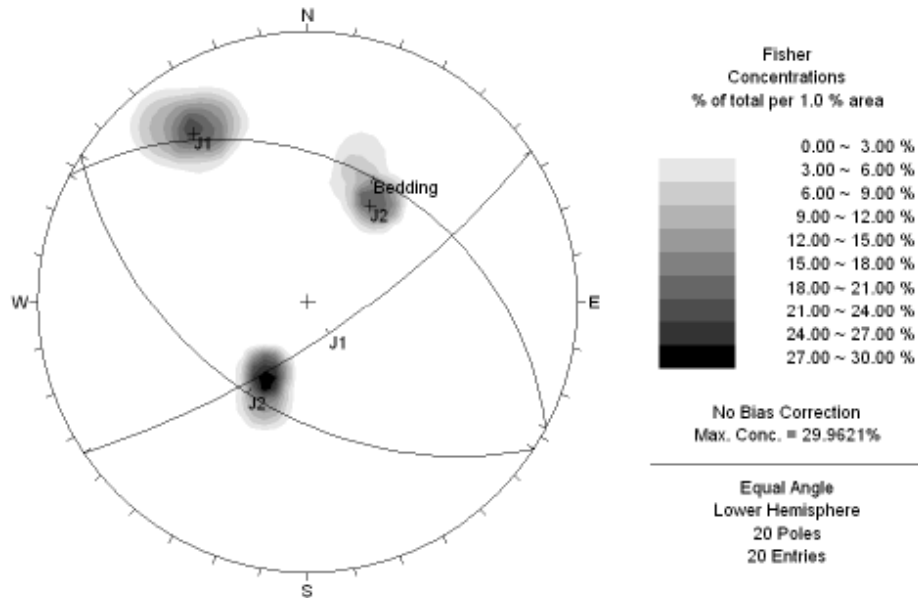


Figure 5.6 Joints in toe of sec\_3 region in Amasya  $146^{\circ}/74^{\circ}$ ,  $213^{\circ}/46^{\circ}$  and  $028^{\circ}/35^{\circ}$

Figures 5.3 to 5.6 indicate that there are almost three joint sets in each section. In section 1, the dominant joint sets have dip and dip direction of  $064^{\circ}/42^{\circ}$ ,  $175^{\circ}/75^{\circ}$  and  $237^{\circ}/66^{\circ}$ . Also, three joint sets of section 2 had orientations  $180^{\circ}/73^{\circ}$ ,  $094^{\circ}/81^{\circ}$  and  $030^{\circ}/45^{\circ}$ , and for section 3 the dip and dip direction of joint sets were recorded as  $146^{\circ}/74^{\circ}$ ,  $213^{\circ}/46^{\circ}$  and  $028^{\circ}/35^{\circ}$ .

Since the region is a folded structure, there are some differences between the dip and the direction of the joint sets. The direction of the joint sets is such a way that rock fall and rock sliding is probable.

Table 5.1 Recorded data of rock discontinuity from scanline for section 1

No.	Distance	Rock type	DIP DIRECTION	DIP	Discontinuity type	JRC	Schmidt Hammer value	Infilling	Thickness (mm)
1	210	Limestone	080 <sup>0</sup>	36 <sup>0</sup>	Bedding	-	26-38-42	-	-
2	242	Limestone	080 <sup>0</sup>	36 <sup>0</sup>	Bedding	-	34-26	Calcite	190
3	285	Limestone	072 <sup>0</sup>	40 <sup>0</sup>	Bedding	-	29	Calcite	5
4	340	Limestone	072 <sup>0</sup>	40 <sup>0</sup>	Bedding	-	34	-	-
5	520	Limestone	064 <sup>0</sup>	47 <sup>0</sup>	Bedding	-	27	Calcite	10
6	542	Limestone	064 <sup>0</sup>	47 <sup>0</sup>	Bedding	-	40	-	-
7	625	Limestone	055 <sup>0</sup>	40 <sup>0</sup>	Bedding	-	-	-	-
8	850	Limestone	062 <sup>0</sup>	45 <sup>0</sup>	Bedding	-	50-30	Calcite	30
9	1100	Limestone	060 <sup>0</sup>	52 <sup>0</sup>	Bedding	-	-	-	-
10	1150	Limestone	060 <sup>0</sup>	45 <sup>0</sup>	Bedding	-	18	-	-
11	1405	Limestone	062 <sup>0</sup>	45 <sup>0</sup>	Bedding	-	-	-	-
12	1440	Limestone	065 <sup>0</sup>	45 <sup>0</sup>	Bedding	-	-	-	-
13	1730	Limestone	062 <sup>0</sup>	40 <sup>0</sup>	Bedding	-	-	-	-
14	1820	Limestone	064 <sup>0</sup>	44 <sup>0</sup>	Bedding	-	48-34	Calcite	10
15	1930	Limestone	064 <sup>0</sup>	45 <sup>0</sup>	Bedding	-	-	-	-
16	1980	Limestone	064 <sup>0</sup>	44 <sup>0</sup>	Bedding	-	-	-	-
17	2040	Limestone	068 <sup>0</sup>	45 <sup>0</sup>	Bedding	-	-	-	-
18	2170	Limestone	062 <sup>0</sup>	45 <sup>0</sup>	Bedding	-	-	-	-
19	2225	Limestone	060 <sup>0</sup>	45 <sup>0</sup>	Bedding	-	-	-	-
20	2265	Limestone	064 <sup>0</sup>	44 <sup>0</sup>	Bedding	-	-	-	-

Continuing table 5.1

No.	Distance	Rock type	DIP DIRECTION	DIP	Discontinuity type	JRC	Schmidt Hammer value	Infilling	Thickness (mm)
21	2310	Limestone	062 <sup>0</sup>	43 <sup>0</sup>	Bedding	-	-	-	-
22	2375	Limestone	062 <sup>0</sup>	45 <sup>0</sup>	Bedding	-	-	-	-
23	2600	Limestone	065 <sup>0</sup>	40 <sup>0</sup>	Bedding	-	-	-	-
24	2670	Limestone	062 <sup>0</sup>	44 <sup>0</sup>	Bedding	-	-	-	-
25	2775	Limestone	062 <sup>0</sup>	45 <sup>0</sup>	Bedding	-	-	-	-
26	2825	Limestone	065 <sup>0</sup>	40 <sup>0</sup>	Bedding	-	-	-	-
27	2880	Limestone	062 <sup>0</sup>	44 <sup>0</sup>	Bedding	-	-	-	-
28	3000	Limestone	065 <sup>0</sup>	47 <sup>0</sup>	Bedding	-	-	-	-
There are also two joint sets that could not be recored directly by scanline which are 175 <sup>0</sup> /75 <sup>0</sup> and 237 <sup>0</sup> /66 <sup>0</sup>									

Table 5.2 Recorded data of rock discontinuity from scanline for section 2

No.	Distance	Rock type	DIP DIRECTION	DIP	Discontinuity type	JRC	Schmidt Hammer value	Infilling	Thickness (mm)
1	0	Limestone	015 <sup>0</sup>	36 <sup>0</sup>	Bedding	-	20-25-40	Calcite	5-10
2	400	Limestone	100 <sup>0</sup>	86 <sup>0</sup>	Joint	-	30-39	Calcite	20
3	400	Limestone	200 <sup>0</sup>	65 <sup>0</sup>	Joint	-	22—24-38	Calcite	20
4	1090	Limestone	040 <sup>0</sup>	55 <sup>0</sup>	Bedding	-	33-36-43	Calcite	20
5	1190	Limestone	093 <sup>0</sup>	85 <sup>0</sup>	Joint	-	43-38	Calcite	10
6	1640	Limestone	020 <sup>0</sup>	84 <sup>0</sup>	Joint	-	34-37-39	-	-
7	2410	Limestone	090 <sup>0</sup>	75 <sup>0</sup>	Joint	-	27-38-39-40	-	-
<p>There is a joint set parallel to surface which is 180<sup>0</sup>/73<sup>0</sup> with spacing of 1.5 m that could not be recorded in scanline</p>									

Table 5.3 Recorded data of rock discontinuity from scanline for toe of section 3

No.	Spacing (cm)	Rock type	DIP DIRECTION	DIP	Discontinuity type	JRC	Schmidt Hammer value	Infilling	Thickness (mm)
1	70	Limestone	31	32	Bedding	-	21-35-39	-	-
2	115	Limestone	31	32	Bedding	-	35	-	-
3	100	Limestone	142	80	Joint	-	-	Calcite	10
4	65	Limestone	20	45	Bedding	-	24	-	-
5	100	Limestone	152	72	Joint	-	20-21-40	Calcite	60
6	120	Limestone	148	75	Joint	-	-	-	-
7	100	Limestone	145	70	Joint	-	-	-	-
8	50	Limestone	25	40	Bedding	-	-	Calcite	30
9	90	Limestone	30	35	Bedding	-	-	-	-
10	90	Limestone	140	78	Joint	-	-	-	-
11	60	Limestone	28	33	Bedding	-	-	-	-
12	50	Limestone	33	34	Bedding	-	-	-	-
13	140	Limestone	153	74	Joint	-	-	-	-
14	60	Limestone	25	45	Bedding	-	-	Calcite	-
15	Were parallel to surface and spacing is ranging from 30 cm to 80 cm	Limestone	200	50	Joint	-	22-22-24-34-42-36	-	-
16		Limestone	200	60	Joint	-		-	-
17		Limestone	215	50	Joint	-		-	-
18		Limestone	215	50	Joint	-		-	-
19		Limestone	215	45	Joint	-		-	-
20		Limestone	215	47	Joint	-		-	-

Surface of the studied joints were drawn on paper and compared with standard profiles suggested by Barton and Choubey (1977) and rated (Figure 2.3). Table 5.4 indicates the statistical descriptions of gathered JRC values. Among the best fitting distributions to JRC value Lognormal distribution was found to be appropriate (Figure 5.7). Table A-1 indicates the goodness of fit obtained in Easyfit software for JRC value.

Table 5.4 Statistical analysis data for JRC

Statistic	Value	Percentile	Value
Sample Size	46	Min	2
Range	18	5%	3.35
Mean	9.1087	10%	4
Variance	21.966	25% (Q1)	6
Std. Deviation	4.6868	50% (Median)	8
Coef. of Variation	0.51454	75% (Q3)	11
Std. Error	0.69102	90%	16.3
Skewness	-0.80172	95%	18
Excess Kurtosis	-0.49338	Max	20

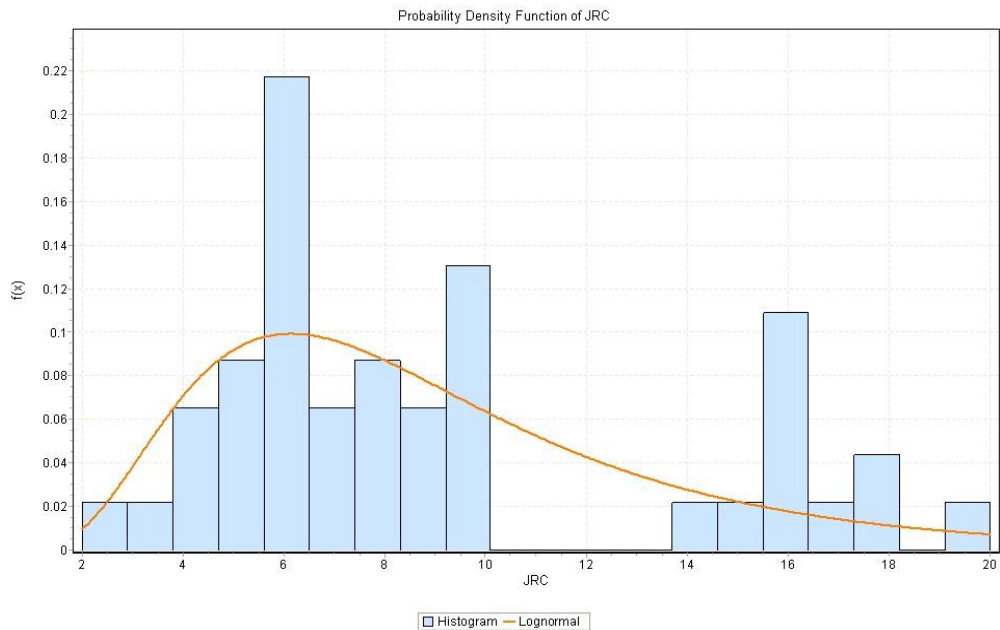


Figure 5.7 Lognormal distribution of joint roughness coefficient (JRC)

Also, joint compressive strength (JCS) values for discontinuity surfaces were obtained by Schmidt hammer. Table 5.5 indicates the distribution of

raw data for JCS, and Figure 5.8 indicates the frequency of joint wall compressive strength (Schmidt Hammer). The raw data obtained by Schmidt hammer are transformed to JCS by Figure 5.9 which integrates the hammer usage direction and density of the rock. Table A-1 indicates the goodness of fit obtained in Easyfit software for JRC value and the appropriate distribution was found to be Beta.

Table 5.5 Statistical data analysis for Schmidt Hammer

Statistic	Value	Percentile	Value
Sample Size	83	Min	8
Range	41	5%	16.4
Mean	32.181	10%	20
Variance	78.028	25% (Q1)	24
Std. Deviation	8.8333	50% (Median)	35
Coef. of Variation	0.27449	75% (Q3)	39
Std. Error	0.96959	90%	42
Skewness	-0.50298	95%	43
Excess Kurtosis	-0.51933	Max	49

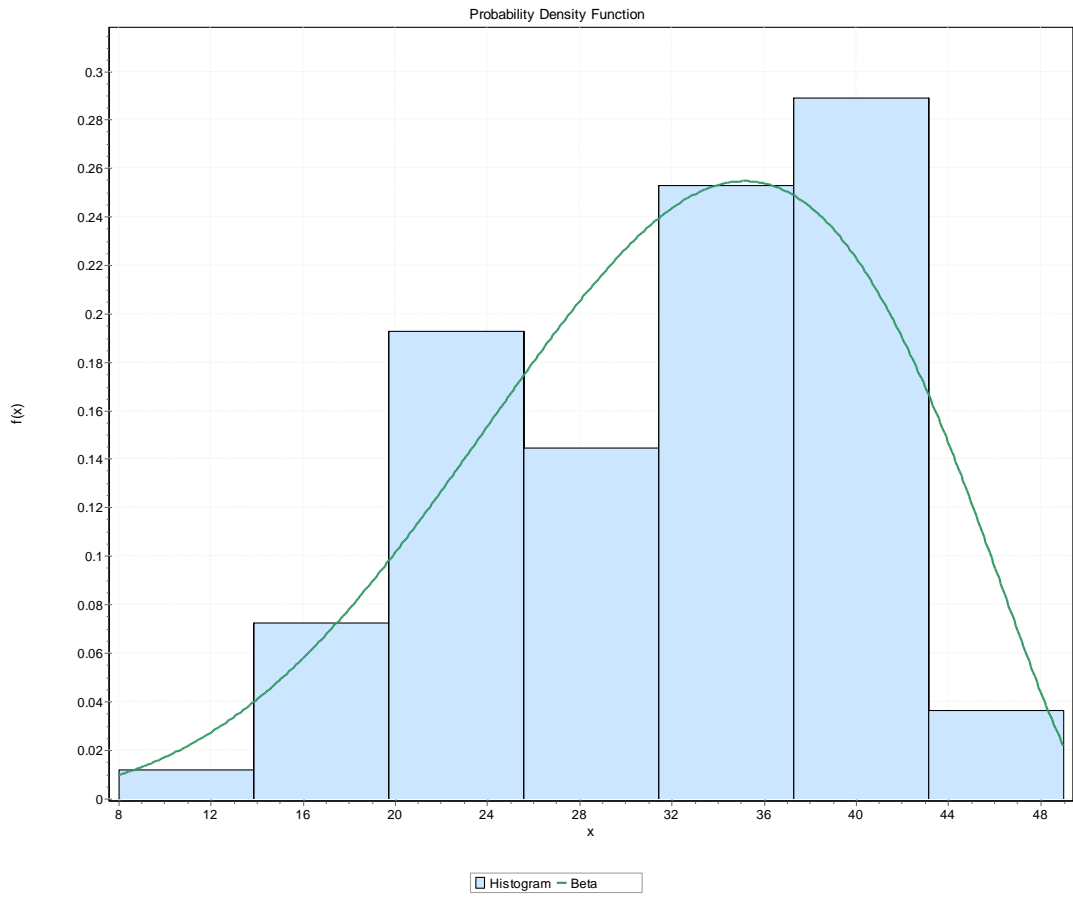
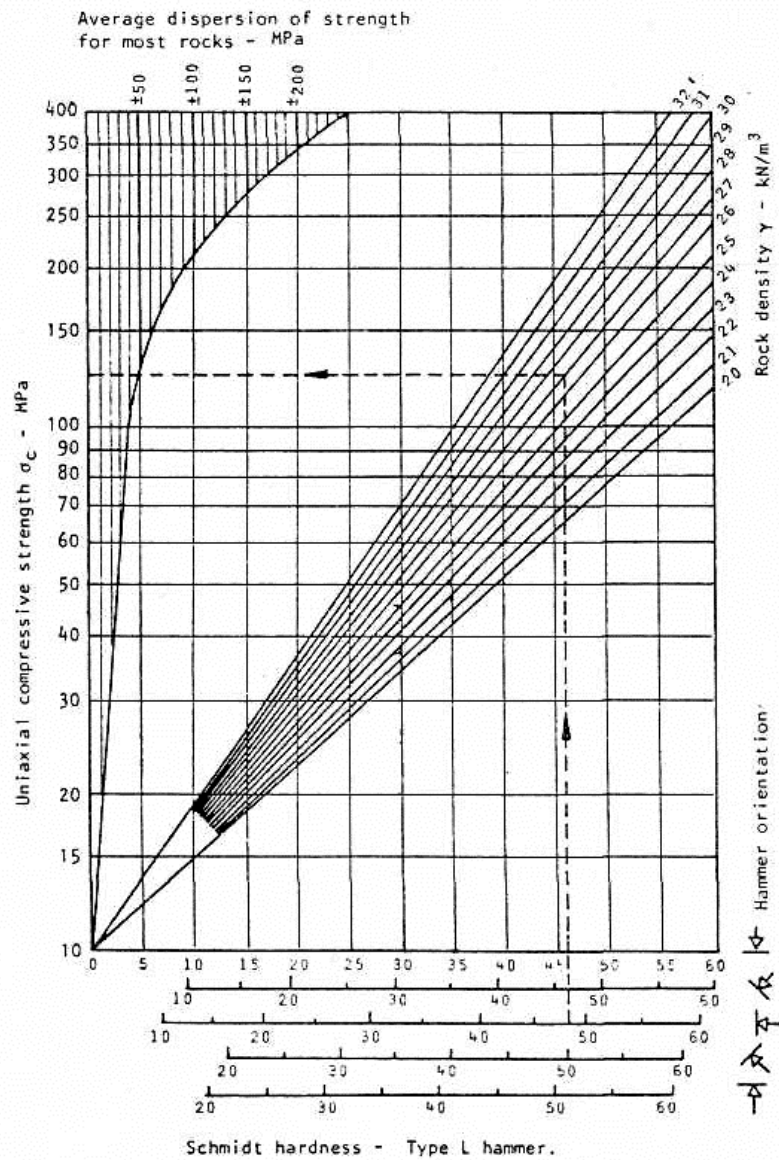


Figure 5.7 The frequency of joint wall compressive strength (Schmidt value, i.e. not transformed)



Relationship between Schmidt hardness and the uniaxial compressive strength of rock, after Deere and Miller

1 MPa = 1 MN/m<sup>2</sup> = 10.2 kg/cm<sup>2</sup> = 145 lb/in<sup>2</sup>

1 kN/m<sup>3</sup> = 102 kg/m<sup>3</sup> = 6.37 lb/ft<sup>3</sup>.

Figure 5.8 Relation between the Schmidt hardness and joint wall strength

One of the most important parameters in the analysis is the basic friction angle of the rock. Five direct shear tests were done to obtain basic friction angle. For S<sub>2</sub>, S<sub>3</sub>, S<sub>4</sub>, S<sub>5</sub> and S<sub>7</sub> samples the obtained basic friction angles were, 32.09, 32.23, 29.16, 33.48 and 29.01, respectively.

The Figures 5.10 to 5.12 indicate the shear stress-shear displacement curves for different applied normal stresses, shear and normal stress relation and relation of joint shear stiffness and normal stress for sample S\_2, respectively. It is to be noted that the joints sheared in S\_2, S\_3, S\_4, S\_5 and S\_7 samples were sawn joints. Figures A.5 to A.16 in appendix A indicate the shear stress-shear displacement curves for different applied normal stresses, shear and normal stress relation and relation of joint shear stiffness and normal stress for other four samples.

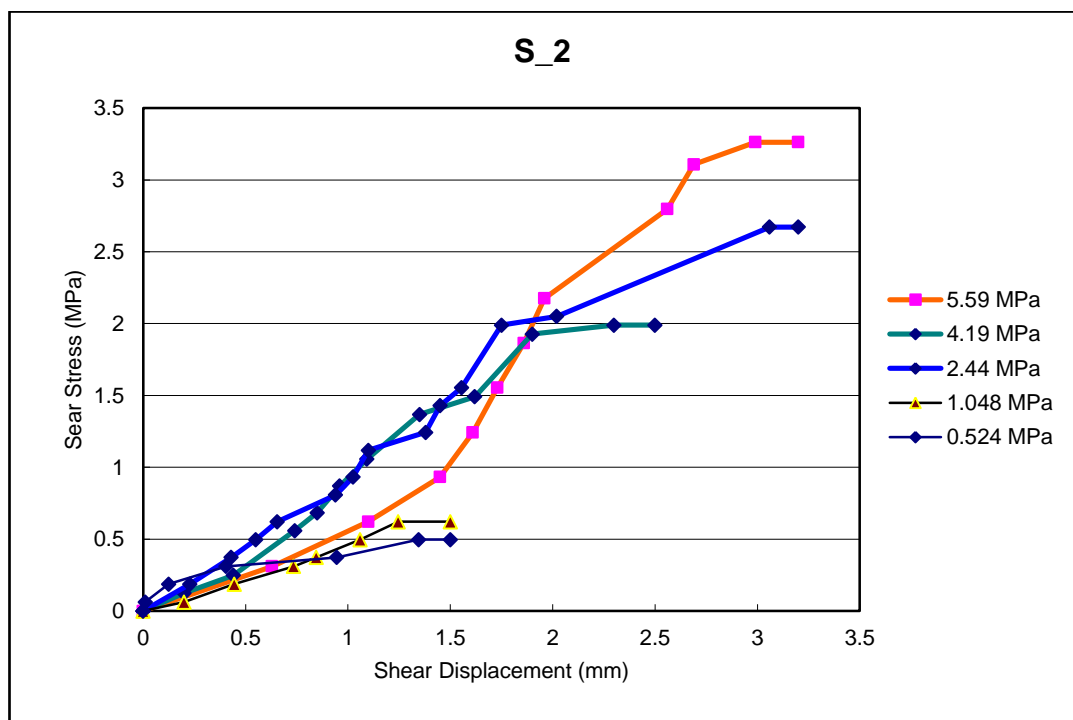


Figure 5.9 Shear stress/displacement curves for joint sample named as S\_2 for different normal stress values

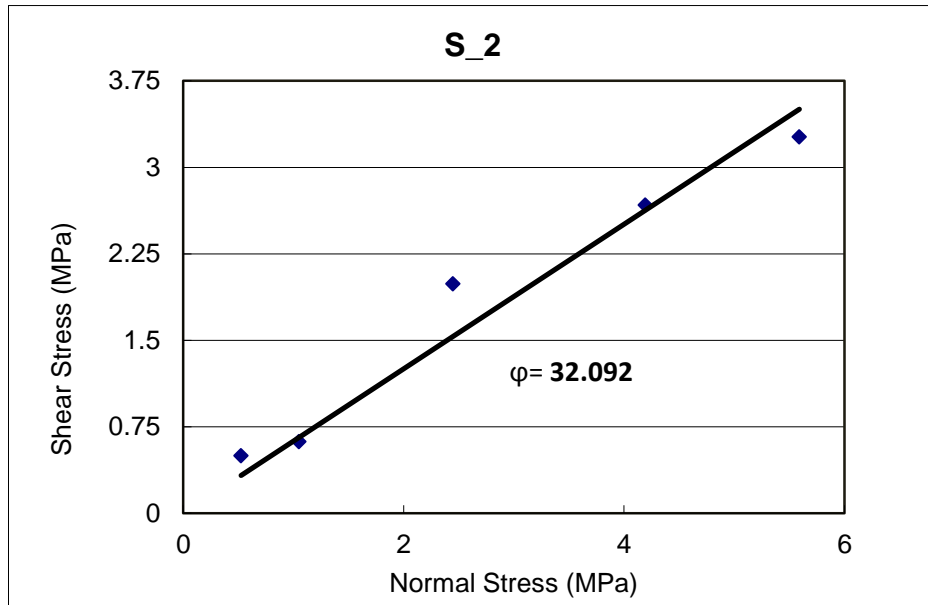


Figure 5.10 Relation of Shear and Normal stresses acted on joint of S\_2 to obtain the basic friction angle of joint surface which is  $32.092^{\circ}$

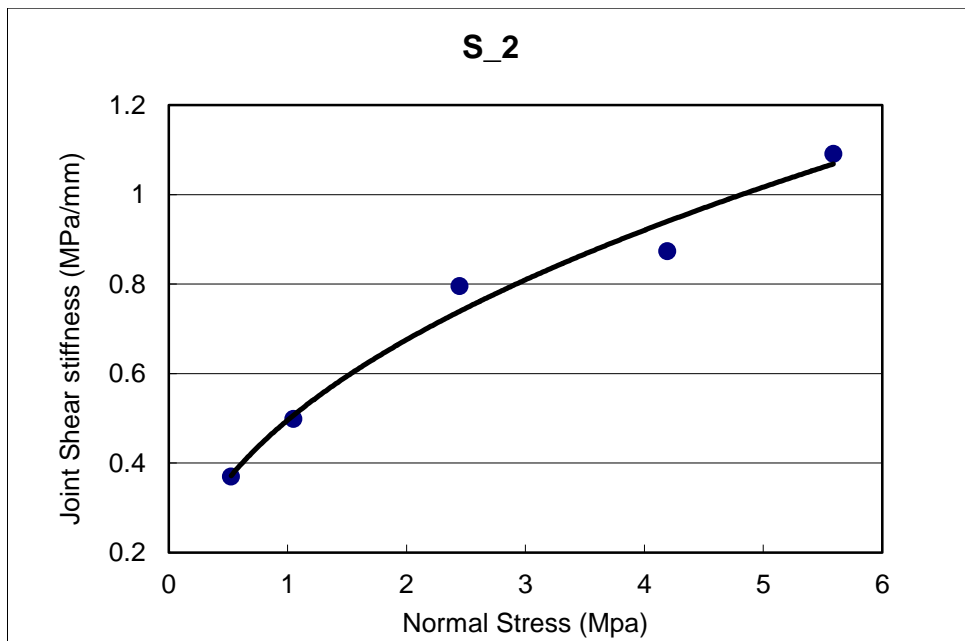


Figure 5.11 Dependency of joint shear stiffness ( $K_s$ ) to normal stress in smooth joint plane (S\_2)

Also, two natural joints were tested by direct shear box and Figures 5.13 to 5.15 indicate the shear stress-shear displacement curves for different applied normal stresses, shear and normal stress relation and relation of joint shear stiffness and normal stress for sample N\_1, respectively. Figures A.1 to A.15 in Appendix A indicate the shear stress-shear displacement curves for different applied normal stresses, shear and normal stress relation and relation of joint shear stiffness and normal stress for sample N\_2.

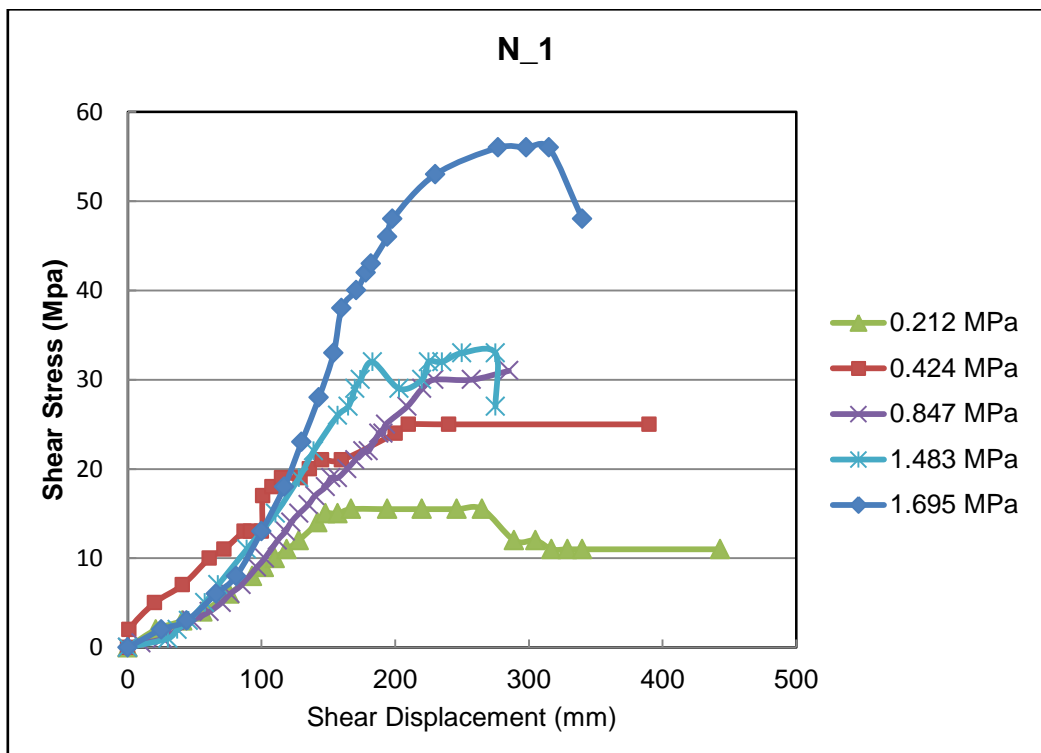


Figure 5.12 Shear stress/displacement curves for joint sample N\_1 for different normal stress values

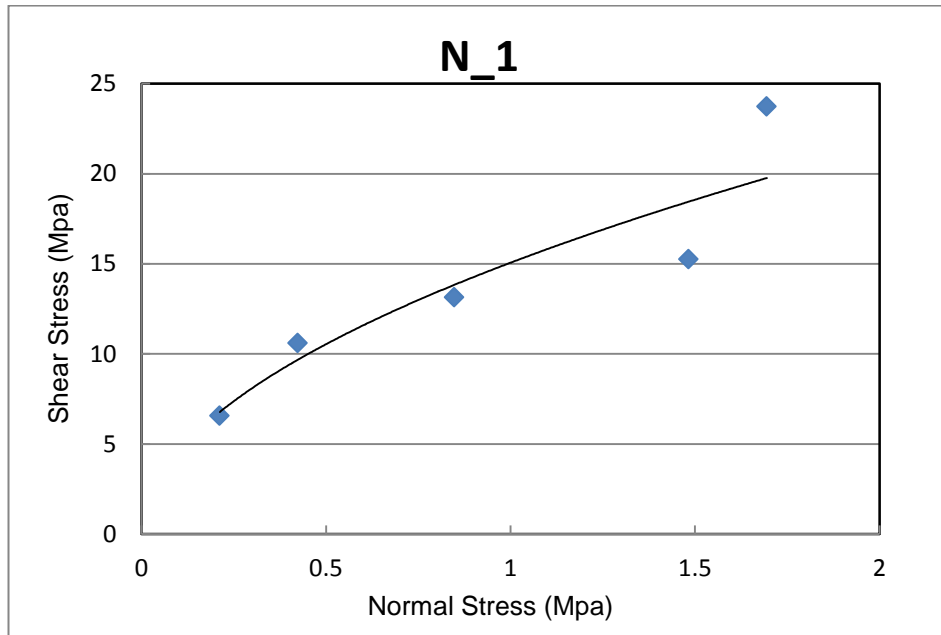


Figure 5.13 Relation of Shear and Normal stresses acted on joint of N\_1

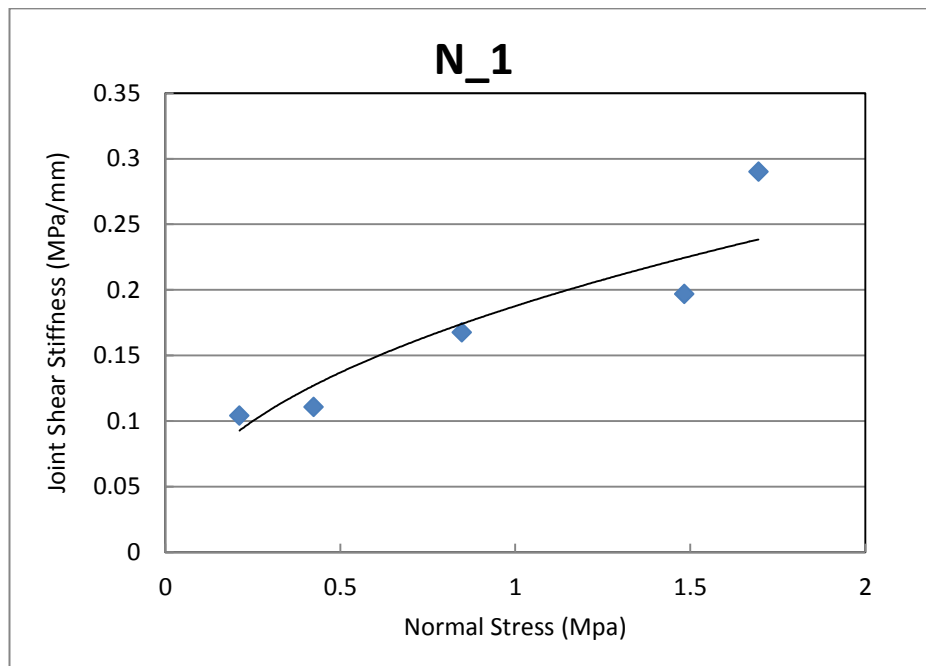


Figure 5.14 Dependency of joint shear stiffness ( $K_s$ ) to normal stress in rough joint plane (N\_1)

Moreover, two axial compressive tests were done to obtain the elastic modulus, Poisson's ratio and compressive strength of the intact rock. The elastic modulus, UCS and Poisson's ratio were 25.15 GPa, 90.28 MPa and 0.1 for sample I, respectively, and 28 GPa, 95.26 MPa and 0.116 for sample II. Figure 5.16 indicates the result of axial compressive loading vs. axial and lateral strains. Figure A.16 indicates the result of axial compressive loading vs. axial and lateral strains sample II in Appendix A.

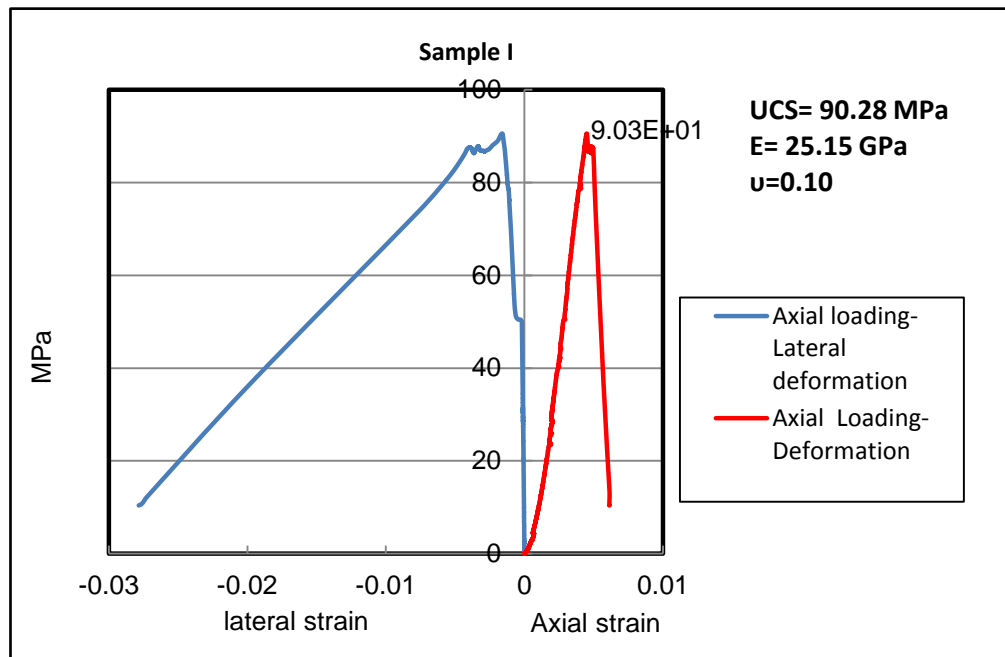


Figure 5.15 Stress-strain curve of sample I

### 5.3 Rock Slope Modeling

Field studies demonstrated that the rock mass in Amasya region is discontinuous and for modeling the rock structure the Discrete Element Modeling should be utilized. As indicated in Figure 5.2, there are different regions in Amasya that suffers from rock slope problems; however, to apply the probabilistic-numerical methodology proposed in this thesis, the Sec\_3 was selected.

This structure, King's Rock Grave, was carved in a limestone cliff containing two dominated discontinuities, the bedding planes and steep joints parallel to the slope face. These discontinuities have increased the potential of planar failure of the King's Grave. Figure 5.17 indicates a view of the King's Grave. The grave is visited by hundreds of visitors daily and there is a restaurant close to the grave. There are some fallen blocks and considerably hanging block which may fall. Moreover, a failure has been occurred on top of the entrance of the grave which has destroyed the half of grave's entrance. Figure 5.19 shows the samples of fallen blocks and a big failure and hanging blocks on the grave structure.

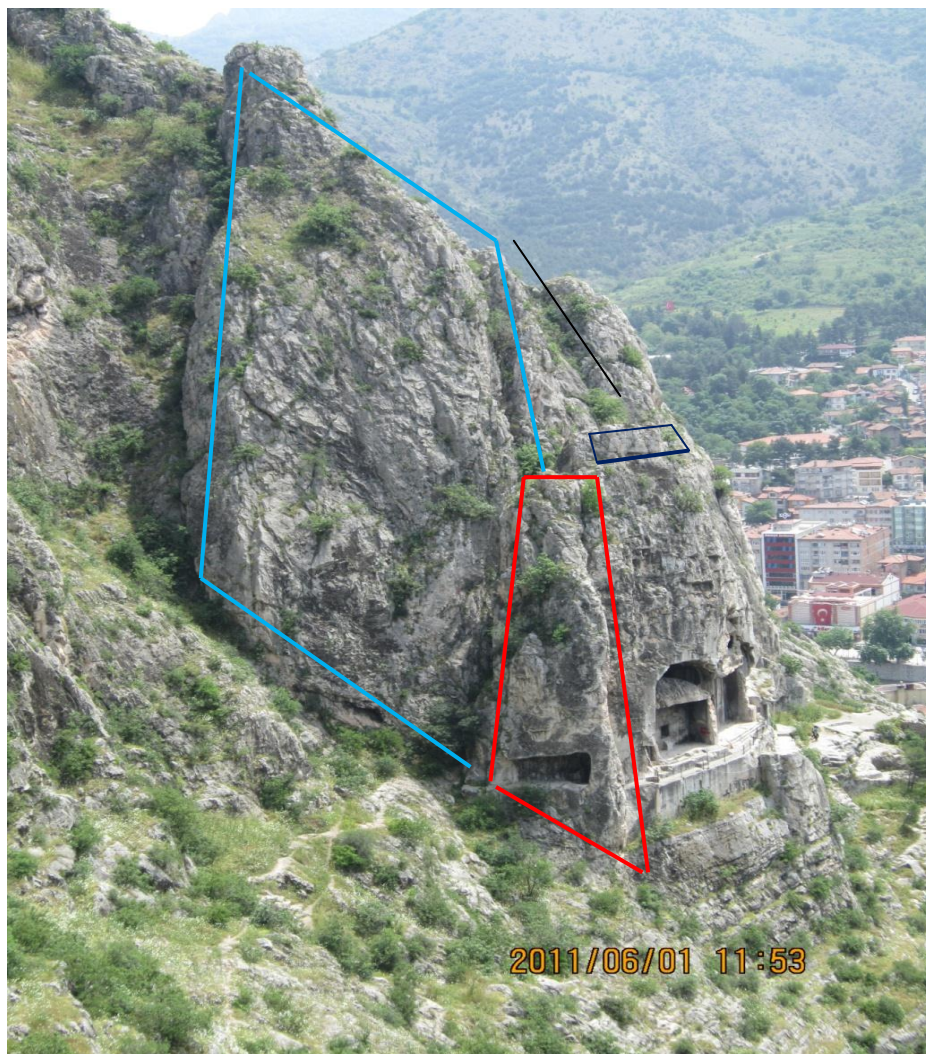


Figure 5.16 King's rock grave, Amasya, Turkey



Figure 5.17 Fallen blocks, big failure and hanging blocks on the grave structure

### 5.3.1 Model construction

The first step was to construct the shape of the structure, since the shape of the structure is complex, the best method would be using laser scanning method and import it to 3DEC medium as a DXF. However, laser scanning is too expensive to be afforded. Instead, combination of laser surveying and differential GPS were applied to obtain the coordinates of the selected points on the structure. As estimation, some planes were defined to draw the schematic of model. The discontinuities also applied to the structure based on data gathered in joint mapping

studies. The geometrical parameters considered in model construction were given in Table 5.6. Figure 5.19 indicates the constructed model of the King's Grave structure.

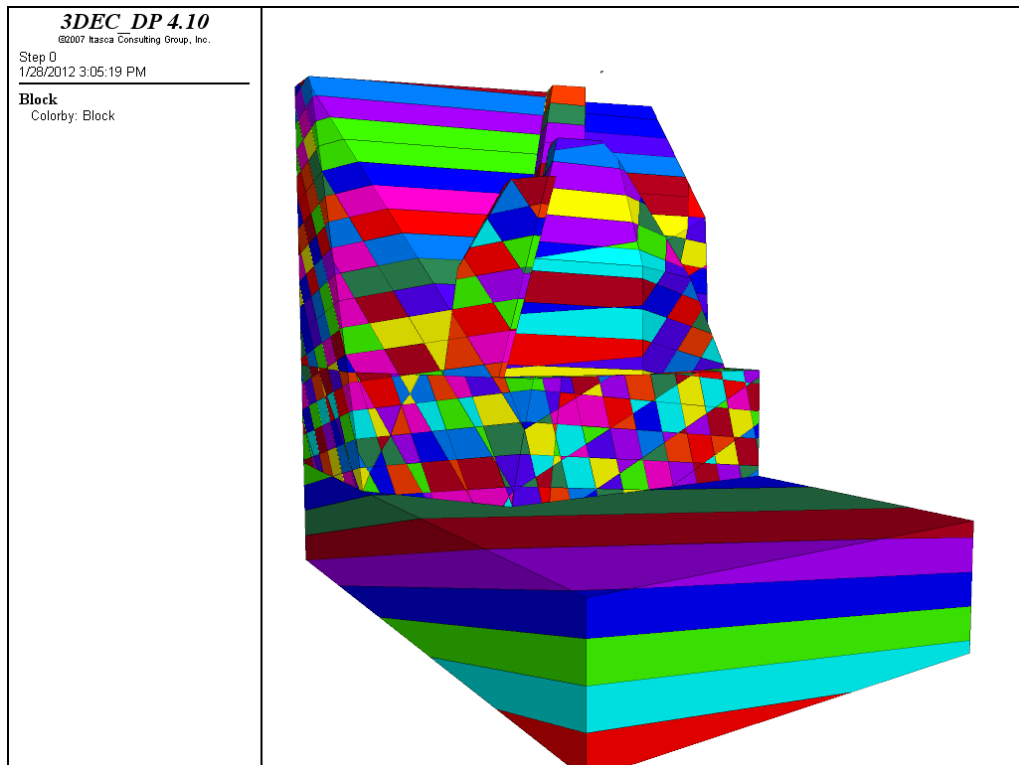


Figure 5.18 Constructed model of the King's Grave

Table 5.6 Joints geometry used in modeling the king's grave

Type of joint	Bedding	Joint 1	Jset 2	Jset 3
Dip ( $^{\circ}$ )	35 $^{\circ}$	87 $^{\circ}$	55 $^{\circ}$	75 $^{\circ}$
Dip Direction ( $^{\circ}$ )	028 $^{\circ}$	180 $^{\circ}$	200 $^{\circ}$	288 $^{\circ}$

However, three dimensional numerical analyses especially those including the discontinuity requires high performance computers. Therefore, the bedding planes were omitted and only the joints parallel to the slope face were included in analysis. Figure 5.20 indicates the final model of the grave to be analyzed by 3DEC. No displacement

(velocity = 0) were applied as boundary conditions in appropriate directions.

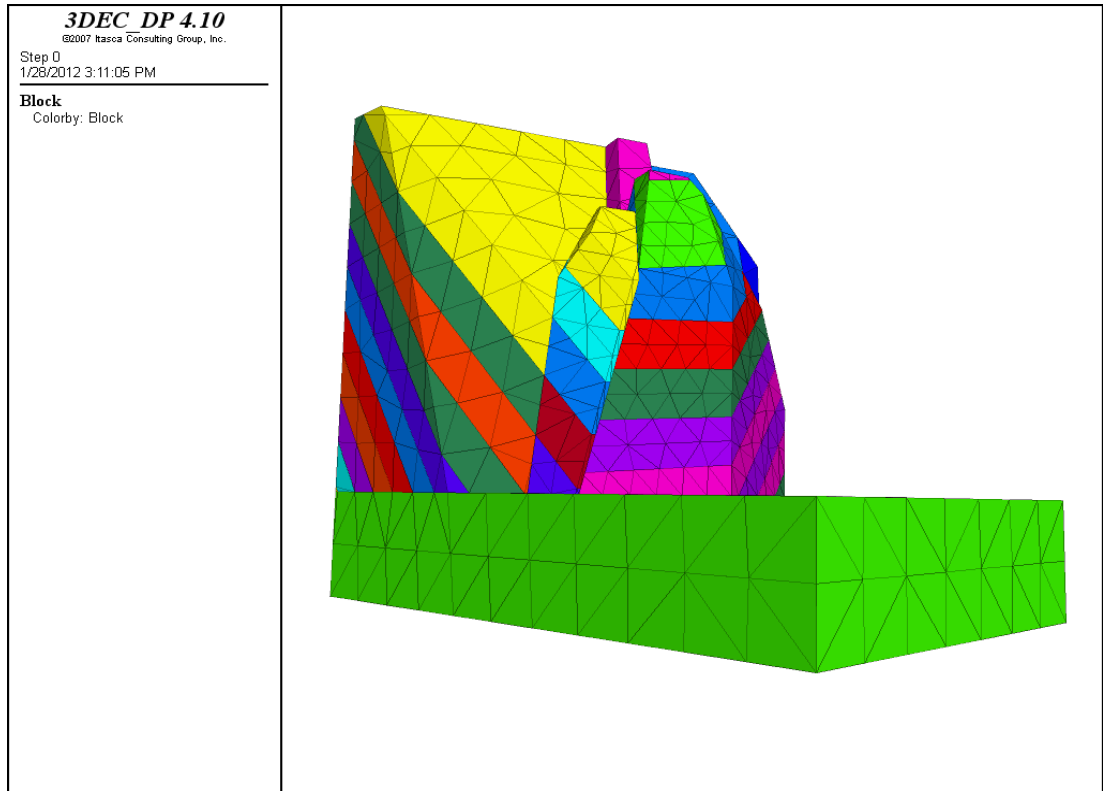


Figure 5.19 Final model of the grave to be analyzed by 3DEC

### 5.3.2 Choice of Block and Joint Constitutive Models and Material Properties

The model constructed is defined with appropriate constitutive laws for both intact rock and discontinuities. Constitutive models are mathematical equations describing the relationship between stress and strain. Since the structure is on the surface and the stress level is low, it was appropriate to use elastic Hook's Law as constitutive model for intact rock. The elastic model also reduces the analysis time.

For modeling a material elastically, three parameters of density, bulk modulus (K) and shear modulus (G) are required. Eqs. 6.1 and 6.2 are used to calculate K and G from Young's modulus and Poisson's ratio:

$$K = \frac{E}{3(1-2\nu)} \quad (5.1)$$

$$G = \frac{E}{2(1+\nu)} \quad (5.2)$$

Based on the laboratory tests the elastic modulus and Poisson's ratio are 26.5 GPa, and 0.11, respectively. K and G were calculated by Eqs. 5.1 and 5.2 and their value are 11.32 GPa and 11.94 GPa respectively. The density was obtained to be 2600 Kg/m<sup>3</sup>.

Fourteen numbers of discontinuities were applied to behave plastically. The other joints behaved elastically and no slip was permitted. Figure 5.21 indicates the ID's of the discontinuity to be analyzed as their material number. It is to be noted that the material number 20 was not permitted to slip however, other joints were model based on Coulomb slip model.

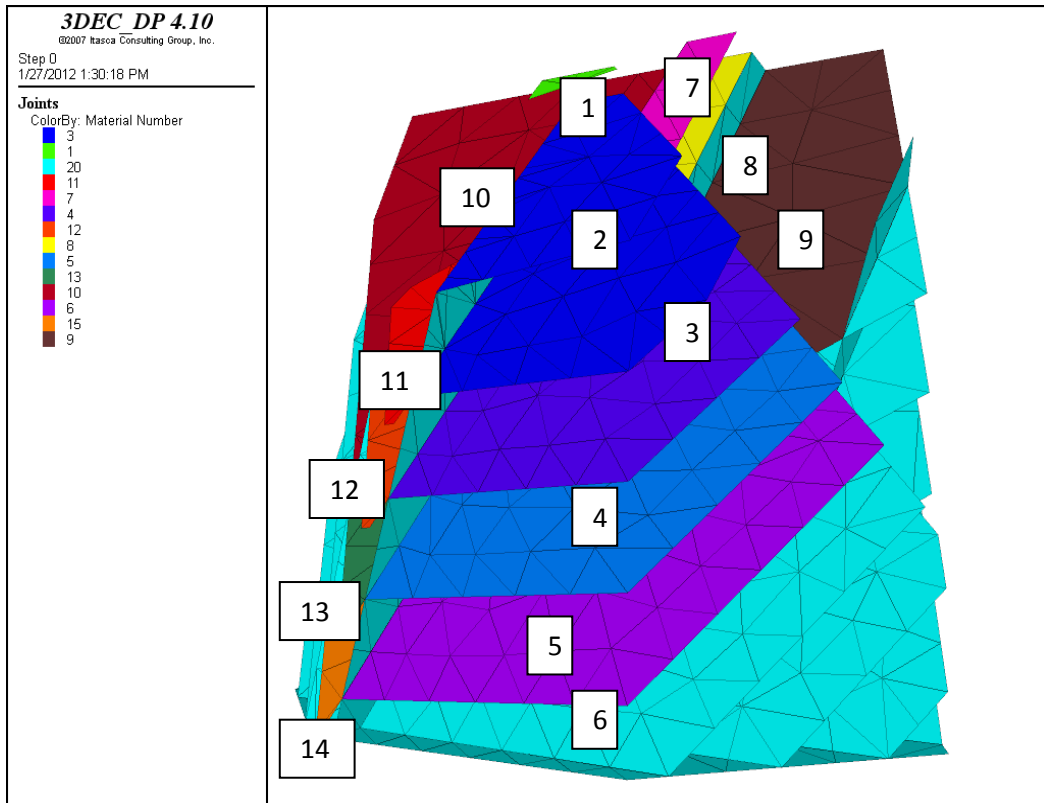


Figure 5.20 Material number of fourteen discontinuities to be analyzed

Before starting analysis, the model should be run to achieve the equilibrium state, for initial loading high  $k_s$ ,  $k_n$ , cohesion, tensile strength and friction angle values were assigned and model run where, all of the joints were behaving elastically, this led the model to reach the equilibrium state.

### 5.3.3 Different realization of random variables

As mentioned in Chapter V, different combination of JRC, JCS, basic friction angle and cohesion variables can be applied to model. The first group of analysis were done with one random variable JRC, in this group it was assumed that the JCS and friction angle are constant for joints and the joints do not have any infilling (added Cohesion=0).

For the second group, the infilling material effect was applied to the model by adding cohesion to the strength of the joint or the discontinuity. This group itself was assessed in two different cases. In one of the cases, the basic friction angle was considered to be  $33^{\circ}$  and this was done for JCS=50 MPa and 70 MPa and different values for JRC and cohesion. In the other case, the basic friction angle was considered to be  $30^{\circ}$  and this was done for JCS=70 MPa and different values for JRC and cohesion. The considered cases are as follows:

1. C=50 kPa, basic friction angle= $33^{\circ}$  and JCS=70 MPa
2. C=50 kPa, basic friction angle= $33^{\circ}$  and JCS=50 MPa
3. C=100 kPa, basic friction angle= $33^{\circ}$  and JCS=70 MPa
4. C=150 kPa, basic friction angle= $33^{\circ}$  and JCS=70 MPa
5. C=200 kPa, basic friction angle= $33^{\circ}$  and JCS=70 MPa
6. C=300 kPa, basic friction angle= $33^{\circ}$  and JCS=70 MPa
7. C=500 kPa, basic friction angle= $33^{\circ}$  and JCS=70 MPa
8. C=50 kPa, basic friction angle= $30^{\circ}$  and JCS=70 MPa
9. C=100 kPa, basic friction angle= $30^{\circ}$  and JCS=70 MPa
10. C=150 kPa, basic friction angle= $30^{\circ}$  and JCS=70 MPa
11. C=200 kPa, basic friction angle= $30^{\circ}$  and JCS=70 MPa
12. C=300 kPa, basic friction angle= $30^{\circ}$  and JCS=70 MPa

13.  $C=500$  kPa, basic friction angle= $33^{\circ}$  and  $JCS=70$  MPa

According to the methodology explained in Chapter IV, the model requires normal stress, instantaneous cohesion and friction angle and  $K_s$  to be calculated for each discontinuity. For example for discontinuity number 5, the normal stress, instantaneous cohesion and friction angle, estimated peak shear displacement and  $K_s$  were obtained 0.197149 MPa,  $53.56^{\circ}$ , 0.1547 MPa, 0.03423 m and 12.32 MPa/m for sample number 3 when the  $JRC=10$ . All the samples were analyzed based on proposed probabilistic-numerical approach described in Chapter IV and the following section discusses the results obtained for each sample.

#### **5.4 Results**

In this thesis, a selected rock slope was modeled and run for different samples of combination of cohesion, friction angle,  $JCS$  and  $JRC$  values reviewed in previous section. The main random variable in this study was the  $JRC$  value of the discontinuities existing in structure. First, it was assumed that the discontinuities do not have infilling material, therefore, the friction angle, the  $JRC$  and the  $JCS$  were input in Barton model to obtain the instantaneous cohesion and friction angle and the shear stiffness. However, the structure collapsed even with high  $JRC$ . Figure 5.22 indicates the state of structure when  $JRC =18$  and the calcite infilling material has not been taken into account. However, this does not seem a reliable result; although there are some failures in the structure it stays stable.

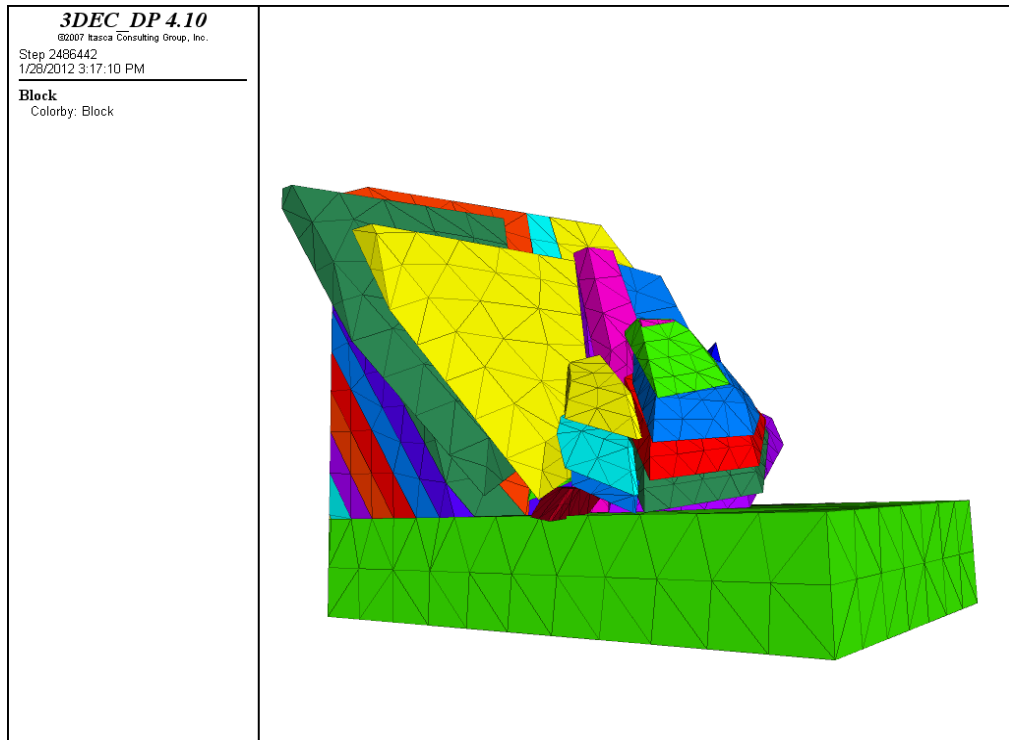


Figure 5.21 State f the structure for JRC=18, JCS=70 MPa,  $\Phi = 33^{\circ}$  and no infilling material

Some of the joints existing in the structure were filled by calcite and in some parts the filled material has been washed by fluids. The filled material certainly increases the strength of the discontinuity. Therefore, the effect of infilling material must be exerted in the analysis. It was assumed that some portion of the joint plane area has calcite as filled material and the other portion is the contact to two walls of joint. For taking this into account, the model was run by assuming different cohesion values such as 50, 100, 150, 200, 300 and 500 kPa.

### 5.4.1 Realizations

1.  $C=50$  kPa, basic friction angle= $33^\circ$  and  $JCS=70$  MPa

In this case, cohesion of 50 kPa was added to run the model for different JRC values. A definite JRC value changes the  $K_s$  and the shear strength of each discontinuity. For  $C=50$  kPa, the JRCs of 15, 13, 11, 10 were given. In cases where JRCs, were 15, 13, 11 the shear displacements are very low in comparison to the allowable peak shear displacement ( $\delta_{peak}$ ). However, when the JRC reduces to lower than 11, the discontinuity no. 1, 2, 3, 4, 7, 11, 12 displaces considerably. However, discontinuity no. 5, 6, 8, 9, 10, 13, and 14 displaced less than  $\delta_{peak}$ . Therefore, if it is assumed that the shear displacement greater than  $\delta_{peak}$  is called as failure, JRC=11 can be considered as the limit state condition for discontinuities when  $C=50$  kPa. Table 5.7 indicates the shear displacement, peak shear displacement and the values calculated for  $K_s$  for each discontinuity.

Figures 5.23 to 5.35 indicate the shear displacement for JRC=10 for fourteen discontinuities. Also, Figures B.1 to B.13 in Appendix B indicate the shear displacement history of each discontinuity for JRC=11 values.

Since the limit state condition for this realization for discontinuities no. 1, 2, 3, 4, 7, 11, 12 is JRC=11, the failure probability for these discontinuities is 76.26% for Lognormal distributions of JRC value, with mean=9.1 and standard deviation of 6.68.

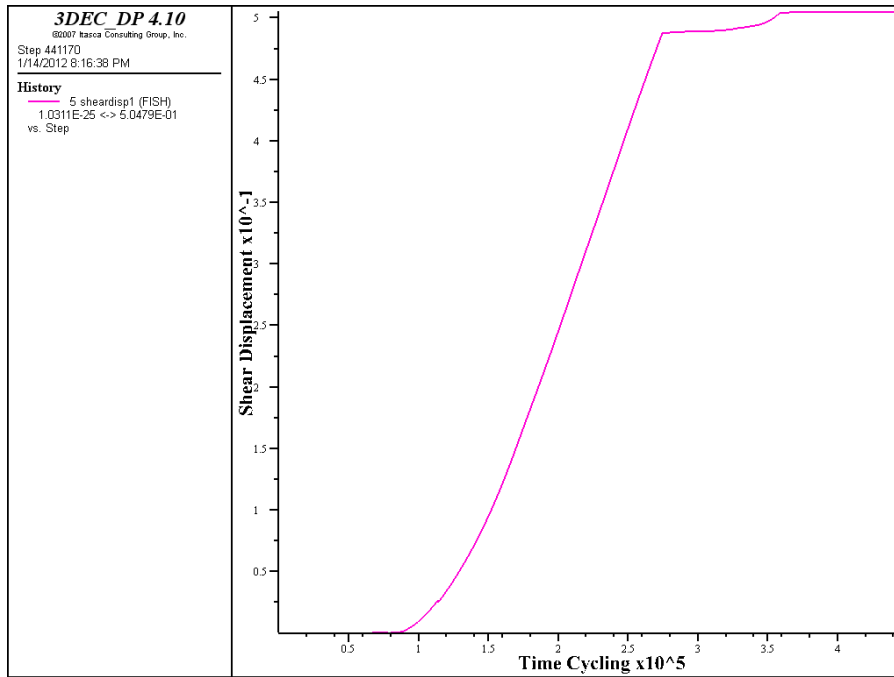


Figure 5.22 Shear displacement of discontinuity 1, for JCS=70, C=50 kPa,  $\Phi=33^\circ$  and JRC=10

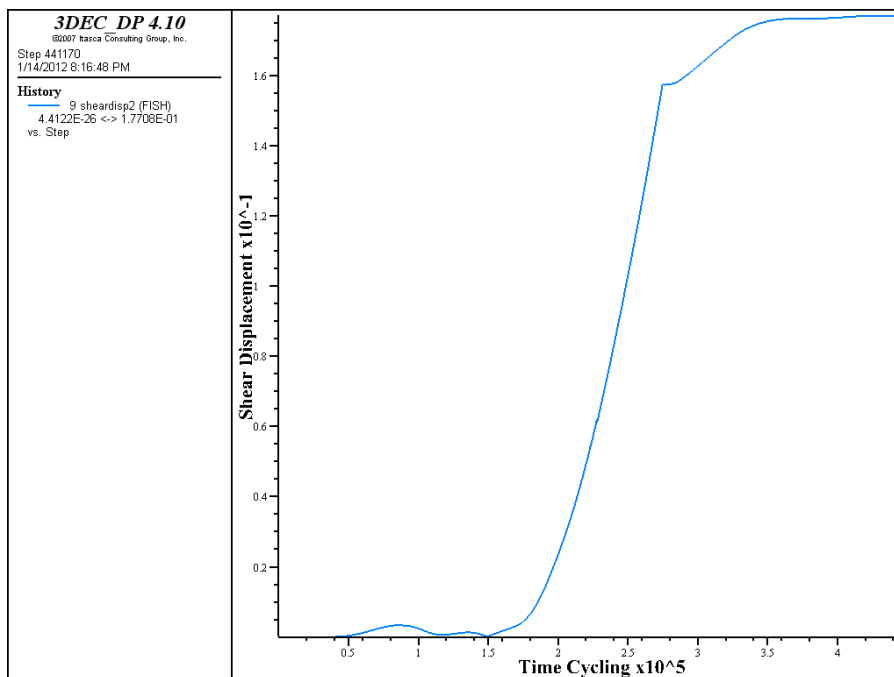


Figure 5.23 Shear displacement of discontinuity 2, for JCS=70 MPa, C=50 kPa,  $\Phi=33^\circ$  and JRC=10

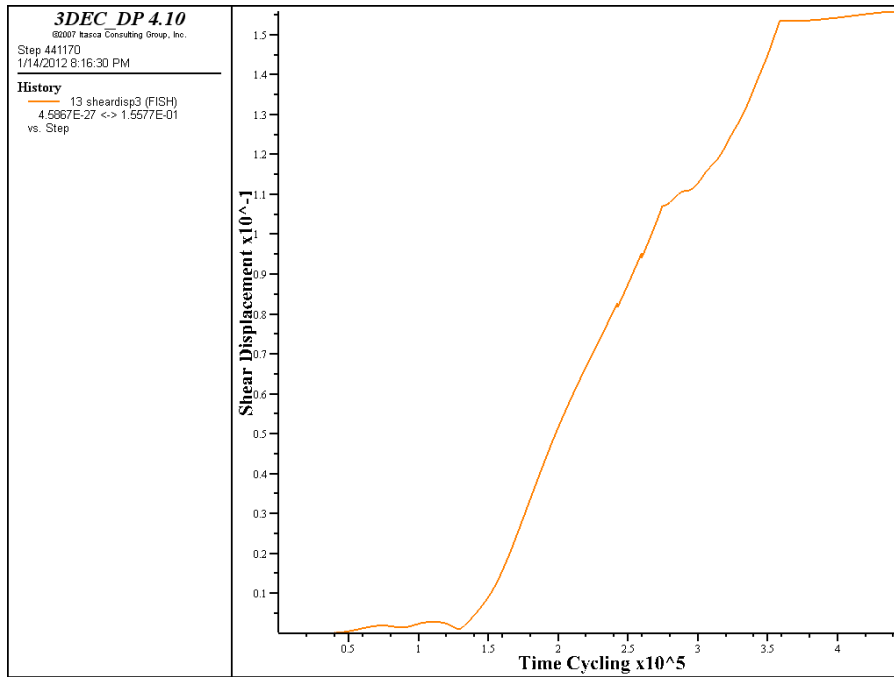


Figure 5.24 Shear displacement of discontinuity 3, for JCS=70 MPa, C=50 kPa,  $\Phi=33^{\circ}$  and JRC=10

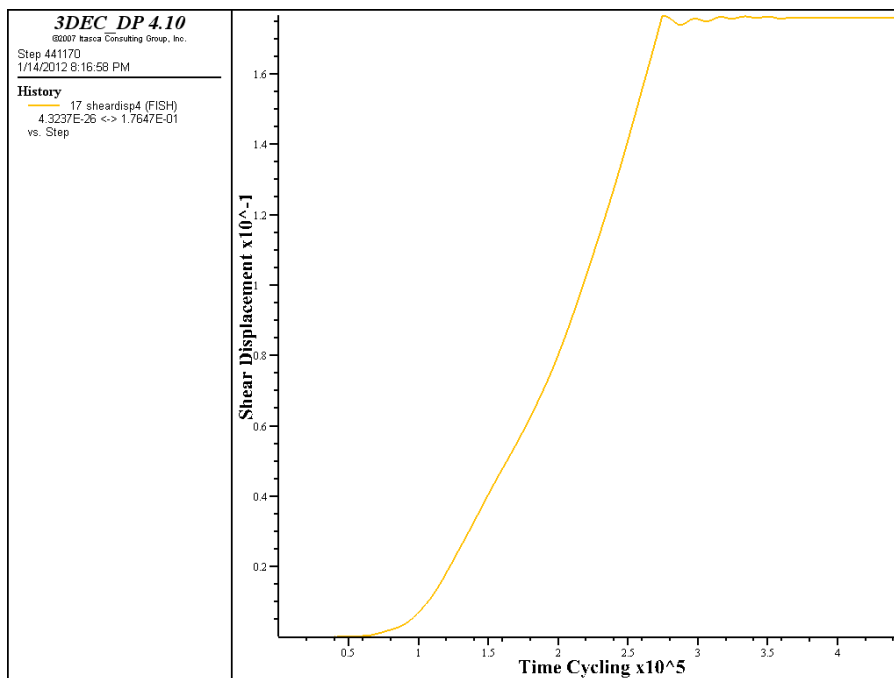


Figure 5.25 Shear displacement of discontinuity 4, for JCS=70 MPa, C=50 kPa,  $\Phi=33^{\circ}$  and JRC=10

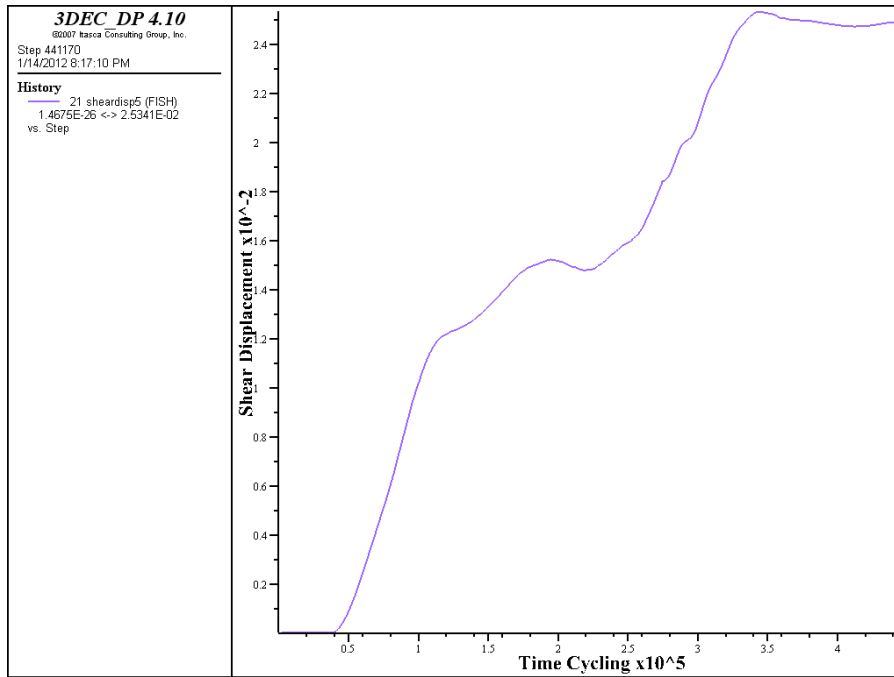


Figure 5.26 Shear displacement of discontinuity 5, for JCS=70 MPa, C=50 kPa,  $\Phi=33^\circ$  and JRC=10

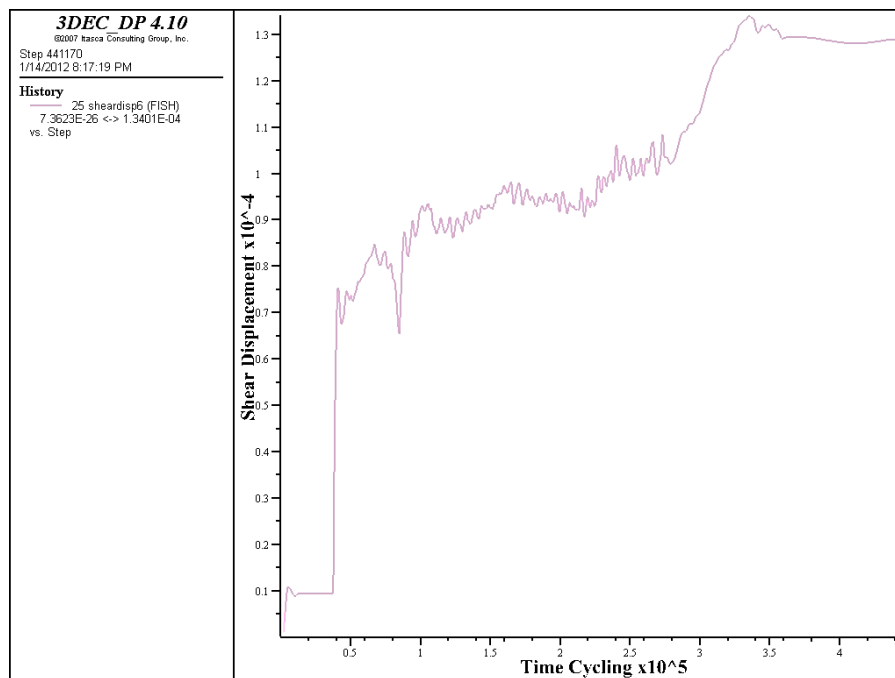


Figure 5.27 Shear displacement of discontinuity 6, for JCS=70 MPa, C=50 kPa,  $\Phi=33^\circ$  and JRC=10

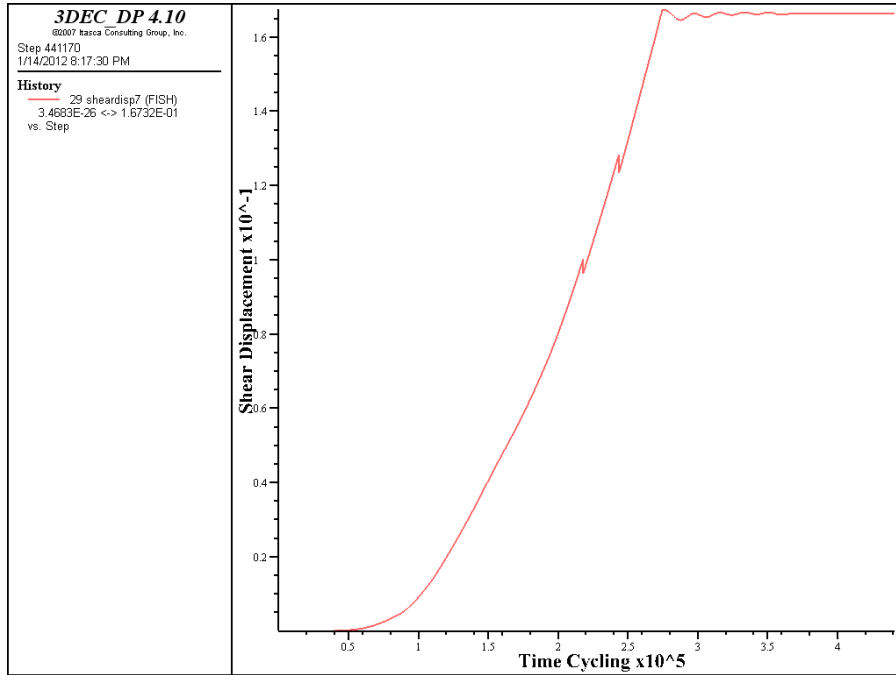


Figure 5.28 Shear displacement of discontinuity 7, for JCS=70 MPa, C=50 kPa,  $\Phi=33^0$  and JRC=10

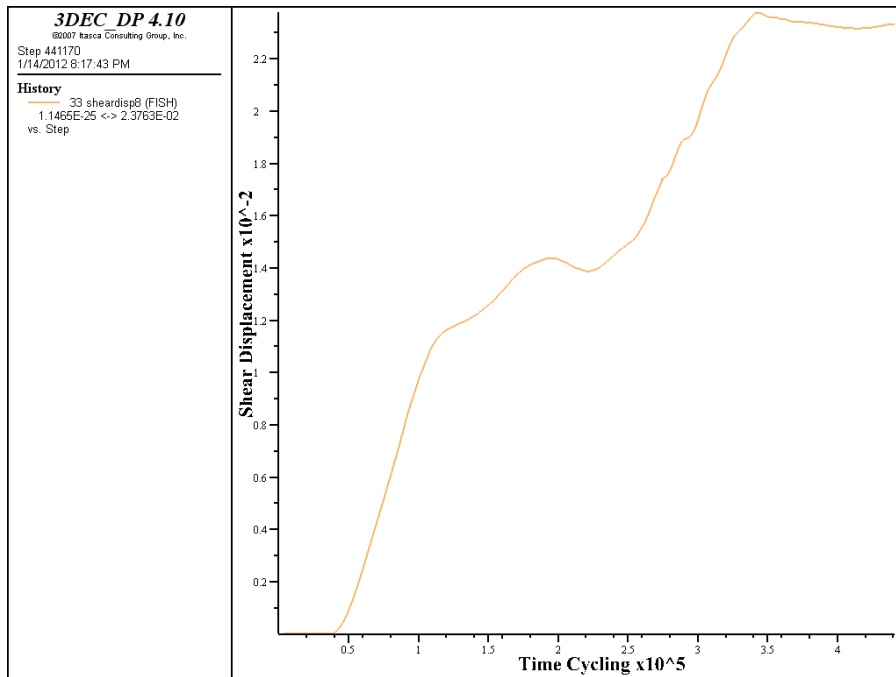


Figure 5.29 Shear displacement of discontinuity 8, for JCS=70 MPa, C=50 kPa,  $\Phi=33^0$  and JRC=10

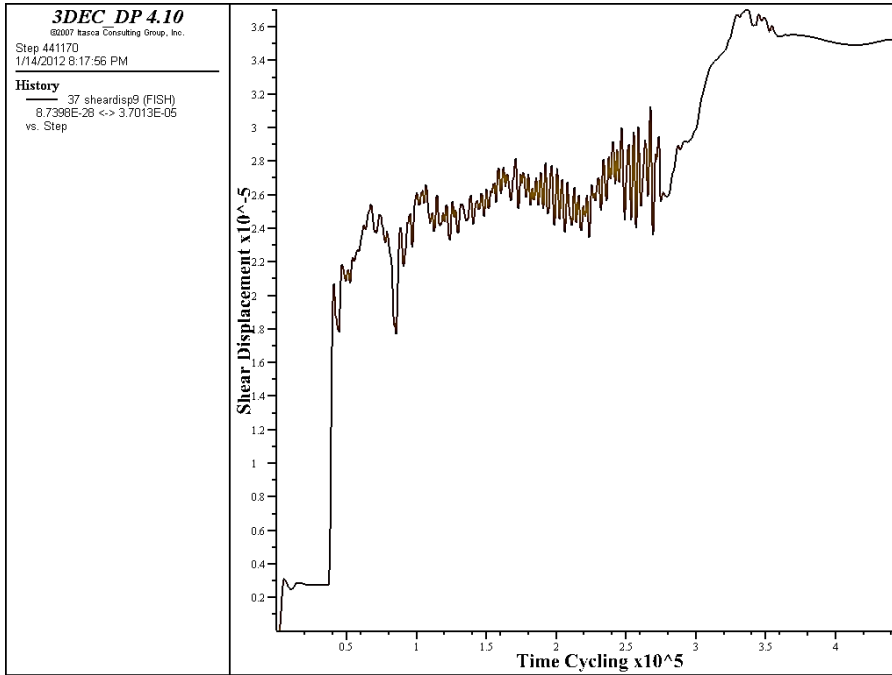


Figure 5.30 Shear displacement of discontinuity 9, for JCS=70 MPa, C=50 kPa,  $\Phi=33^\circ$  and JRC=10

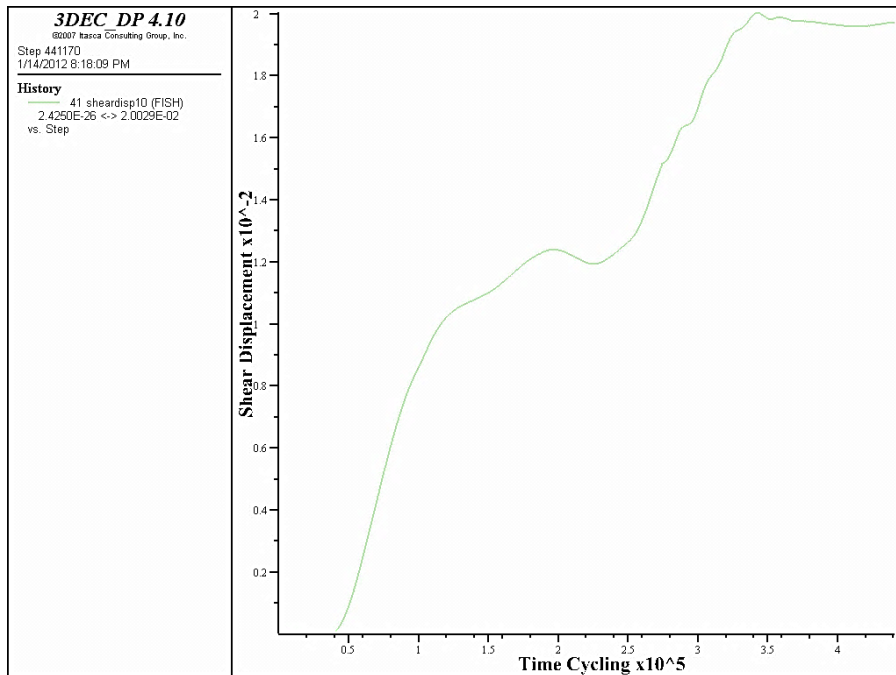


Figure 5.31 Shear displacement of discontinuity 10, for JCS=70 MPa, C=50 kPa,  $\Phi=33^\circ$  and JRC=10

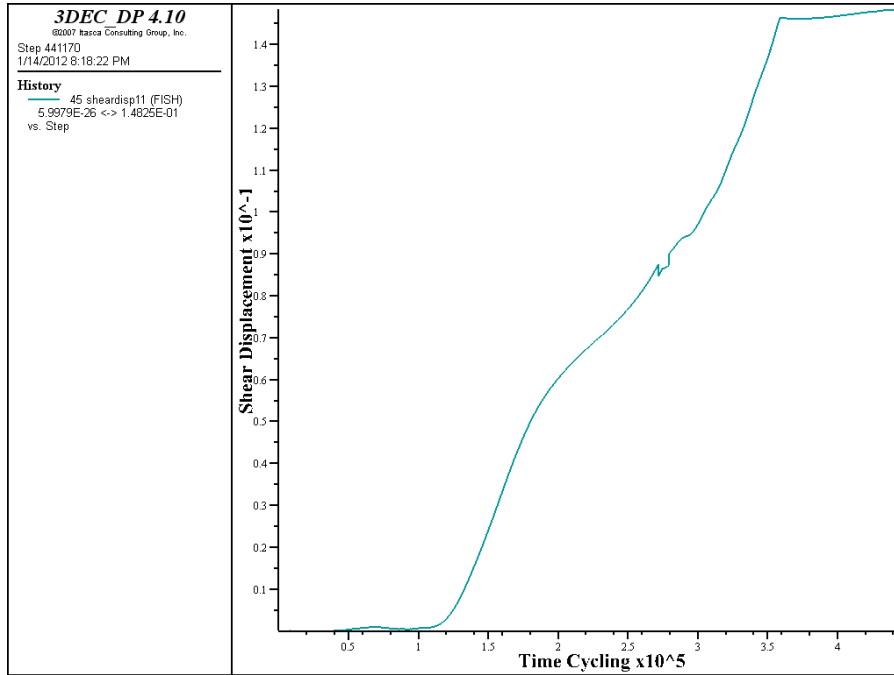


Figure 5.32 Shear displacement of discontinuity 11, for JCS=70 MPa, C=50 kPa,  $\Phi=33^{\circ}$  and JRC=10

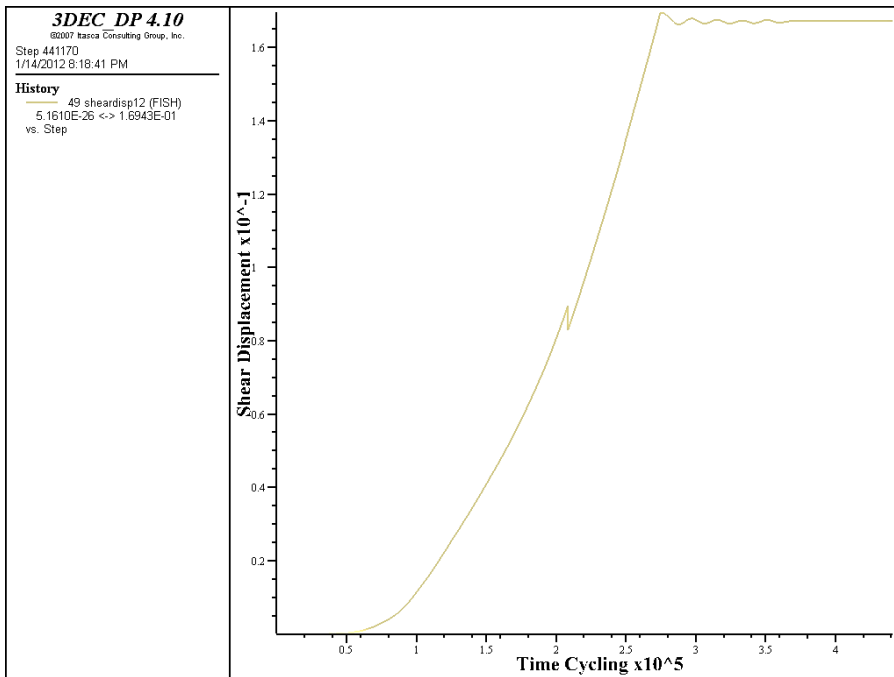


Figure 5.33 Shear displacement of discontinuity 12, for JCS=70 MPa, C=50 kPa,  $\Phi=33^{\circ}$  and JRC=10

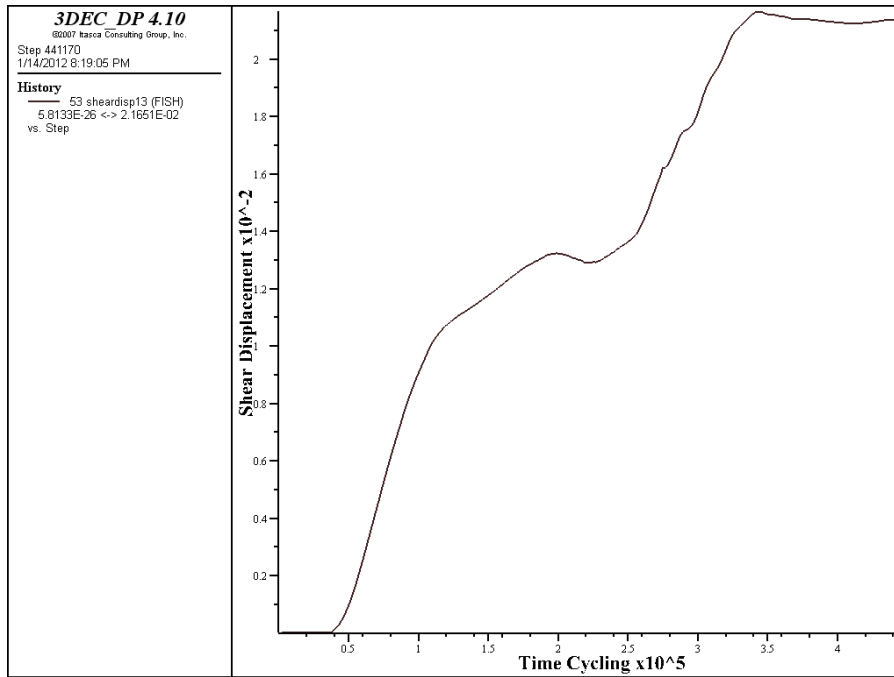


Figure 5.34 Shear displacement of discontinuity 13, for JCS=70 MPa, C=50 kPa,  $\Phi=33^{\circ}$  and JRC=10

Table 5.7 Shear deformation, peak shear deformation of Barton model for friction= 33, coh.=0.05 MPa, different JCS, JRC and Ks

Cohesion		JCS		C R J		*Not in Equilibrium state	** In Equilibrium state			Discontinuity ID										State
						1	2	3	4	5	6	7	8	9	10	11	12	13	14	
	50	11	J	$\delta$ (m)	<b>0.7</b>	<b>0.202</b>	<b>0.14</b>	<b>0.164</b>	0.03	0.0001	<b>0.155</b>	0.023	3.3e-5	0.019	<b>0.136</b>	<b>0.156</b>	0.021	7.5e-5	**	
				$\delta_{peak}$ (m)	0.006	0.037	0.04	0.036	0.04	0.04	0.08	0.07	0.06	0.03	0.03	0.033	0.023	0.023		
				Ks (MPa/m)	13.06	3.65	5.53	8.22	10.87	13.68	2.65	3.65	3.23	6.31	7.23	9.04	15.52	21.84		
		12	J	$\delta$ (m)	9.8e-6	0.0001	3.5e-5	1.2e-5	0.0005	3.4e-5	3.1e-5	$\frac{0.000}{5}$	9.9e-6	0.0006	4.6e-5	1.9e-5	0.0006	4.5e-5	**	
				$\delta_{peak}$ (m)	0.006	0.038	0.04	0.037	0.036	0.036	0.078	0.074	0.0661	0.031	0.028	0.034	0.024	0.024		
				Ks (MPa/m)	14.01	3.95	5.96	8.75	11.51	14.41	2.84	3.9	3.47	6.79	7.77	9.62	16.46	22.99		
	70	10	J	$\delta$ (m)	<b>0.505</b>	<b>0.177</b>	<b>0.16</b>	<b>0.176</b>	0.025	0.0001	<b>0.166</b>	0.023	2.9e-6	0.0197	<b>0.148</b>	<b>0.167</b>	0.021	7.9e-5	**	
				$\delta_{peak}$ (m)	0.006	0.036	0.04	0.035	0.034	0.0342	0.073	0.07	0.0623	0.0288	0.0265	0.032	0.022	0.022		
				Ks (MPa/m)	12.8	3.57	5.47	8.17	10.86	13.73	2.61	3.62	3.19	6.22	7.13	8.99	15.48	21.94		
		11	J	$\delta$ (m)	1.0e-5	0.0001	7.2e-5	1.9e-5	0.001	4.1e-5	7.1e-5	0.001	1.2e-5	0.0014	0.0001	3.7e-5	0.001	4.5e-5	**	
				$\delta_{peak}$ (m)	0.006	0.037	0.04	0.036	0.035	0.036	0.075	0.072	0.0643	0.0297	0.0273	0.033	0.023	0.023		
				Ks (MPa/m)	13.15	3.7	5.65	8.42	11.17	14.08	2.7	3.73	3.29	6.43	7.37	9.26	15.93	22.5		
13	J	$\delta$ (m)	1.7e-6	0.0001	1.7e-5	1.9e-5	3.4e-5	9.8e-6	1.8e-5	$\frac{2.3e-}{5}$	2.9e-6	1.9e-5	1.3e-5	1.8e-5	3.5e-5	1.5e-5	**			
		$\delta_{peak}$ (m)	0.006	0.039	0.04	0.038	0.037	0.037	0.08	0.076	0.0679	0.0314	0.0289	0.035	0.024	0.024				
		Ks (MPa/m)	89.44	4.83	7.03	10.22	13.29	16.49	3.39	4.57	4.12	8.11	9.26	11.23	19.07	26.27				

2.  $C=50$  kPa, basic friction angle= $33^{\circ}$  and JCS= $50$  MPa

To investigate the effect of JCS variation on model, the JCS values also reduced to 50 MPa in this case, Table 5.8 indicates the shear displacement of each discontinuity for this condition. For this case the JRC lower than 12 can be considered as limit state function based on the shear displacement and its comparison with peak shear displacement estimated by Barton.

Since the limit state condition for this sample for discontinuities no. 1, 2, 3, 4, 7, 11, 12 is JRC=12, therefore, the failure probability for these discontinuities is 81.75%.

Comparing the sample number 1 and 2 indicates that if for constant  $C=50$  kPa, basic friction angle= $33^{\circ}$  the JCS reduced from 70 MPa to 50 MPa, failure probability increases about 5.5 %.

3.  $C=100$  kPa, basic friction angle= $33^{\circ}$  and JCS= $70$  MPa

In this case, cohesion of 100 kPa was added to run the model for different JRC values. For  $C=100$  kPa, the JRCs of 2, 3, 5, 9, 9.8 and 10 were given to the model. For JRCs, equal to 9.8 and 10 the shear displacements are very low in comparison to the allowable peak shear displacement. However, when the JRC reduces to lower than 9.8, the discontinuities no. 1, 2, 3, 4, 5, 7, 8, 10, 11, 12, 13 displaced considerably. However, discontinuity no. 6 and 14 displaced less than estimated peak shear displacement. Therefore, if it is assumed that the shear displacement greater than peak is called as failure, JRC= 9.8 can be considered as the limit state criterion for our discontinuity for this sample.

Since the limit state condition for this sample for the discontinuities no. 1, 2, 3, 4, 5, 7, 8, 10, 11, 12, 13 is  $JRC=9.8$ , the failure probability for these discontinuities is 68.07%.

Comparing the sample number 1 and 3 indicates that if for constant  $JCS=70$  MPa, basic friction angle= $33^{\circ}$  the cohesion increased from 50 kPa to 100 kPa, the failure probability decreases about 8.2 %.

*4. =150 kPa, basic friction angle= $33^{\circ}$  and  $JCS=70$  MPa*

In this case, cohesion of 150 kPa was added to run the model for different JRC values. For  $C=150$  kPa, the JRCs of 7, 7.4, 8 and 9 were given to the model. For  $JRC=9$  all the discontinuities' displacements are negligible. However, for JRCs of 7.4 and 8 only discontinuity no. 1 displaced more than estimated peak shear displacement. However, when the JRC reduces to lower than 7.4, all the discontinuities except discontinuity no. 6, 9 and 14 displaced considerably. Therefore, if it is assumed that the shear displacement greater than peak is called as failure, for discontinuity no. 1  $JRC=9$  and for others except discontinuity no.6, 9 and 14 the  $JRC=7.4$  can be considered as the limit state criterion for this sample. Table 5.9 indicates the shear displacement, peak shear displacement and the values calculated for  $K_s$  for each discontinuity.

Since the limit state condition for this sample for the discontinuities no. 1, 2, 3, 4, 5, 7, 8, 10, 11, 12, 13 is  $JRC=7.4$ , the failure probability for these discontinuities is 41.47%.

Comparing the samples number 3 and 4 indicates that if for constant  $JCS=70$  MPa, basic friction angle= $33^{\circ}$  the cohesion increased from 100 kPa to 150 kPa, the failure probability decreases about 26.6. %.

Table 5.8 Shear deformation, peak shear deformation of Barton model for friction= 33, cohesion=0.15 MPa, JCS=70 MPa and different JRC values and joint shear stiffness for each discontinuity

68

*Not in Equilibrium state		** In Equilibrium state		Discontinuity ID														State
Cohesion	JCS	JRC															State	
			1	2	3	4	5	6	7	8	9	10	11	12	13	14		
0.15 MPa	70	7	$\bar{\delta}$ (m)	1.31	1.306	0.49	0.17	0.153	0.0001	0.16	0.15	3.2e-5	0.131	0.469	0.155	0.148	0.0001	*
			$\bar{\delta}_{peak}$ (m)	0.005	0.032	0.034	0.031	0.031	0.03	0.065	0.062	0.055	0.023	0.024	0.029	0.02	0.02	
			Ks (MPa/m)	31.45	6.33	7.73	10.4	12.9	15.52	3.84	4.78	4.6	9.37	10.51	11.39	18.72	24.64	
		7.4	$\bar{\delta}$ (m)	0.011	0.001	8.7e-5	0.0003	0.002	7e-5	0.001	0.002	1.5e-5	0.002	7.6e-5	0.001	0.002	6.8e-5	**
			$\bar{\delta}_{peak}$ (m)	0.005	0.033	0.035	0.032	0.032	0.031	0.066	0.063	0.056	0.026	0.024	0.029	0.020	0.020	
			Ks (MPa/m)	31.07	6.3	7.74	10.43	12.95	15.6	3.83	4.79	4.6	9.36	10.51	11.42	18.8	24.77	
		8	$\bar{\delta}$ (m)	0.012	0.001	5.9e-5	1.7e-5	0.002	6.3e-5	2.9e-5	0.001	1.6e-5	0.001	5.8e-5	1.7E-5	0.001	6.1e-5	**
			$\bar{\delta}_{peak}$ (m)	0.005	0.033	0.036	0.033	0.032	0.032	0.068	0.065	0.058	0.027	0.025	0.03	0.021	0.021	
			Ks (MPa/m)	30.58	6.27	7.77	10.5	13.07	15.76	3.84	4.82	4.62	9.37	10.53	11.51	18.96	25.03	
		9	$\bar{\delta}$ (m)	4.8e-6	8e-5	1.6e-5	2.2e-5	2.8e-5	3.3e-5	1.9e-5	2.2e-5	6.9e-6	2e-5	1.1e-5	2e-5	3e-5	4.e-5	**
			$\bar{\delta}_{peak}$ (m)	0.006	0.035	0.038	0.034	0.034	0.034	0.072	0.069	0.061	0.028	0.026	0.032	0.022	0.022	
			Ks (MPa/m)	29.9	6.31	7.97	10.86	13.56	16.38	3.93	4.97	4.73	9.57	10.77	11.9	19.66	26.01	

5.  $C=200$  kPa, basic friction angle= $33^{\circ}$  and  $JCS=70$  MPa

In this case, cohesion of 200 kPa was added to run the model for different JRC values. For  $C=200$  kPa, the JRCs of 2, 5 and 7 were given to the model. For  $JRC=7$  all the discontinuities' displacements are negligible. However, for JRCs of 5 only discontinuity no. 1 displaced more than estimated peak shear displacement. However, when the JRC reduces to lower than 5, all the discontinuities except discontinuity no. 6, 9 and 14 displaced considerably. Therefore, if it is assumed that the shear displacement greater than peak is called as failure, for discontinuity no. 1  $JRC=7$  and for others except discontinuity no. 6, 9 and 14 the  $JRC=5$  can be considered as the limit state criterion for this sample. Table 5.9 indicates the shear displacement, peak shear displacement and the values calculated for  $K_s$  for each discontinuity.

Since the limit state condition for this sample for the discontinuities no. 1, 2, 3, 4, 5, 7, 8, 10, 11, 12, 13 is  $JRC=5$ , the failure probability for these discontinuities is 18.88% Lognormal distribution of JRC value.

Comparing the sample number 1 and 5 indicates that if for constant  $JCS=70$  MPa, basic friction angle= $33^{\circ}$  the cohesion increased from 50 kPa to 200 kPa, the failure probability decreases about 57%.

Table 5.9 Shear deformation, peak shear deformation of Barton model for friction= 33, cohesion=0.2 MPa, JCS =70 and different JRC values and joint shear stiffness for each discontinuity

		*Not in Equilibrium state	** In Equilibrium state	Discontinuity ID														
Cohesion	JCS	JRC		1	2	3	4	5	6	7	8	9	10	11	12	13	14	State
			0.2 kPa	70	2	$\delta(m)$	<b>0.596</b>	<b>0.596</b>	<b>0.531</b>	<b>0.178</b>	<b>0.156</b>	0.0002	<b>0.166</b>	<b>0.140</b>	4e-5	<b>0.132</b>	<b>0.519</b>	<b>0.164</b>
$\delta_{peak}(m)$	0.004	0.021				0.023	0.021	0.02	0.02	0.043	0.041	0.037	0.017	0.016	0.019	0.013	0.013	
$K_s$ (MPa/m)	59.98	10.85				11.88	14.95	17.62	20.42	6.02	7.05	7.16	14.91	16.53	16.33	25.96	32.23	
5	$\delta(m)$	<b>0.042</b>			0.002	4.7e-5	0.001	0.003	0.0001	0.002	0.003	2e-5	0.002	2.8e-5	0.002	0.003	8.3e-5	**
	$\delta_{peak}(m)$	0.005			0.029	0.031	0.028	0.027	0.027	0.058	0.056	0.05	0.023	0.021	0.0257	0.018	0.018	
	$K_s$ (MPa/m)	45.09			8.44	9.58	12.33	14.78	17.34	4.82	5.77	5.75	11.89	13.23	13.48	21.67	27.42	
7	$\delta(m)$	3e-6			0.0004	6.6e-5	5e-5	5.3e-5	6.2e-5	4e-5	4e-5	1e-5	2e-5	2.4e-5	4.5e-5	6e-5	6.2e-5	**
	$\delta_{peak}(m)$	0.005			0.032	0.034	0.031	0.03	0.0304	0.065	0.062	0.055	0.026	0.024	0.0287	0.02	0.0198	
	$K_s$ (MPa/m)	41.06			7.9	9.2	12.01	14.53	17.17	4.61	5.59	5.51	11.32	12.64	13.13	21.25	27.17	

6.  $C=300$  kPa, basic friction angle= $33^{\circ}$  and  $JCS=70$  MPa

In this case, cohesion of 300 kPa was added to run the model for different JRC values. For  $C=300$  kPa, for  $JRC=2$  all the discontinuities' displacements are negligible and since the range of JRC is greater than 2, therefore, for  $C=300$  the model can be called safe and failure probability is zero. Table 5.10 indicates the shear displacement, peak shear displacement and the values calculated for  $K_s$  for each discontinuity.

7.  $C=500$  kPa, basic friction angle= $33^{\circ}$  and  $JCS=70$  MPa

In this case, cohesion of 500 kPa was added to run the model for different JRC values. For  $C=500$  kPa, for  $JRC=2$  and 5 all the discontinuities' displacements are negligible and since the range of JRC is greater than 2, therefore, for  $C=500$  the model can be called safe and failure probability is zero. Table 5.11 indicates the shear displacement, peak shear displacement and the values calculated for  $K_s$  for each discontinuity.

Table 5.10 Shear deformation, peak shear deformation of Barton model for friction= 33, cohesion=0.3 MPa, JCS=70 MPa, JRC=2 values and joint shear stiffness for each discontinuity

*Not in Equilibrium state		** In Equilibrium state		Discontinuity ID														State
Cohesion	JCS	JRC		1	2	3	4	5	6	7	8	9	10	11	12	13	14	
0.3 kPa	70	2	$\delta$ (m)	2 e-6	0.0002	1.7e-5	1e-5	0.0004	8e-5	9e-6	0.0004	2e-5	0.0004	2e-5	1e-5	0.0004	7e-5	**
			$\delta_{peak}$ (m)	0.003	0.021	0.02	0.02	0.02	0.02	0.04	0.04	0.037	0.017	0.02	0.019	0.013	0.013	
			Ks (MPa/m)	89.01	15.59	16.32	19.82	22.59	25.4	8.35	9.49	9.89	20.81	22.9	21.6	33.61	39.88	

Table 5.11 Shear deformation, peak shear deformation of Barton model for friction= 33, cohesion=0.5 MPa, JCS=70 MPa, JRC=2 and 5 values and joint shear stiffness for each discontinuity

*Not in Equilibrium state		** In Equilibrium state		Discontinuity ID														State
Cohesion	JCS	JRC		1	2	3	4	5	6	7	8	9	10	11	12	13	14	
0.5 kPa	70	2	$\bar{\delta}$ (m)	1.1e-6	2.5e-5	2.8e-6	7e-6	1.3e-5	1e-5	5e-6	8e-6	3e-6	6e-6	2e-6	6e-6	1e-5	1.9e-5	**
			$\bar{\delta}_{peak}$ (m)	0.003	0.02	0.022	0.02	0.02	0.02	0.043	0.041	0.037	0.017	0.016	0.019	0.013	0.013	
			Ks (MPa/m)	147.1	25.1	25.2	29.55	32.53	35.35	13.01	14.35	15.35	32.62	35.81	32.15	48.92	55.19	
		5	$\bar{\delta}$ (m)	1.4e-6	3.3e-5	3.9e-6	8.7e-6	1.6e-5	9e-6	6e-6	1e-5	3e-6	7e-6	3e-6	8e-6	2e-5	1.2e-5	**
			$\bar{\delta}_{peak}$ (m)	0.005	0.03	0.03	0.028	0.027	0.027	0.06	0.06	0.05	0.023	0.021	0.026	0.018	0.018	
			Ks (MPa/m)	109.5	18.96	19.42	23.12	25.79	28.37	9.99	11.16	11.8	24.97	27.47	25.17	38.64	44.39	

8.  $C=50$  kPa, basic friction angle= $30^{\circ}$  and  $JCS=70$  MPa

In this case, cohesion of 50 kPa was added to run the model for different JRC values. For  $C=50$  kPa and friction angle of  $30^{\circ}$  the JRCs of 11 and 12 were given. For JRCs, equal to 12 the shear displacements are very low in comparison to the allowable peak shear displacement. However, when the JRC reduces to 11, the discontinuity no. 1, 2, 3, 4, 5, 7, 8, 10, 11, 12 and 13 displaces considerably. However, discontinuity no. 6, 9 and 14 displaced less than estimated peak shear displacement. Therefore, if it is assumed that the shear displacement greater than peak is called as failure,  $JRC=12$  can be considered as the limit state criterion for our discontinuity when  $C=50$  kPa and friction angle of  $30^{\circ}$ . Table 5.12 indicates the shear displacement, peak shear displacement and the values calculated for  $K_s$  for each discontinuity.

Since the limit state condition for this sample for discontinuities no. 1, 2, 3, 4, 7, 11, 12 is  $JRC=12$ , the failure probability for these discontinuities is 81.75%.

Comparing the sample number 1 and 8 indicates that if for constant  $JCS=70$  MPa, cohesion= 50 kPa the basic friction angle reduced from  $33^{\circ}$  to  $30^{\circ}$ , the failure probability increases about 5 %.

Table 5.12 Shear deformation, allowable peak shear deformation for cohesion=0.05 MPa, JCS=70 and different JRC values and joint shear stiffness for each discontinuity

		*Not in Equilibrium state		** In Equilibrium state		Discontinuity ID														
Cohesion	Friction	JCS	JRC															State		
				1	2	3	4	5	6	7	8	9	10	11	12	13	14			
0.05 MPa	30	70	11	$\bar{\delta}$ (m)	1.70	1.70	0.69	0.167	0.142	0.0002	0.16	0.136	4e-5	0.118	0.646	0.159	0.135	0.0001	*	
				$\bar{\delta}_{peak}$ (m)	0.006	0.037	0.04	0.036	0.035	0.035	0.075	0.072	0.064	0.03	0.027	0.033	0.023	0.023		
				Ks (MPa/m)	12.65	3.495	5.29	7.84	10.37	13.04	2.53	3.482	3.09	6.03	6.91	8.62	14.8	20.82		
	12	$\bar{\delta}$ (m)	1.1e-5	0.0002	6e-5	1e-5	0.001	5e-5	8e-5	0.002	1e-5	0.002	9e-5	4e-5	0.002	5.e-5	*			
		$\bar{\delta}_{peak}$ (m)	0.006	0.0381	0.04	0.037	0.036	0.036	0.08	0.074	0.066	0.031	0.028	0.034	0.024	0.024				
		Ks (MPa/m)	13.54	3.773	5.67	8.363	11.0	13.77	2.72	3.72	3.31	6.49	7.42	9.2	15.73	21.98				

9.  $C=100$  kPa, basic friction angle= $30^0$  and  $JCS=70$  MPa

In this case, cohesion of 100 kPa was added to run the model for different JRC values. For  $C=100$  kPa and friction angle of  $30^0$  the JRCs of 10, 10.5 and 11 were given. For JRCs, equal to 10.5 and 11 the shear displacements are very low in comparison to the allowable peak shear displacement. However, when the JRC reduces to 10, the discontinuity no. 1, 2, 3, 4, 7, 8, 10, 11 and 12 displaces considerably. However, discontinuity no. 6, 9, 13 and 14 displaced less than estimated peak shear displacement. Therefore, if it is assumed that the shear displacement greater than peak is called as failure,  $JRC= 10.5$  can be considered as the limit state condition when  $C=100$  kPa and friction angle of  $30^0$ . Table 5.13 indicates the shear displacement, peak shear displacement and the values calculated for  $K_s$  for each discontinuity.

Since the limit state condition for this sample for discontinuities no. 1, 2, 3, 4, 7, 11, 12 is  $JRC=10.5$ , the failure probability for these discontinuities is 73.08%.

Comparing the sample number 3 and 9 indicates that if for constant  $JCS=70$  MPa, cohesion= 100 kPa the basic friction angle reduced from  $33^0$  to  $30^0$ , the failure probability increased about 4-5%.

Comparing the sample number 8 and 9 indicates that if for constant  $JCS=70$  MPa, basic friction angle= $30^0$  the cohesion increased from 50 kPa to 100 kPa, the failure probability decreases about 8%.

10.  $C=150$  kPa, basic friction angle= $30^0$  and  $JCS=70$  MPa

In this case, cohesion of 150 kPa was added to run the model for different JRC values. For  $C=150$  kPa and friction angle of  $30^0$  the JRC of 9.5 was given. For  $JRC=9.5$  the shear displacements for all discontinuities except

no. 1 are very low in comparison to the allowable peak shear displacement. Therefore, if it is assumed that the shear displacement greater than peak is called as failure, JRC= 10 can be considered as the limit state condition when  $C=150$  kPa and friction angle is  $30^{\circ}$ . Table 5.14 indicates the shear displacement, peak shear displacement and the values calculated for  $K_s$  for each discontinuity.

Since the limit state condition for this sample for discontinuities no. 1, 2, 3, 4, 7, 11, 12 is JRC=10, therefore, the failure probability for these discontinuities is 69.57%.

Comparing the sample number 4 and 10 indicates that if for constant JCS=70 MPa, cohesion= 150 kPa the basic friction angle reduced from  $33^{\circ}$  to  $30^{\circ}$ , the failure probability increases about 28%.

Comparing the sample number 9 and 10 indicates that if for constant JCS=70 MPa, basic friction angle= $30^{\circ}$  the cohesion increased from 100 kPa to 150 kPa, the failure probability decreases about 3%.

Table 5.13 Shear deformation, allowable peak shear deformation for cohesion=0.1 MPa, friction angle=30, JRC=70 MPa, different JRC values and joint shear stiffness for each discontinuity

66		*Not in Equilibrium state		** In Equilibrium state		Discontinuity ID														State
		Cohesion	JCS	Friction	JRC	1	2	3	4	5	6	7	8	9	10	11	12	13	14	
0.1 MPa	70	30	10	$\delta$ (m)	0.59	0.146	0.189	0.165	0.019	0.0001	0.156	0.017	3e-5	0.014	0.19	0.159	0.016	8e-5	**	
				$\delta_{peak}$ (m)	0.006	0.036	4e-2	0.035	0.034	0.034	0.073	0.07	0.062	0.029	0.026	0.032	0.022	0.022		
				Ks (MPa/m)	20.66	4.69	6.29	8.85	11.3	13.89	3.07	4.01	3.71	7.42	8.40	9.71	16.29	22.10		
	10.5	$\delta$ (m)	0.0001	0.0003	7e-5	0.0001	0.002	6.3e-5	0.0003	0.002	2e-5	0.002	9.8e-5	0.0003	0.002	6e-5	**			
		$\delta_{peak}$ (m)	0.006	0.036	0.039	0.036	0.035	0.035	0.074	0.071	0.063	0.029	0.027	0.033	0.023	0.023				
		Ks (MPa/m)	20.74	4.76	6.41	9.03	11.53	14.16	3.13	4.08	3.78	7.55	8.56	9.90	16.62	22.53				
	11	$\delta$ (m)	6e-6	8.2e5	8e-5	8e-5	0.0002	5.1e-5	9.5e-5	0.0002	1e-5	0.0002	7.9e-5	9.8e-5	0.0002	5e-5	**			
		$\delta_{peak}$ (m)	0.006	0.037	0.04	0.036	0.035	0.035	0.075	0.072	0.064	0.03	0.027	0.033	0.023	0.023				
		Ks (MPa/m)	20.92	4.85	6.55	9.23	11.78	14.46	3.19	4.18	3.86	7.71	8.74	10.12	16.98	23				

Table 5.14 Shear deformation, allowable peak shear deformation for cohesion=0.15 MPa, JCS=70 MPa, JRC=9.5 and joint shear stiffness for each discontinuity

1001

*Not in Equilibrium state		** In Equilibrium state		Discontinuity ID															
Cohesion	JCS	Friction	JRC		1	2	3	4	5	6	7	8	9	10	11	12	13	14	State
0.15 MPa	70	30	9.5	$\delta$ (m)	0.013	0.0005	5e-5	0.0002	0.001	7e-5	0.0003	0.001	2e-5	0.001	6e-5	0.0003	0.001	6.4e-5	**
				$\delta_{peak}$ (m)	0.006	0.035	0.037	0.034	0.033	0.033	0.071	0.068	0.06	0.028	0.03	0.031	0.022	0.022	
				Ks (MPa/m)	29.55	6.051	7.46	10.04	12.44	14.9	3.69	4.62	4.44	9.02	10.13	11	18.1	23.7	

11.  $C=200$  kPa, basic friction angle= $30^{\circ}$  and  $JCS=70$  MPa

In this case, cohesion of 200 kPa was added to run the model for different JRC values. For  $C=200$  kPa and friction angle of  $30^{\circ}$  the JRCs of 5, 7 and 8 were given. For JRCs, equal to 8 the shear displacements are very low in comparison to the allowable peak shear displacement. However, when the JRC reduces to 7 only discontinuity 1 and when JRC reduces to 8, the discontinuity no. 1, 3, 4, 7, 11 and 12 displaces considerably. However, discontinuity no. 6, 9, 13 and 14 displaced less than estimated peak shear displacement. Therefore, if it is assumed that the shear displacement greater than peak is called as failure,  $JRC=8$  for discontinuity 1 and  $JRC=7$  for others can be considered as the limit state condition when  $C=200$  kPa and friction angle of  $30^{\circ}$ . Table 5.15 indicates the shear displacement, peak shear displacement and the values calculated for  $K_s$  for each discontinuity.

Since the limit state condition for this sample for discontinuities no. 1, 3, 4, 7, 11 and 12 is  $JRC=7$ , therefore, the failure probability for these discontinuities is 30.08%.

Comparing the sample number 5 and 11 indicates that if for constant  $JCS=70$  MPa, cohesion= 200 kPa the basic friction angle reduced from  $33^{\circ}$  to  $30^{\circ}$ , the failure probability increases about 27%.

Comparing the sample number 10 and 11 indicates that if for constant  $JCS=70$  MPa, basic friction angle= $30^{\circ}$  the cohesion increased from 150 kPa to 200 kPa, the failure probability decreases about 39.5%.

Table 5.15 Shear deformation, allowable peak shear deformation for cohesion=0.2 MPa, friction angle=30, JCS=70 MPa and different JRC and joint shear stiffness for each discontinuity

		*Not in Equilibrium state	** In Equilibrium state	Discontinuity ID														State	
Cohesion	JCS	Friction	JRC	1	2	3	4	5	6	7	8	9	10	11	12	13	14		
				0.2 MPa	70	30	5	$\bar{\delta}$ (m)	<b>0.29</b>	0.016	<b>0.064</b>	<b>0.18</b>	0.012	0.0001	<b>0.16</b>	0.01	2.8.e-5	0.007	<b>0.073</b>
$\bar{\delta}_{peak}$ (m)	0.005	0.029	0.030					0.028	0.027	0.027	0.058	0.056	0.05	0.023	0.021	0.026	0.018	0.018	
Ks (MPa/m)	44.86	8.3	9.28					11.82	14.04	16.35	4.68	5.55	5.58	11.57	12.86	12.91	20.64	25.82	
7	$\bar{\delta}$ (m)	<b>0.039</b>	0.001				0.0001	0.0002	0.002	8.1e-5	0.0003	0.002	1.7e-5	0.001	9.1e-5	0.0004	0.002	7e-5	* *
	$\bar{\delta}_{peak}$ (m)	0.005	0.032				0.034	0.031	0.030	0.03	0.065	0.062	0.055	0.026	0.024	0.029	0.02	0.02	
	Ks (MPa/m)	40.76	7.73				8.86	11.44	13.73	16.11	4.45	5.35	5.31	10.96	12.21	12.51	20.13	25.46	
8	$\bar{\delta}$ (m)	3e-6	0.0004				6.1e-5	6.5e-5	9.1e-5	6.3e-5	7e-5	0.0001	1.3e-5	9e-5	3.9e-5	6.3e-5	9.6e-5	6.3e-5	* *
	$\bar{\delta}_{peak}$ (m)	0.005	0.033				0.036	0.032	0.032	0.032	0.068	0.065	0.058	0.027	0.025	0.03	0.021	0.021	
	Ks (MPa/m)	39.4	7.58				8.8	11.43	13.78	16.22	4.41	5.33	5.27	10.84	12.09	12.5	20.19	25.65	

102

12.  $C=300$  kPa, basic friction angle= $30^0$  and  $JCS=70$  MPa

In this case, cohesion of 300 kPa was added to run the model for different JRC values. For  $C=300$  kPa and friction angle of  $30^0$  the JRCs of 3 and 5 were given. For  $JRC=5$  all the discontinuities' displacements are negligible. However, for  $JRC=3$  only discontinuity no. 1 displaced more than estimated peak shear displacement Table 5.16 indicates the shear displacement, peak shear displacement and the values calculated for  $K_s$  for each discontinuity.

Since the limit state condition for this sample for discontinuity no. 1 is  $JRC=3$ , therefore, the failure probability for these discontinuities is 0.297%.

Comparing the sample number 6 and 12 indicates that if for constant  $JCS=70$  MPa, cohesion= 300 kPa the basic friction angle reduced from  $33^0$  to  $30^0$ , the failure probability increases about 0.3%. Comparing the sample number 11 and 12 indicates that if for constant  $JCS=70$  MPa, basic friction angle= $30^0$  the cohesion increased from 200 kPa to 300 kPa, the failure probability decreases about 30%.

13.  $C=500$  kPa, basic friction angle= $33^0$  and  $JCS=70$  MPa

In this case, cohesion of 500 kPa was added to run the model for different JRC values. For  $C=500$  kPa and friction angle of  $30^0$  for  $JRC=2$  and 5 all the discontinuities' displacements are negligible and since the range of JRC is greater than 2, therefore, for  $C=500$  kPa the model can be called safe and failure probability is zero. Table 5.17 indicates the shear displacement, peak shear displacement and the values calculated for  $K_s$  for each discontinuity.

Table 5.16 Shear deformation, allowable peak shear deformation for cohesion=0.3 MPa, friction angle=30, JCS=70 MPa and different JRC and joint shear stiffness for each discontinuity

		*Not in Equilibrium state		** In Equilibrium state		Discontinuity ID														
Cohesion	JCS	Friction	JR			1	2	3	4	5	6	7	8	9	10	11	12	13	14	State
				0.3 MPa	70	30	3	$\bar{\delta}$ (m)	<b>0.025</b>	0.0006	2.9e-5	3.6e-5	0.0006	8.3e-5	4e-5	0.0006	12e-5	0.0005	2.e-5	
$\bar{\delta}_{peak}$ (m)	0.004	0.024	0.026					0.023	0.023	0.023	0.049	0.047	0.042	0.019	0.018	0.022	0.015	0.015		
Ks (MPa/m)	77.93	13.65	14.27					17.29	19.65	22.02	7.3	8.28	8.65	18.21	20.08	18.84	29.27	34.57		
5	$\bar{\delta}$ (m)	2e-6	0.0002		4e-6	4.4e-6	6.1e-5	7.4e-5	9e-6	5.3e-5	2e-5	2.9e-5	1e-5	3e-6	7e-5	7.2e-5				
	$\bar{\delta}_{peak}$ (m)	0.005	0.029		0.03	0.028	0.027	0.027	0.058	0.056	0.05	0.023	0.021	0.026	0.018	0.018				
	Ks (MPa/m)	66.32	11.8		12.56	15.42	17.71	20.02	6.41	7.35	7.6	15.93	17.61	16.81	26.3	31.47				

Table 5.17 Shear deformation, allowable peak shear deformation for cohesion=0.5 MPa, JCS=70 MPa, JRC=2 and joint shear stiffness for each discontinuity

		*Not in Equilibrium state		** In Equilibrium state		Discontinuity ID														
105	Cohesion	JCS	Friction	JRC		1	2	3	4	5	6	7	8	9	10	11	12	13	14	State
	0.5 MPa	70	30	2	$\bar{\delta}$ (m)	1e-6	3e-5	3e-6	7e-6	1e-5	1 e-5	4.e-6	9e-6	3 e-6	6e-6	2e-6	6e-6	1e-5	2e-5	**
					$\bar{\delta}_{peak}$ (m)	0.003	0.021	0.023	0.02	0.02	0.02	0.043	0.04	0.037	0.017	0.016	0.019	0.013	0.013	
Ks (MPa/m)					146.9	24.94	24.89	29.	31.73	34.3	12.87	14.1	15.18	32.3	35.43	31.55	47.82	53.44		

## 5.5 Discussions of the Results

The main variable considered in this study was JRC, however, the effect of other influential parameters such as friction angle; JCS and cohesion of the filled material have been studied. The samples were planned such a way that can be also considered as the effect of weathering process on discontinuity planes. As the weathering reduces the values of friction angle, JCS and the strength of filled material the sample also considers the status of the structure in future.

The analysis indicated that the increase of cohesion decreases the displacements and failure probability of the structure. Also, reduction of basic friction angle and joint wall compressive strength increase the probability of failure and increases the displacement. Figure 5.36 indicates the reduction of failure probability due to increase in cohesion value for both basic friction angle of  $33^{\circ}$  and  $30^{\circ}$ .

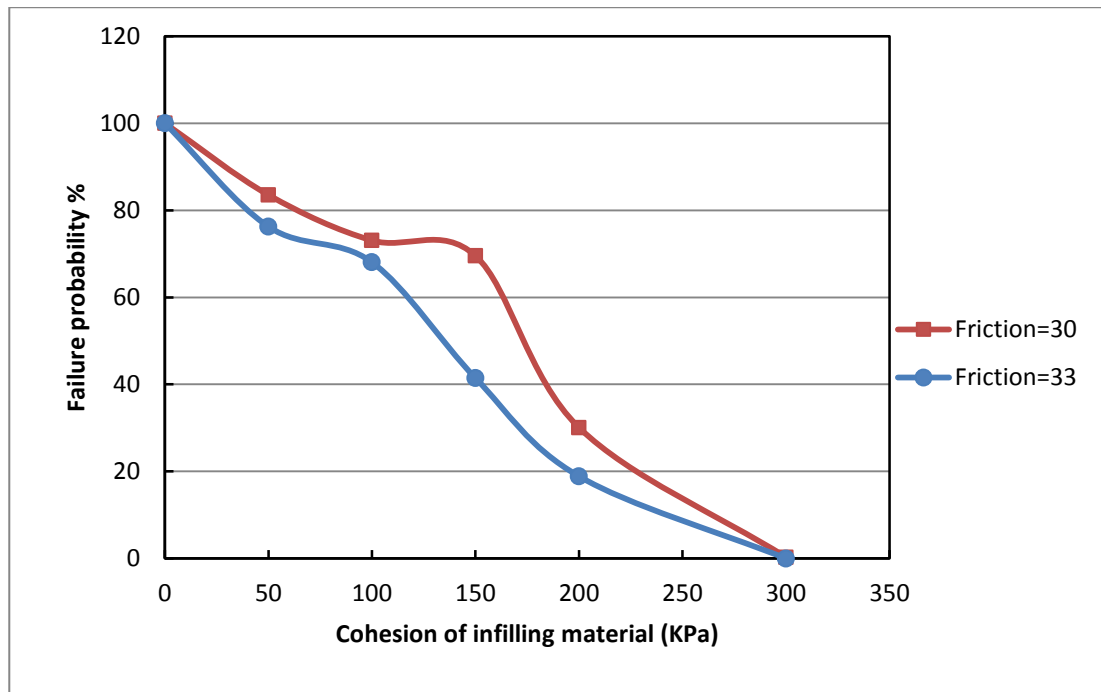


Figure 5.35 Relation of cohesion and failure probability of discontinuities

The model was run about thirty five times for different cohesion, basic friction angle, JCS and JRC values. The shear displacements of each discontinuity for all of the runs were fitted appropriate distribution functions and the probability of  $\bar{\delta} > \bar{\delta}_{peak}$  was calculated that is the probability of failure of corresponding discontinuity. Figure 5.37 indicates that Beta distribution is fitted for shear displacement of discontinuity no. 1.

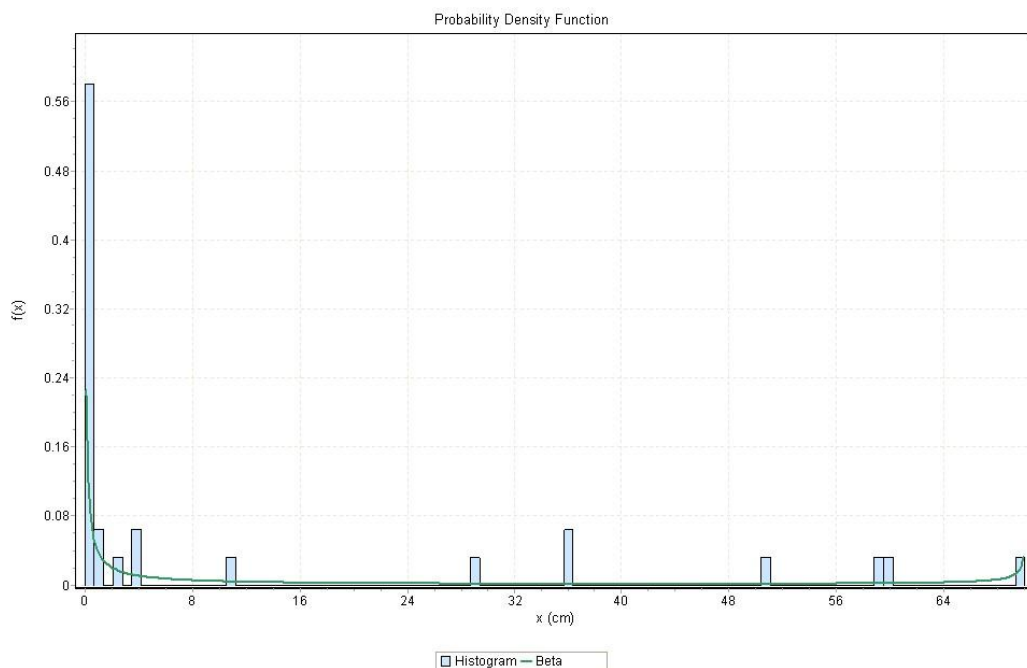


Figure 5.36 Beta distribution of shear displacement of discontinuity no. 1

Figures C.1 to C.13 indicate the statistical distribution of shear displacement for discontinuities no. 2 to 14 respectively in Appendix C. Since for different cohesion, basic friction angle, JCS and JRC values the  $\bar{\delta}_{peak}$  changes, the average, minimum and maximum value of  $\bar{\delta}_{peak}$  were used to calculate the probability of failure and its corresponding reliability index. Table 5.18 indicates the average, minimum and maximum value of  $\bar{\delta}_{peak}$ , the probability of failure and its corresponding reliability index for each discontinuity.

The  $\beta < 1$  is considered as failure state therefore, the discontinuities no. 1, 2, 10, 11 and 13 have failed and other discontinuities are in safe condition.

Table 5.18 Failure probability and corresponding reliability index ( $\beta$ ) for average, minimum and maximum value of  $\delta_{peak}$  for each discontinuity

The ID of discontinuities	1	2	3	4	5	6	7	8	9	10	11	12	13	14
$\delta_{Peak\_Avreage}$ (cm)	0.52	3.22	3.42	3.13	3.07	3.07	6.56	6.26	5.57	2.58	2.42	2.89	2.00	2.00
$\delta_{Peak\_min}$ (cm)	0.3	2	2	2	2	2	4	4	3.7	1.7	1.6	1.9	1.3	1.3
$\delta_{Peak\_max}$ (cm)	0.7	4	4	4	3.9	3.9	8.3	8	7.1	3.14	3	3.7	2.5	2.5
$P_f(\delta > \delta_{Peak\_Avreage})$ %	47.683	21.26	3.798	4.445	4.586	0	4.813	5.04	0	11.765	12.463	10.602	18.576	0
$P_f(\delta > \delta_{Peak\_max})$ %	50.458	23.84	9.175	9.175	9.175	0	2.86	2.86	0	16.925	17.781	15.421	22.593	0
$P_f(\delta > \delta_{Peak\_min})$ %	46.15	20.04	2.86	2.86	2.995	0	3.817	3.958	0	9.814	10.242	8.402	16.704	0
$\beta_{Ave}$	<b>0.058</b>	<b>0.797</b>	1.7746	1.7012	1.6864	INF	1.663	1.641	INF	1.1868	1.1521	1.248	<b>0.8936</b>	INF
$\beta_{min}$	-	<b>0.712</b>	1.3301	1.3301	1.3301	INF	1.902	1.9018	INF	<b>0.9571</b>	<b>0.9237</b>	1.0185	<b>0.7523</b>	INF
$\beta_{max}$	<b>0.0966</b>	<b>0.84</b>	1.9018	1.9018	1.8815	INF	1.772	1.7556	INF	1.2922	1.2679	1.3785	<b>0.9659</b>	INF

## CHAPTER VI

### CONCLUSIONS AND RECOMMEDATIONS

In this research, three dimensional distinct element method using 3DEC software was combined with probability for analyzing of rock slope stability and a probabilistic-numerical approach has been developed. To follow the methodology practically, a slope containing a historical grave in Amasya Turkey was selected to be analyzed. The shear behavior of rock discontinuities were modeled plastically by applying Barton models.

The model of rock slope was given different samples of realization of random variables such as JRC, cohesion, JCS and friction angle. The analysis indicated that if the calcite as the infilling of the rock joints is not included in the analysis, even for a higher value for JRC the slope fails tremendously. Although there are some failed discontinuities in the field, however, tremendous failure of model without calcite effect is not rational. To take the infilling material's effect into account it was assumed that the joint planes are controlled by both frictional parameters like JRC and cohesion of the calcite. For this purpose, for different values of cohesion the model was run for different JRC values. The variation of JRC and cohesion were controlling the stability of the model. Because, both the shear strength and joint shear stiffness are dependent on JRC and cohesion.

In field, it was observed that the weathering of the infilling material might be one of the parameters that were affected the instabilities, to model this, the range of 50 kPa to 500 kPa was considered to be used in the model. Model

was totally stable for cohesion bigger than 300 kPa even for lower JRC like JRC=2. However, by decreasing the cohesion the discontinuity displaced considerably.

To calculate the failure probability of the discontinuities, for definite values of JCS, friction angle and cohesion, the realization of JRC (random variable) was varied and the stability condition of the structure was investigated. And for any sample, the failure probability of each discontinuity was obtained.

The study indicated that for constant values of cohesion, basic friction angle and joint wall's compressive strength the reduction of joint roughness (JRC) increases the failure probability, because, it reduces the strength and the shear stiffness of the joint plane and consequently the increment of shear displacement. Furthermore, the reduction of compressive strength of joint wall (JCS) from 70 MPa to 50 MPa increases the failure probability about 8%. Also, the reduction of basic friction angle from  $33^{\circ}$  to  $30^{\circ}$  for constant cohesion and JCS values increases the failure probability from 0.3% to 28% depending on the different pairs of cohesion and JCS.

Moreover, results indicated that for a case in which the JCS=70 MPa and the basic friction angle is  $33^{\circ}$ , reduction of cohesion of infilling material due to weathering from 300 kPa to 200, 150, 100 and 50 kPa has increased the failure probability about 18.88%, 41.47%, 68.07% and 76.26% respectively, which indicates that during time the weathering that reduces the strength of the infilling material increases the possibility of failure of the slope. Also, for a case in which the JCS=70 MPa and the basic friction angle is  $30^{\circ}$ , reduction of cohesion of infilling material due to weathering from 500 kPa to 300, 200, 150, 100 and 50 kPa has increased the failure probability about 0.3%, 30%, 69.57%, 73% and 81.75% respectively. These results confirm the importance of the weathering effects on stability of the slope.

In this research, the thirty five realizations of random variables were run; the shear displacements of each discontinuity for all thirty five realizations were fitted appropriate distribution functions. For shear displacements lower than estimated peak shear displacement by Barton formula the failure probability and the corresponding reliability index ( $\beta$ ) were obtained. By assuming  $\beta < 1$  as failure, the discontinuities number 1, 2, 10 and 11 are in failure state. Also, the results indicated that the discontinuities number 6, 9 and 14 are totally safe.

For future works the following recommendations are made:

The study area has a complex topography; therefore it is difficult to construct the model of the rock slope. According to the Barton models the strength parameters of the rock discontinuity are dependent on normal stress acting on the discontinuities. Therefore, the shape of the model affects the normal stress and shear stress therefore the behavior of the rock discontinuities. Thus, application of the laser scanning and the photogrammetric methods to achieve more precise results is recommended.

In this study, some of Barton models were used to model the behavior of the rock discontinuities, and the Barton models were equalized by Coulomb model that assumes perfect Elastic-Plastic behavior. However, it is clear that the Joint Shear Stiffness is nonlinear and the strength of the rock discontinuity reduces to lower than its peak value after shearing. Also, existence of asperities on the discontinuity plane increases the role of dilatancy in stability of the discontinuities. Therefore, it is recommended to use other models of Barton in future works.

Moreover, in this thesis the role of bedding planes were omitted, due to the heavy computational load in DEM, however, the existence of bedding planes reduce the size of blocks that influences the displacement of the blocks.

Thus, it is also recommended to apply more joint sets to derive more realistic results.

## REFERENCES

- Akgun H, Kockar M,K. (2004). Design of anchorage and assessment of the stability of openings in silty, sandy limestone: A case study in Turkey. *International Journal of Rock Mechanics and Mining Science*(41), 37-49.
- Ang, A.H.S., and Tang, W.H. (1984). *Probability Concepts in Engineering Planning and Design* (Vol. 2). John Wiley and Sons.
- Bobet, A. (2010). Numerical Methods in Geomechanics. *The Arabian Journal for Science and Engineering*, 35, 27-48.
- Bolle, A. Bonnechere F. and Arnould R. (1987). A probabilistic approach of slope stability in fractured rock . *Proc. of 6th. Cong. Rock mechanics*, (pp. 301-303).
- Brady, B. (1987). *Boundary Element and Linked Methods for Underground Excavation*. England: Allen and Unwin.
- Chen S. G., and Zhao J. (n.d.). A Study of UDEC Modelling for Blast Wave Propagation in Jointed Rock Masses. *International Journal of Rock Mechanics and Mining Sciences*, 35(1), 93-99.
- Cundall P. A. (1988). Formulation of a Three-Dimensional Distinct Element Model - Part I. A Scheme to Detect and Represent Contacts in a System Composed of Many Polyhedral Blocks. *International Journal of Rock Mechanics and Mining Sciences*, 25(3), 107-116.
- Ditlevsen, O. (1981). *Uncertainty modeling: with applications to multidimensional civil engineering systems*. New York: McGraw-Hill.
- Duzgun, H.S.B. and Bhasin R.K. (2009). Probabilistic Stability Evaluation of Oppstadhornet Rock Slope Norway. *Rock Mechanics and Rock Engineering*, 42, 724-749.
- Duzgun, H.S.B. and Özdemir, A.,. (2006). Landslide Risk Assessment and Management by Decision Analytical Procedure for Dereköy, Konya, Turkey. *Natural Hazards*, 39, 245-263.

- Duzgun, H.S.B., Yucemen M.S. and Karpuz, C. (2003). A Methodology for Reliability-Based Design of Rock Slopes. *Rock Mechanics and Rock Engineering*, 36, 95-120.
- Duzgun, H.S.B., Yucemen M.S. and Pasamehmetoglu, A.G. (1995). Plane Failure Analysis of Rock Slopes: A Reliability Approach. *International Journal of Surface Mining and Reclamation*, 9, 1-6.
- Duzgun, S. (1994). *Plane Failure Analysis of Rock Slopes. A Reliability Approach*. Ankara, Turkey: M.Sc. Thesis, Middle East Technical University.
- Eberhardt E. , Stead D., and Coggan J. S. (2004). Numerical Analysis of Initiation and Progressive Failure in Natural Rock Slopes - The 1991 Randa Rockslide. *International Journal of Rock Mechanics and Mining Sciences*, 41, 69-87.
- Esterhuizen, G. (1990). Combined Point Estimate and Monte Carlo Techniques for the Analysis of Wedge Failure in Rock Slope. *Proc. of Static and Dynamic Considerations in Rock Engineering Symp*, (pp. 125-132).
- Fadlelmula Fadlelseed, M. M. (2007). *Probabilistic modeling of failure in rock slopes*. Turkey: M.Sc. Thesis, Middle East Technical University.
- Feng P. . (1997). *Probabilistic treatment of the sliding wedge*. Manitoba, Canada: M.Sc. Thesis, University of Manitoba Winnipeg,.
- Goodman, R.E., Bray, J.W. (1976). Toppling of rock slopes. *Proceedings of the Specialty Conference on Rock Engineering for Foundations and Slopes* (pp. 201–223). New York: American Society of Civil Engineers.
- Griffiths, D.V., Fenton, G.A., and Tveten, D.E. (2005). Probabilistic passive earth pressure analysis by the Random Finite Element Method. *Proceedings of the 11th International Conference on Computer Methods and Advances in Geomechanics (IACMAG 05)*.4, pp. 235-249. Turin: Patron Editore.
- Griffiths, D.V., Fenton, G.A., and Tveten, D.E.,. (2005). Probabilistic passive earth pressure analysis by the Random Finite Element Method. *Proceedings of the 11th International Conference on Computer Methods and Advances in Geomechanics (IACMAG 05)*.4, pp. 235-249. Turin: Patron Editore, Bologna.
- Hammah, R.E., Yacoub, T.E. and Curran, J.H. (2009). Numerical modeling of slope uncertainty due to rock mass jointing. *Proceedings of the International Conference on Rock Joints and Jointed Rock Masses*, (pp. 7-8). Tucson, Arizona.

- Harr, M. (1981). *Mecanique des milieux formes de particules*. Lausanne: Presses Polytechniques Romandes.
- Hasofer, A.M. and Lind, N.C. (1974). Exact and invariant second-moment code format . *J.Engrg. Mech., ASCE*, 100(1), 111-121.
- Heok, E. and Bray, J.W. (1974). *Rock Slope Engineering*. London: Institution of Mining and Metallurgy.
- Heuze F. E. and Morris J. P. ., (2007). "Insights Into Ground Shock in Jointed Rocks and the Response of Structures Therein. *International Journal of Rock Mechanics and Mining Sciences*, 44(5), 647-676.
- Jimenez-Rodriguez, R., Sitar, N. (2007). Rock wedge stability analysis using system reliability methods. *Rock Mechanics ad Rock Engineering*, 40(4), 419-427.
- Jimenez-Rodriguez, R., Sitar, N., Chacón,J. (2006). System reliability approach to rock slope stability. *International Journal of Rock Mechanics and Mining Sciences*, 847-859.
- Jing L. (2003). A Review of Techniques, Advances and Outstanding Issues in Numerical Modeling for Rock Mechanics and Rock Engineering. *International Journal of Rock Mechanics and Mining Sciences*, 283–353.
- Jing L. and Hudson J.A. (2002). Numerical Methods in Rock Mechanics. *International Journal of Rock Mechanics and Mining Sciences*, 39, 409–427.
- Kim, H.S., Major, G. and Ross, B.D.,. (1978). A General Probabilistic Analysis for 3-Dimensional Wedge Failure. Nevada: Proc. 19th. U.S. Symp. Rock Mechanics, Makay School of Mines.
- Kimance, J. P., Howe, J. H. (1991). A combined geostatistical and first order second moment reliability analysis of slopes in Kaolinsed granite. *Proc., 7th ISRM Congress on Rock Mechanics*, (pp. 905–911).
- Kirsten, H. (1983). Significance of the Probability of Failure in Rock Slopes. *The Civil Engineer iin South Africa*, 25(1), 17-27.
- Krahn J. (2003). The 2001 R.M. Hardy Lecture: The limits of limit equilibrium analyse. *Canadian Geotechnical Journal*, 40(3), 643-660.
- Li, D., Zhou, C. Lu,W., Jiang, Q. (2009). A system reliability approach for evaluating stability of rock wedges with correlated failure modes. *Computers and Geotechnics*, 36(8), 1298-1307.
- Low, B. (1997). Reliability analysis of rock wedges. *Journal of Geotechnical and Geoenvironmental Engineerin*, 123(6), 498-505.

- Low, B. K. (1996). Practical probabilistic approach using spreadsheet . *ASCE Geotechnical Special Publication No. 58, Proc., Uncertainty in the geologic Environment – From Theory to Practice*, (pp. 1284-1302 ). Madison, Wisconsin.
- Low, B. K. (1997). Reliability analysis of rock wedges. *J. Geotech. Geoenviron. Engng.*, 123(6), 498–505.
- Low, B. K. (2003). Practical Probabilistic Slope Stability Analysis . *Proceedings, Soil and Rock America 2003. 12th Panamerican Conference on Soil Mechanics and Geotechnical Engineering and 39th U.S. Rock Mechanics Symposium*, (pp. 2777-2784).
- Major, G., Kim, H.S. and Ross, B.D. (1978). Application of Monte Carlo Techniques to Stability Analysis. Nevada: Proc. 19th. U.S. Symp. Rock Mechanics, Makay School of Mines.
- Moarefvand P., Verdel. (2008). The probabilistic distinct element method. *International Journal for Numerical and Analytical Methods in Geomechanics*, 32(5), 559-577.
- Morris, P., and Stoter, H.J. (1983). Open Cut Slope Design Using Probabilistic Methods. *Proc. Of 5th ISRM Symposium*, 1.
- Muralha, J. & Trunk, U. (1993). Stability of Rock Slopes-Evaluation of Failure Probabilities by the Monte Carlo and First Order Reliability Methods. *Proc. of Assessment and Prevention of Failure Phenomena in Rock Engineering*, (pp. 759-765).
- Nguyen, V.U., and Chowdhurym R.N. (1985). Simulation for Risk Analysis with Correlated Variables. *Geotechnique*, 35.
- Pande G. N. , Beer G., and Williams J. R. . (1990). *Numerical Methods in Rock Mechanics* . West Sussex, England: John Wiley and Sons, Ltd.
- Park, H., West, T.R. . (2001). Development of a probabilistic approach for rock wedge failure. *Engineering Geology*, 59 (3-4), 233-251.
- Potyondy D. O. and Cundall P. A. (2004). A Bonded-Particle Model for Rock. *International Journal of Rock Mechanics and Mining Sciences*, 41, 1329-1364.
- Priest, S.D., and Brown, E.T. (1983). Probabilistic Stability Analysis of Variable Rock Slopes. *Trans. Instn. Min. Metal.*, 92.
- Rosenbleuth, E. (1975). Point Estimates for Probability Moments. *70(10)*. Proc. Nat. Acad. Sci. USA .

- Scavia, C., Barla, G., Bernaudo, V. (1990). Probabilistic stability analysis of block toppling failure in rock slopes. *International Journal of Rock Mechanics and Mining Sciences*, 26(7), 465-478.
- Tan X.H. and J. Wang. (2009). Finite element reliability analysis of slope stability. *J Zhejiang Univ Sci*, 645–652.
- Tatone, B.S.A., Grasselli, G. (2010). ROCKTOPPLE: A spreadsheet-based program for probabilistic block-toppling analysis . *Computers and Geosciences*, 98-114.
- Taylor L. M. and Preece D. S. . (1992). Simulation of Blasting Induced Rock Motion Using Spherical Element Models . *Engineering Computations*, 9, 243-252.
- Wang J.C., W.H. Tan, S.W. Feng and R.D. Zhou. (2000). Reliability analysis of an open pit coal mine slope. *International Journal of Rock Mechanics and Mining Sciences*, 37(4), 715–721.
- Wong. F. S., 1985. , “Slope stability and response surface method. *Journal of Geotechnical and Geoenvironmental Engineering ASC*, 111(1), 32–53.

## APPENDIX A:

### FIELD DATA AND LABORATORIAL TESTS RESULTS

Table A 1 Goodness of Fit for JRC

#	Distribution	Kolmogorov Smirnov		Anderson Darling		Chi-Squared	
		Statistic	Rank	Statistic	Rank	Statistic	Rank
1	Beta	0.16392	38	1.2237	29	8.0468	15
2	Burr	0.13243	21	0.77664	8	9.131	33
3	Burr (4P)	0.1263	6	0.97813	23	8.6035	18
4	Cauchy	0.16028	36	2.6619	43	7.4223	14
5	Chi-Squared	0.15296	33	1.235	30	2.8066	3
6	Chi-Squared (2P)	0.15791	34	2.1859	40	3.1091	5
7	Dagum	0.12937	15	0.72097	2	8.977	21
8	Dagum (4P)	0.13139	18	0.79967	10	9.1487	35
9	Erlang	0.25747	52	5.012	47	6.5777	13
10	Erlang (3P)	0.17329	41	1.337	34	3.4504	6
11	Error	0.19426	45	2.0759	38	5.9883	9
12	Error Function	0.75982	59	79.811	59	235.33	54

Table A.1- Continued

13	Exponential	0.31373	55	5.7404	51	17.634	49
14	Exponential (2P)	0.23558	50	3.4396	45	13.259	47
15	Fatigue Life	0.11729	3	0.75408	5	8.9858	23
16	Fatigue Life (3P)	0.12787	10	0.80935	15	9.1142	31
17	Frechet	0.15904	35	1.0889	28	1.1611	1
18	Frechet (3P)	0.13343	23	0.80527	13	9.1387	34
19	Gamma	0.13238	20	0.97779	22	9.1114	29
20	Gamma (3P)	0.12885	14	0.87724	21	9.6288	41
21	Gen. Extreme Value	0.13358	24	0.84422	17	9.3357	38
22	Gen. Gamma	0.14214	27	1.0451	26	8.9287	20
23	Gen. Gamma (4P)	0.12884	13	0.87348	20	9.6262	40
24	Gen. Pareto	0.12705	7	8.2742	54	N/A	
25	Gumbel Max	0.14445	30	1.0362	25	2.9899	4
26	Gumbel Min	0.2493	51	5.7022	50	12.058	46
27	Hypersecant	0.19713	46	2.5946	42	6.1971	12
28	Inv. Gaussian	0.13812	25	0.87273	19	9.0077	24
29	Inv. Gaussian (3P)	0.12827	11	0.80594	14	9.1117	30
30	Johnson SB	0.16085	37	8.3345	55	N/A	
31	Kumaraswamy	0.17223	40	5.2802	49	N/A	
32	Laplace	0.21735	49	3.0293	44	11.674	45

Table A.1 Continued							
33	Levy	0.44556	58	11.545	57	49.255	53
34	Levy (2P)	0.37176	56	7.659	53	24.874	51
35	Log-Gamma	0.11446	2	0.75633	6	8.7722	19
36	Log-Logistic	0.11233	1	0.75169	4	9.2407	37
37	Log-Logistic (3P)	0.12984	16	0.73749	3	8.9831	22
38	Log-Pearson 3	0.12838	12	0.80377	12	9.1195	32
39	Logistic	0.18212	43	2.3688	41	6.1619	11
40	Lognormal	0.12482	5	0.76242	7	9.0087	25
41	Lognormal (3P)	0.12999	17	0.80311	11	9.1002	27
42	Nakagami	0.14525	31	1.2567	31	9.8069	42
43	Normal	0.18546	44	2.129	39	6.1104	10
44	Pareto	0.37477	57	10.356	56	21.051	50
45	Pareto 2	0.29285	54	5.1989	48	30.011	52
46	Pearson 5	0.1216	4	0.72086	1	1.4887	2
47	Pearson 5 (3P)	0.13178	19	0.79548	9	9.1008	28
48	Pearson 6	0.13333	22	0.84084	16	9.1644	36
49	Pearson 6 (4P)	0.12705	8	0.8675	18	9.6236	39
50	Pert	0.14225	28	1.0808	27	8.3214	16
51	Power Function	0.20182	47	6.1407	52	N/A	
52	Rayleigh	0.14892	32	1.2586	32	9.8586	44

Table A.1 Continued							
53	Rayleigh (2P)	0.16862	39	1.5638	36	5.8743	8
54	Reciprocal	0.28924	53	4.7135	46	14.717	48
55	Rice	0.14328	29	1.2611	33	9.8121	43
56	Student's t	0.93053	60	153.64	60	1778.3	55
57	Triangular	0.1801	42	1.5744	37	5.6397	7
58	Uniform	0.20597	48	13.243	58	N/A	
59	Weibull	0.13934	26	1.5409	35	9.0295	26
60	Weibull (3P)	0.12775	9	0.98776	24	8.5932	17
61	Johnson SU	No fit					

Table A 2 Goodness of Fit for Schmidt Hammer value

	Distribution	Kolmogorov Smirnov		Anderson Darling		Chi-Squared	
		Statistic	Rank	Statistic	Rank	Statistic	Rank
1	Beta	0.10715	9	0.86793	5	10.287	4
2	Burr	0.12986	18	1.438	12	14.414	15
3	Burr (4P)	0.10077	5	0.89059	7	10.18	3
4	Cauchy	0.15071	26	3.6726	37	22.403	28

Table A.2 Continued							
5	Chi-Squared	0.19053	44	3.9163	40	24.898	32
6	Chi-Squared (2P)	0.15857	27	2.122	22	14.894	21
7	Dagum	0.08591	2	0.55436	1	5.3414	2
8	Dagum (4P)	0.6739	58	100.07	58	313.43	53
9	Erlang	0.20104	47	3.517	36	22.849	29
10	Erlang (3P)	0.1389	19	1.7239	18	15.043	23
11	Error	0.12885	17	1.3678	11	13.779	14
12	Error Function	0.94086	59	521.59	60	N/A	
13	Exponential	0.38022	52	20.011	52	93.524	49
14	Exponential (2P)	0.30743	51	15.285	50	55.683	46
15	Fatigue Life	0.17918	37	3.1686	32	31.134	38
16	Fatigue Life (3P)	0.14439	23	1.6948	17	14.891	17
17	Frechet	0.22001	50	5.8142	46	27.672	34
18	Frechet (3P)	0.19033	43	8.8348	48	N/A	
19	Gamma	0.17397	35	2.8411	28	33.046	41
20	Gamma (3P)	0.14918	25	1.7966	21	14.893	19
21	Gen. Extreme Value	0.08925	3	4.699	43	N/A	
22	Gen. Gamma	0.16911	31	2.5228	26	28.793	36
23	Gen. Gamma (4P)	0.11685	13	1.1314	10	10.756	7

Table A.2 Continued							
24	Gen. Pareto	0.11727	14	12.198	49	N/A	
25	Gumbel Max	0.20684	48	5.3378	45	37.801	44
26	Gumbel Min	0.10773	10	0.9709	9	5.2253	1
27	Hypersecant	0.17136	32	2.7557	27	23.664	31
28	Inv. Gaussian	0.18956	42	3.9743	41	25.011	33
29	Inv. Gaussian (3P)	0.14257	20	1.6544	16	14.933	22
30	Johnson SB	0.08186	1	4.6906	42	N/A	
31	Kumaraswamy	0.1055	8	0.84197	3	10.314	6
32	Laplace	0.19969	46	3.8253	39	27.711	35
33	Levy	0.55744	57	28.689	56	190.4	52
34	Levy (2P)	0.4958	56	21.994	54	109.75	50
35	Log-Gamma	0.18261	40	3.4312	34	31.428	39
36	Log-Logistic	0.17803	36	3.1913	33	32.036	40
37	Log-Logistic (3P)	0.12089	15	1.6091	14	16.527	24
38	Log-Pearson 3	0.10171	6	0.86383	4	13.068	11
39	Logistic	0.15889	28	2.2115	24	11.535	10
40	Lognormal	0.17367	34	2.9871	31	30.372	37
41	Lognormal (3P)	0.14622	24	1.7513	20	14.718	16
42	Nakagami	0.15973	29	2.9237	30	16.528	25
43	Normal	0.14327	21	1.6368	15	14.893	20

Table A.2 Continued							
44	Pareto	0.40952	54	24.803	55	35.379	43
45	Pareto 2	0.39654	53	21.439	53	117.62	51
46	Pearson 5	0.17985	38	3.7343	38	34.649	42
47	Pearson 5 (3P)	0.1641	30	2.1772	23	18.999	26
48	Pearson 6	0.18098	39	2.8939	29	23.023	30
49	Pearson 6 (4P)	0.14431	22	1.7451	19	14.892	18
50	Pert	0.10807	11	0.88244	6	13.104	12
51	Power Function	0.18634	41	3.4831	35	19.703	27
52	Rayleigh	0.20989	49	7.3287	47	56.528	47
53	Rayleigh (2P)	0.19638	45	5.0816	44	44.758	45
54	Reciprocal	0.42406	55	31.557	57	63.937	48
55	Rice	0.1725	33	2.2236	25	13.757	13
56	Student's t	0.99237	60	514.78	59	54758.0	54
57	Triangular	0.09243	4	0.69343	2	11.308	9
58	Uniform	0.11028	12	16.407	51	N/A	
59	Weibull	0.12659	16	1.4756	13	10.309	5
60	Weibull (3P)	0.10193	7	0.93133	8	11.251	8
61	Johnson SU	No fit					

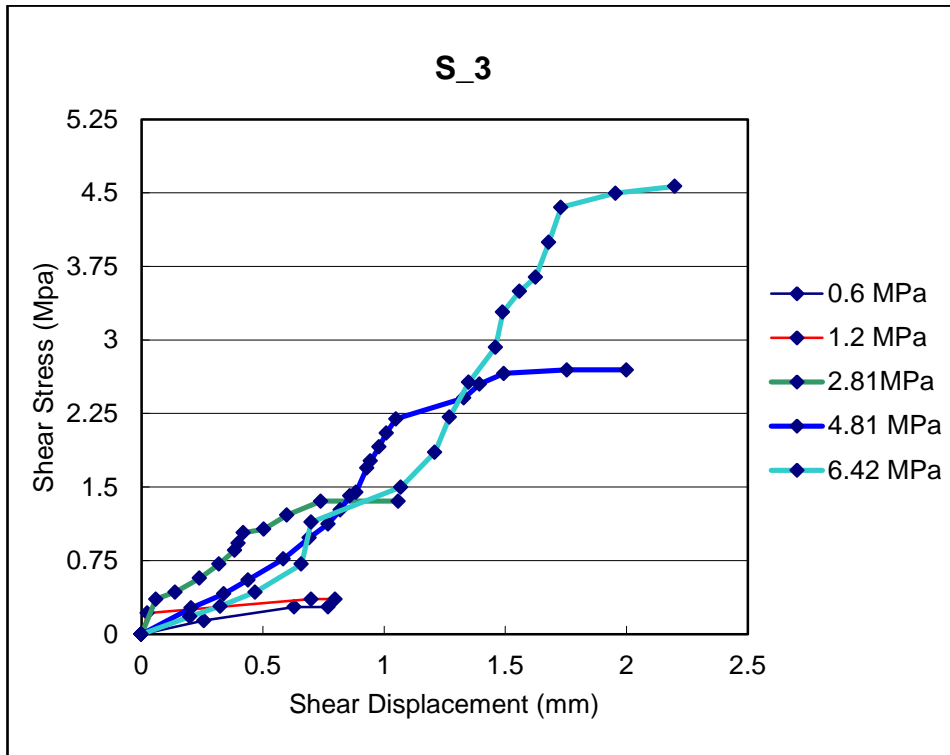


Figure A. 1 Shear stress/displacement curves for joint sample named as S\_3 for different normal stress values

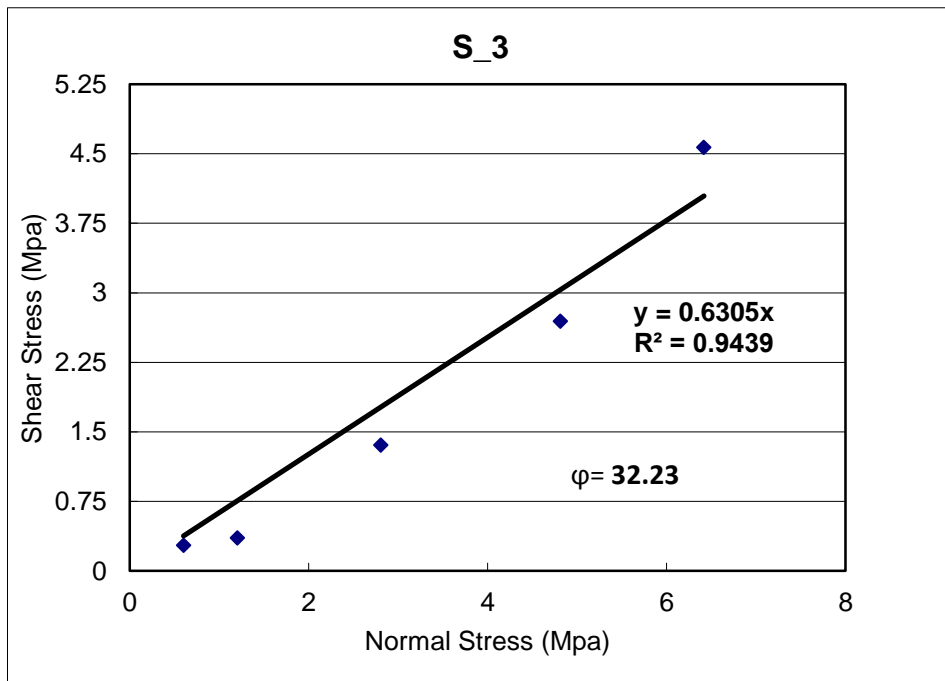


Figure A. 2 Relation of Shear and Normal stresses acted on joint of S\_3 to obtain the basic friction angle of joint surface which is 32.23

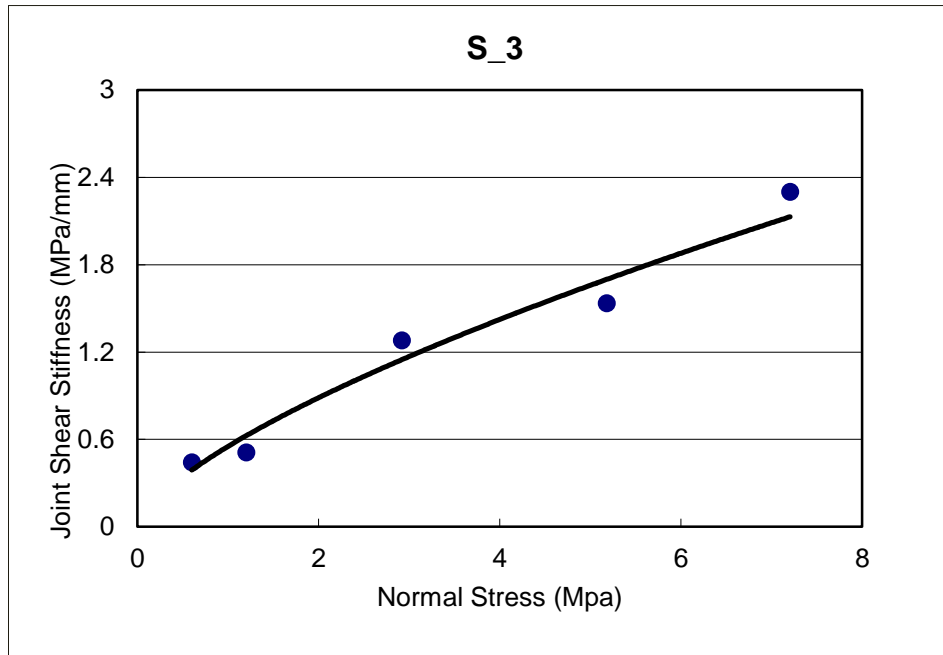


Figure A. 3 Dependency of joint shear stiffness (Ks) to normal stress in smooth joint plane (S\_3)

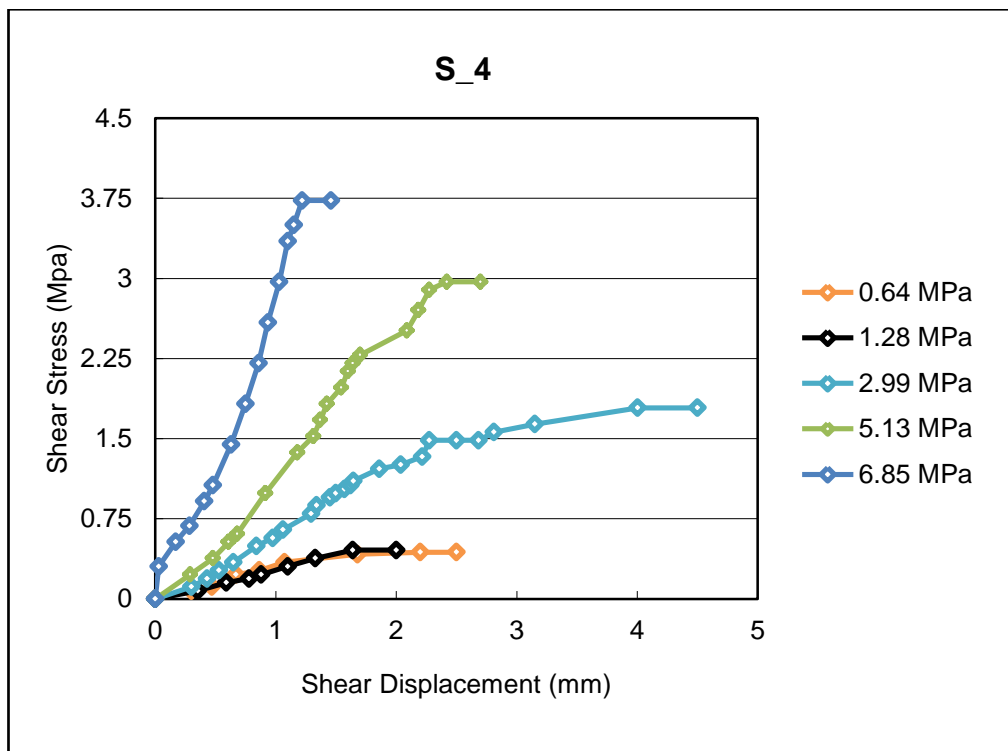


Figure A.4 Shear stress/displacement curves for joint sample named as S\_4 for different normal stress values

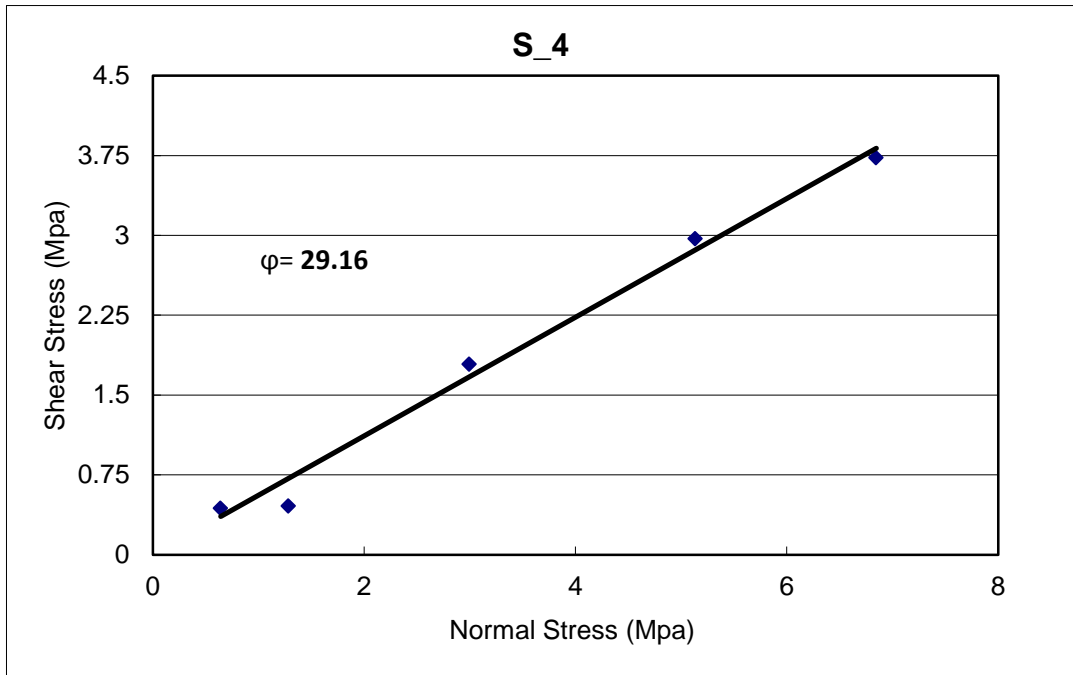


Figure A.5 Relation of Shear and Normal stresses acted on joint of S\_4 to obtain the basic friction angle of joint surface which is 29.16

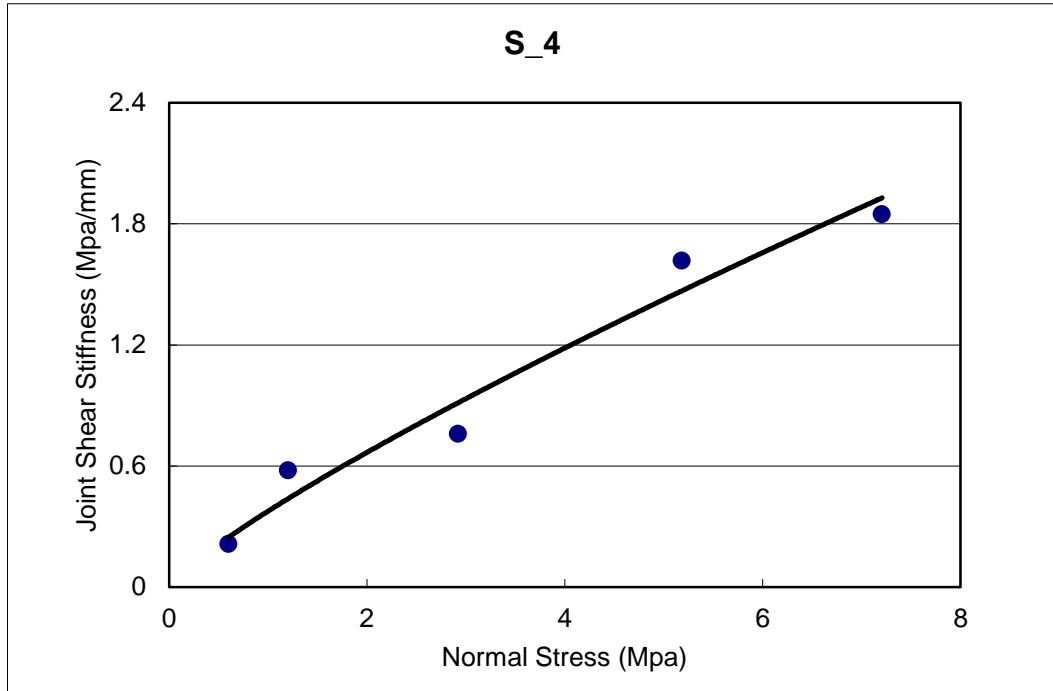


Figure A.6 Dependency of joint shear stiffness (Ks) to normal stress in smooth joint plane (S\_4)

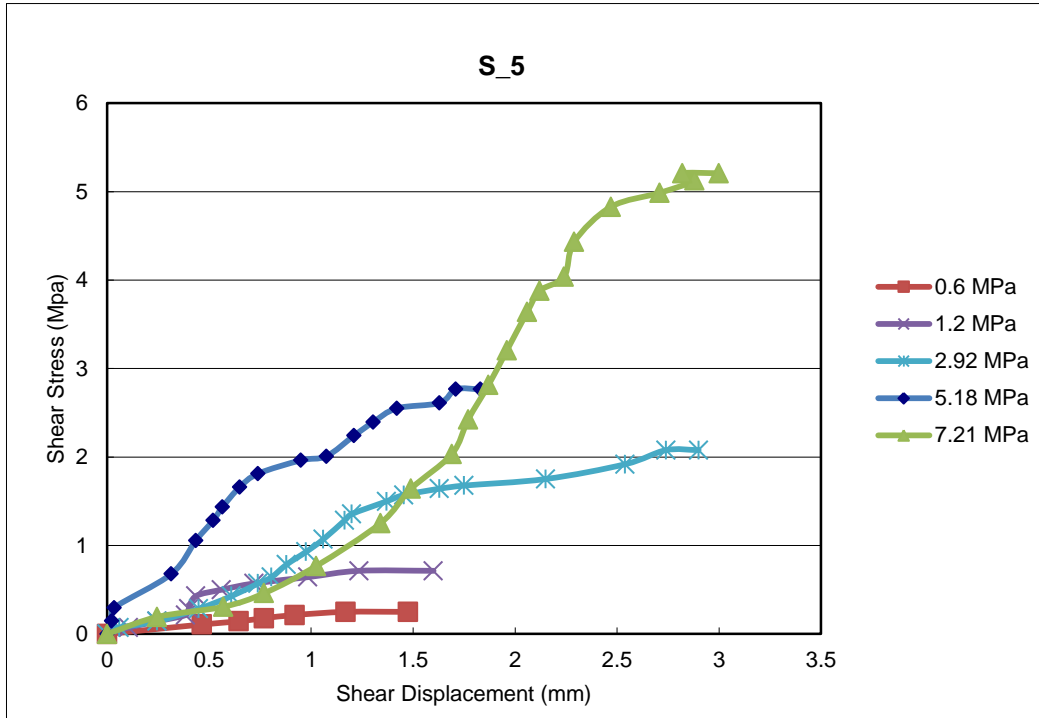


Figure A.7 Shear stress/displacement curves for joint sample named as S\_5 for different normal stress values

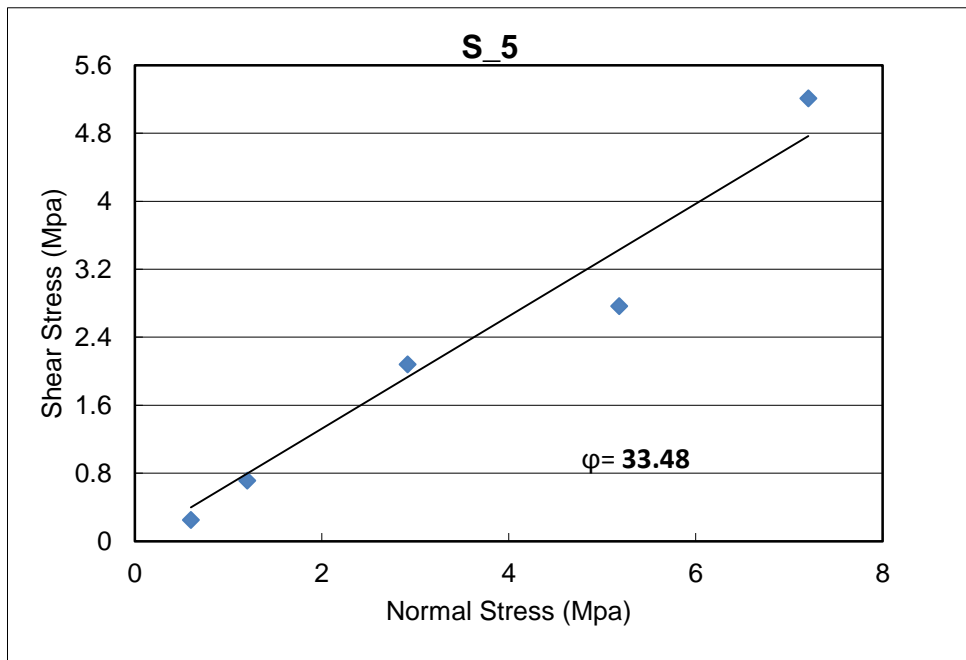


Figure A.8 Relation of Shear and Normal stresses acted on joint of S\_5 to obtain the basic friction angle of joint surface which is 33.48

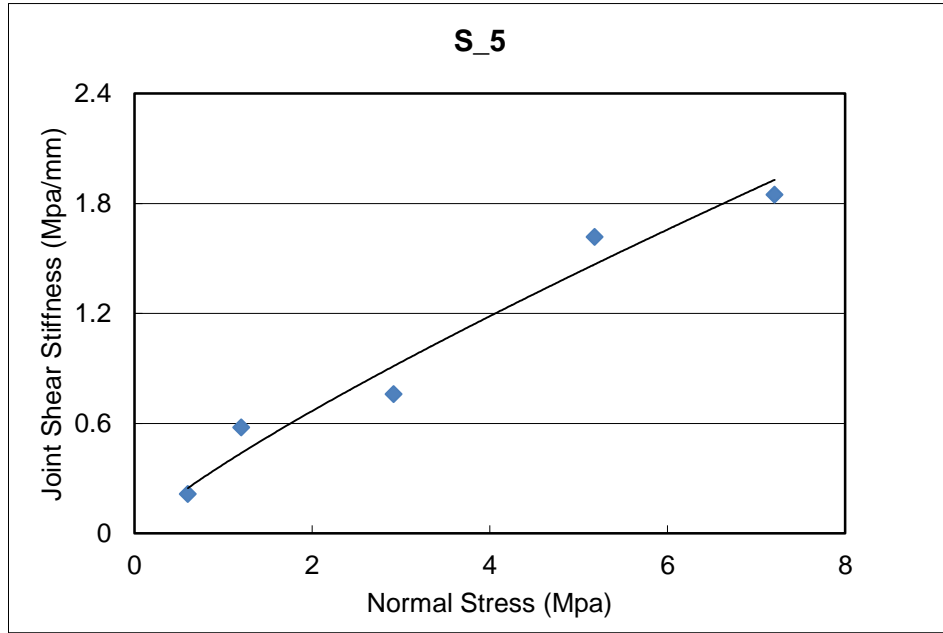


Figure A.9 Dependency of joint shear stiffness ( $K_s$ ) to normal stress in smooth joint plane (S\_5)

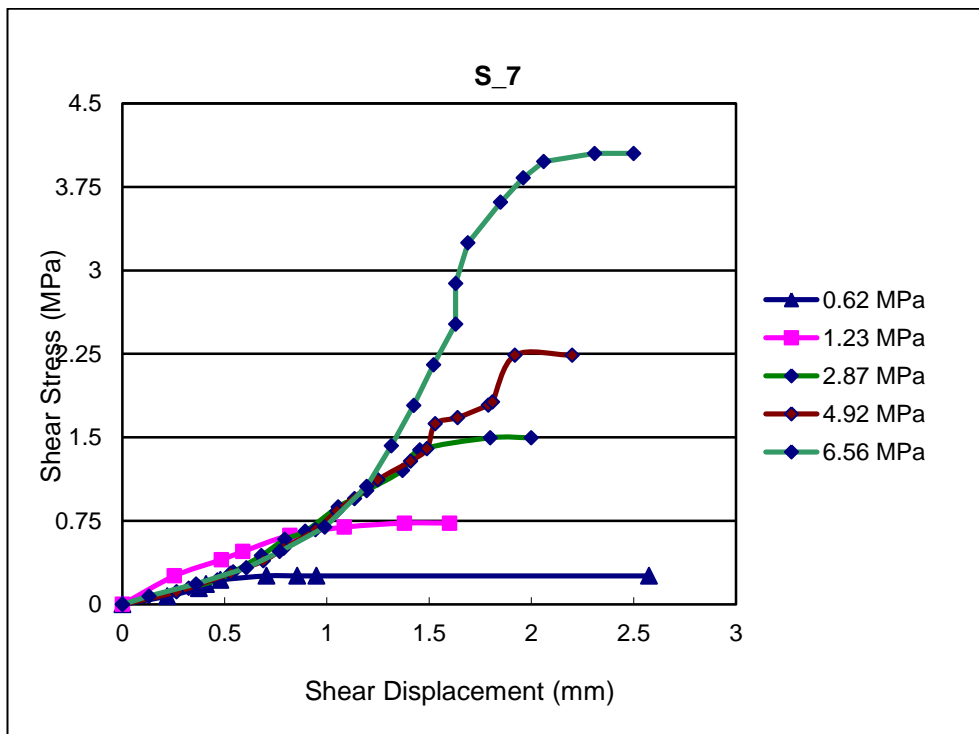


Figure A.10 Shear stress/displacement curves for joint sample named as S\_5 for different normal stress values

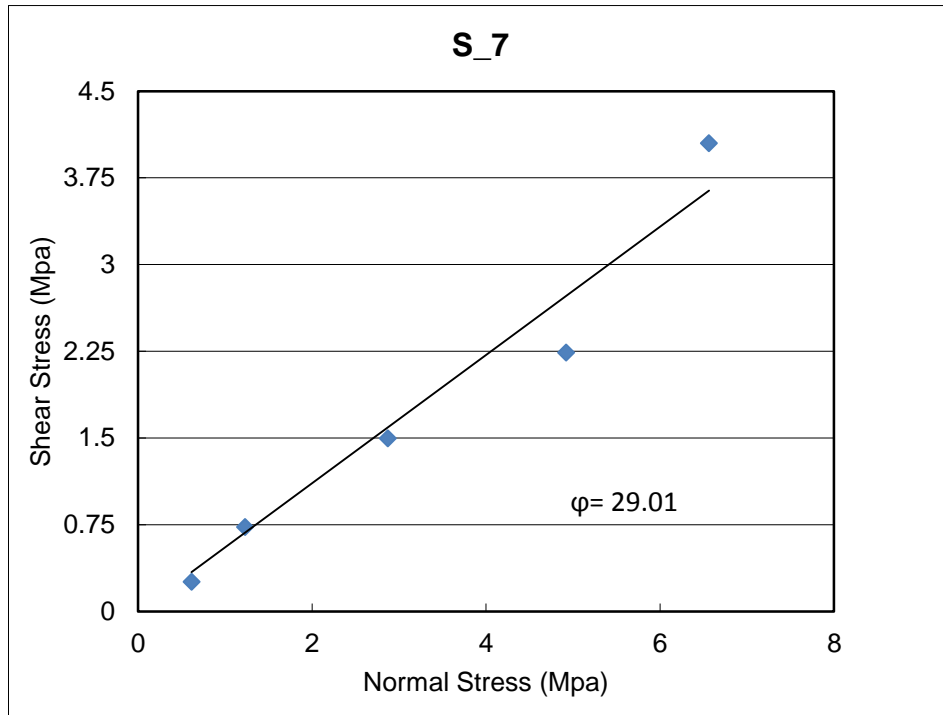


Figure A.11 Relation of Shear and Normal stresses acted on joint of S\_5 to obtain the basic friction angle of joint surface which is 29

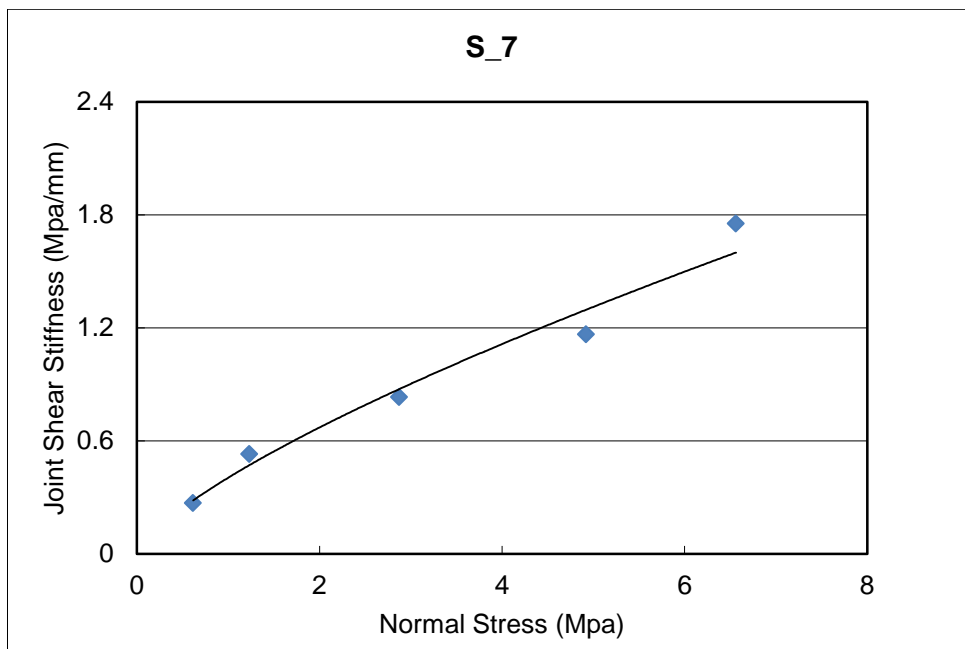


Figure A. 12 Dependency of joint shear stiffness (Ks) to normal stress in smooth joint plane (S\_5)

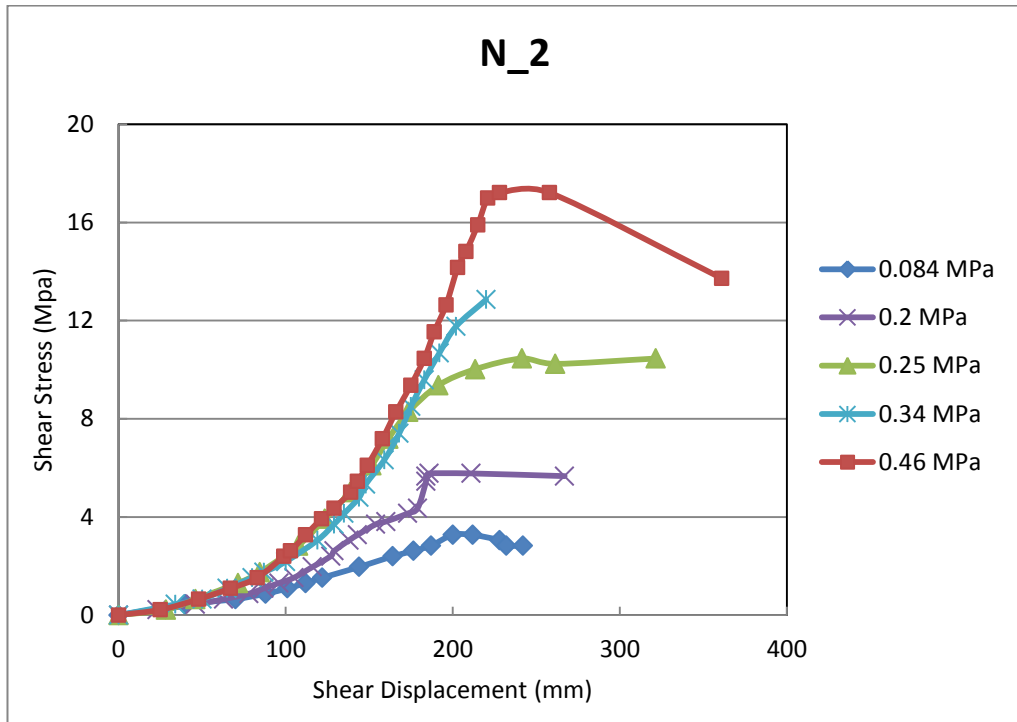


Figure A. 13 Shear stress/displacement curves for joint sample named as N\_2 for different normal stress values

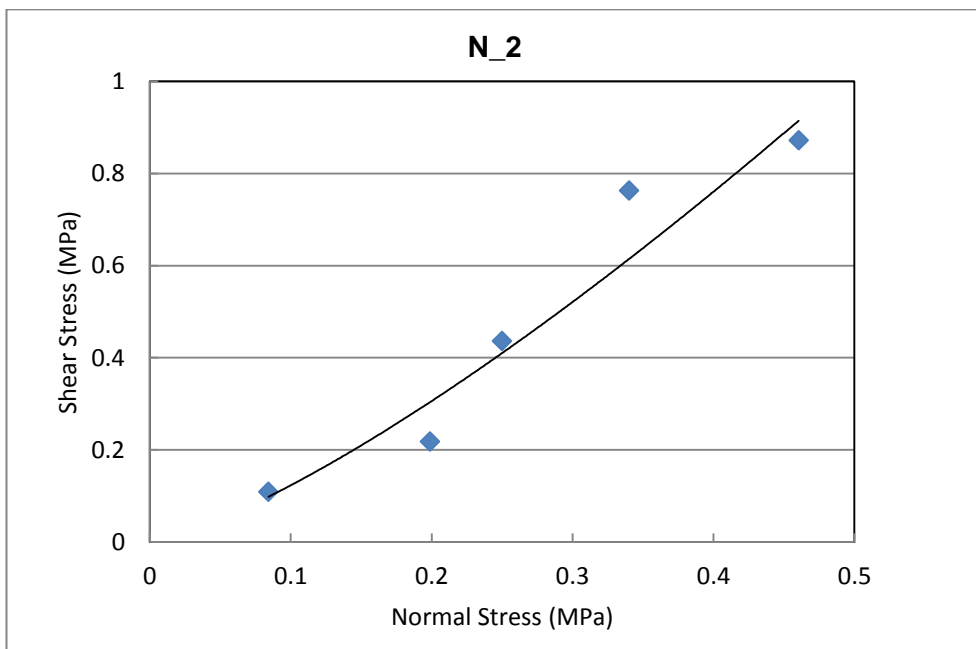


Figure A.14 Relation of Shear and Normal stresses acted on joint of N\_2

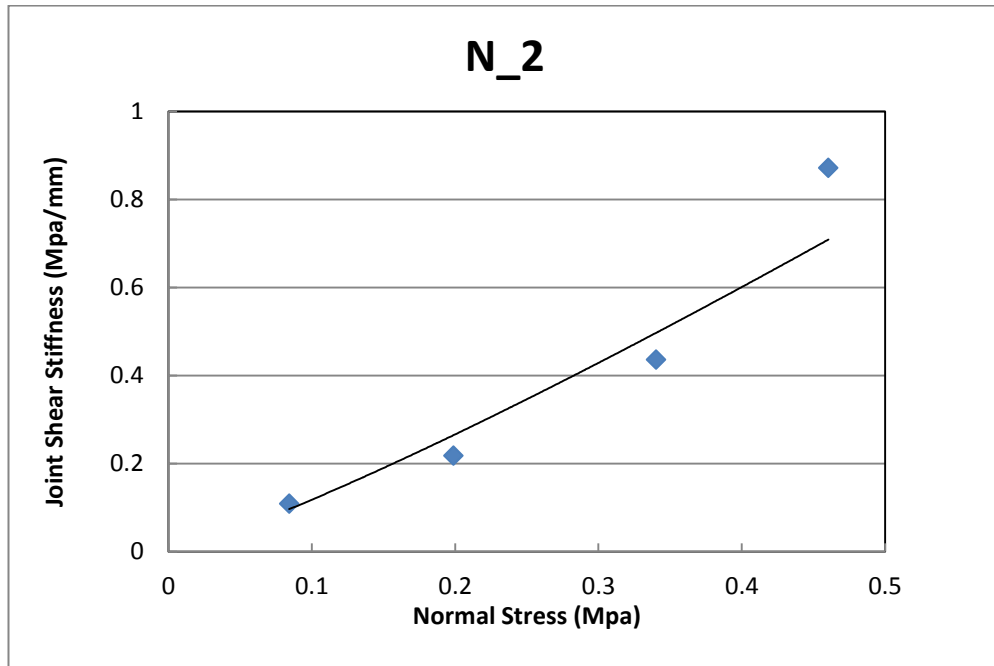


Figure A.15 Dependency of joint shear stiffness (Ks) to normal stress in rough joint plane (N\_2)

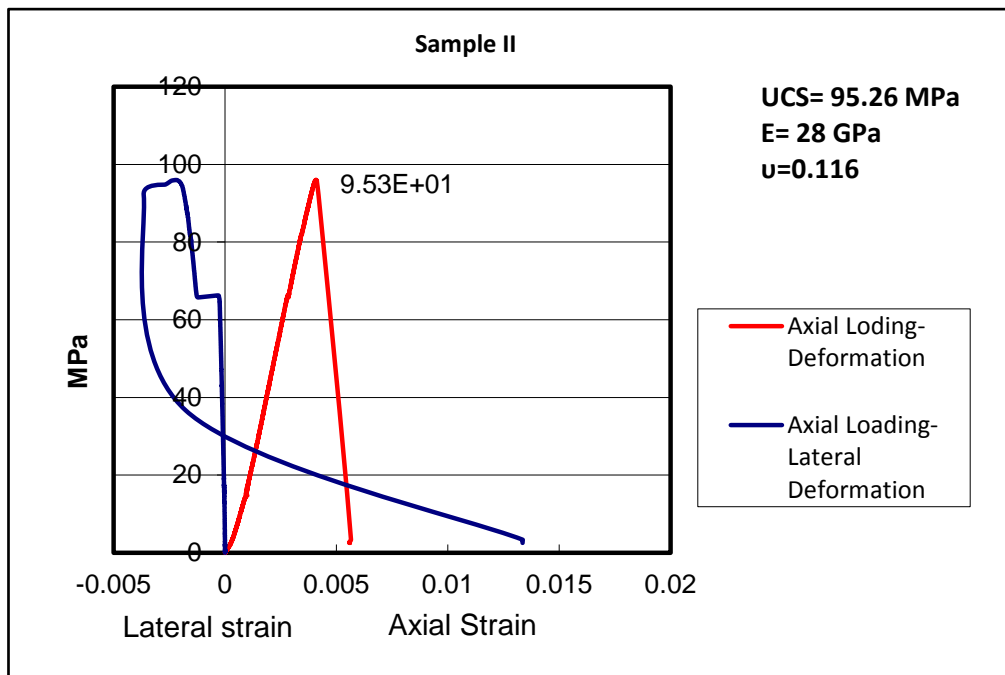


Figure A.16 Stress-strain curve of sample II

## APPENDIX B

### DISTRIBUTIONS OF SHEAR DISPLACEMENT

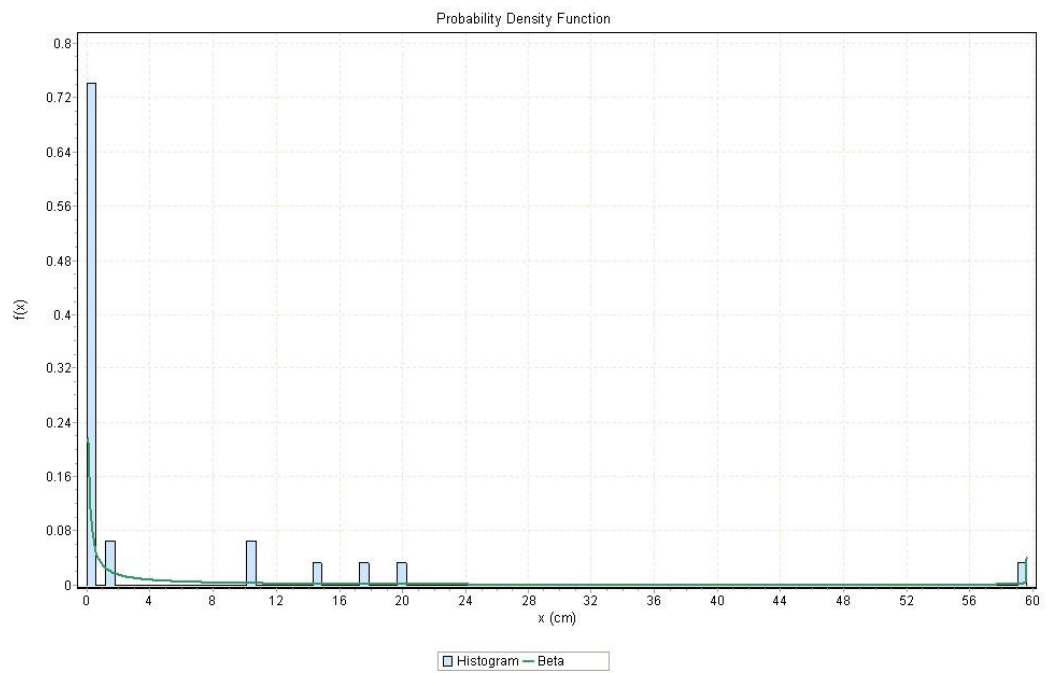


Figure B.1 Beta distribution of shear displacement of discontinuity no. 2

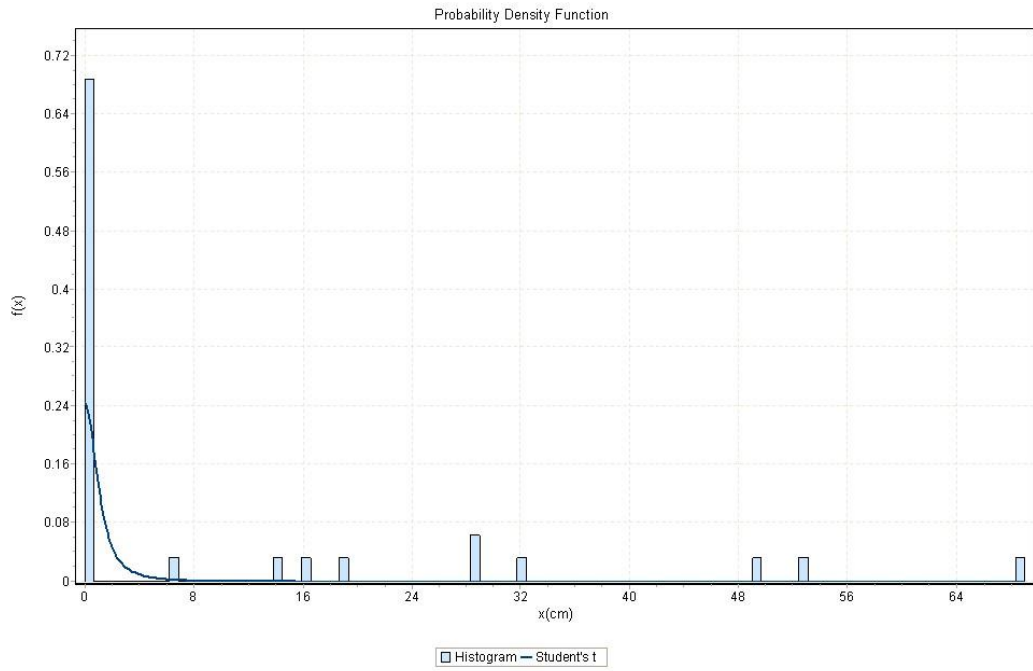


Figure B.2 Student's distribution of shear displacement of discontinuity no. 3

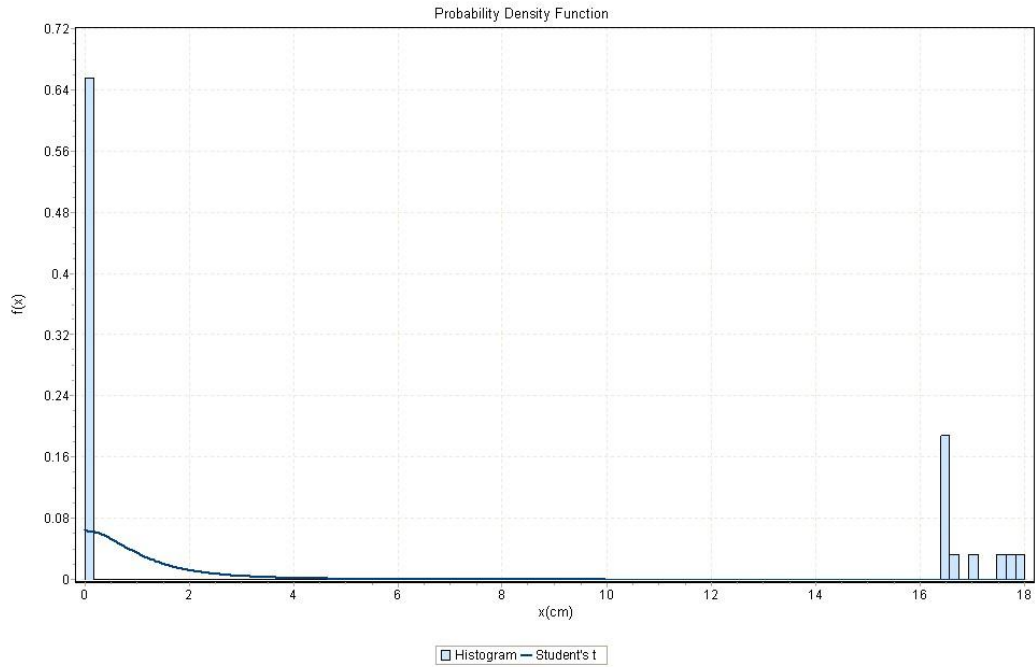


Figure B.3 Student's distribution of shear displacement of discontinuity no. 4

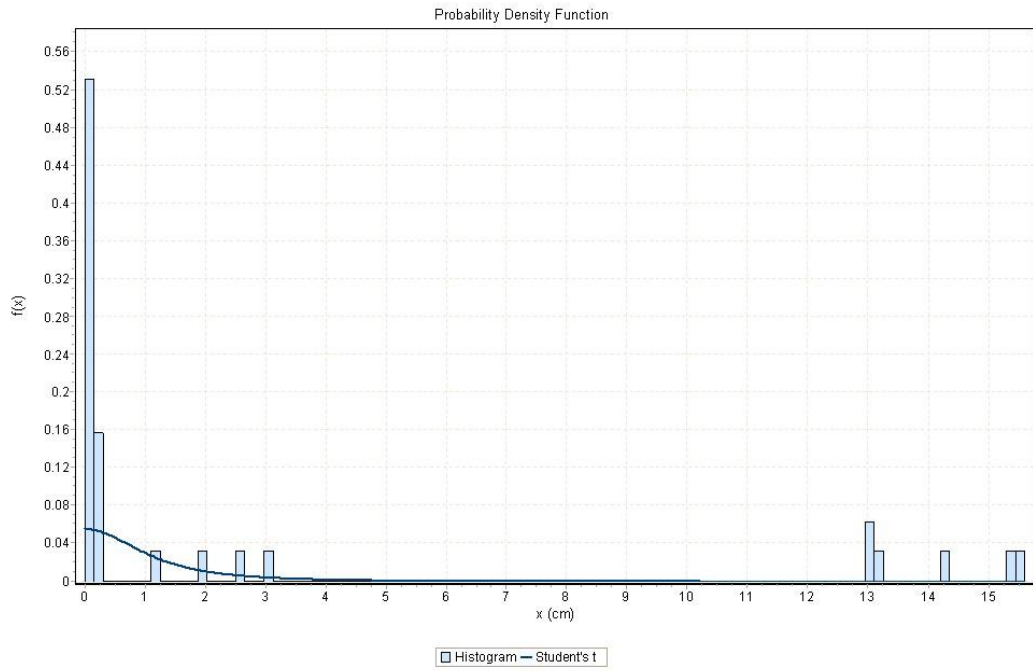


Figure B.4 Student's distribution of shear displacement of discontinuity no. 5

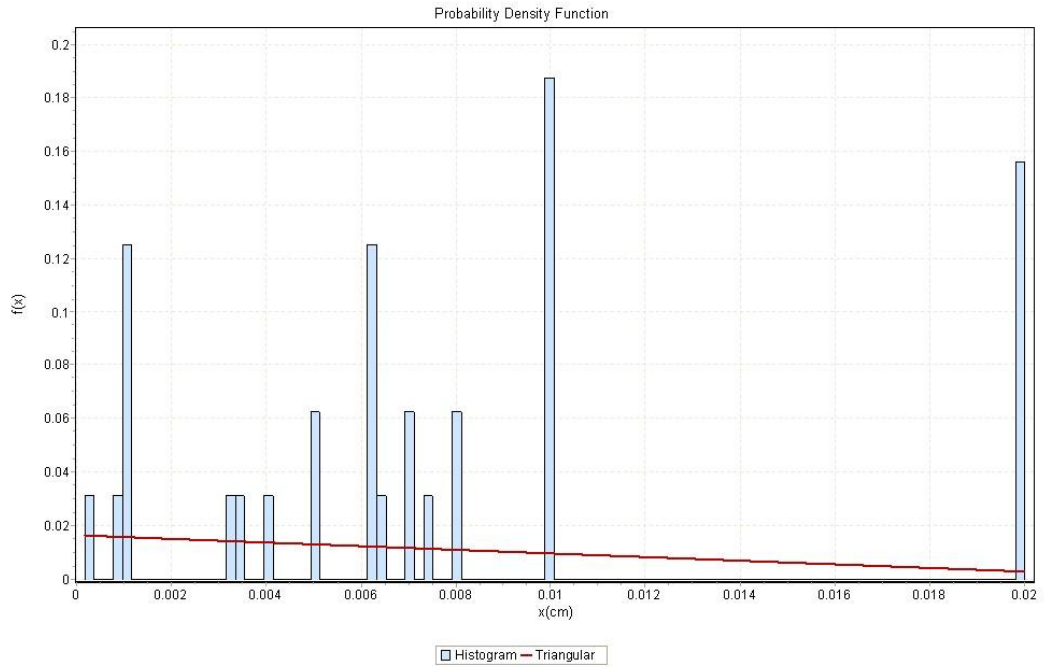


Figure B.5 Triangular distribution of shear displacement of discontinuity no. 6

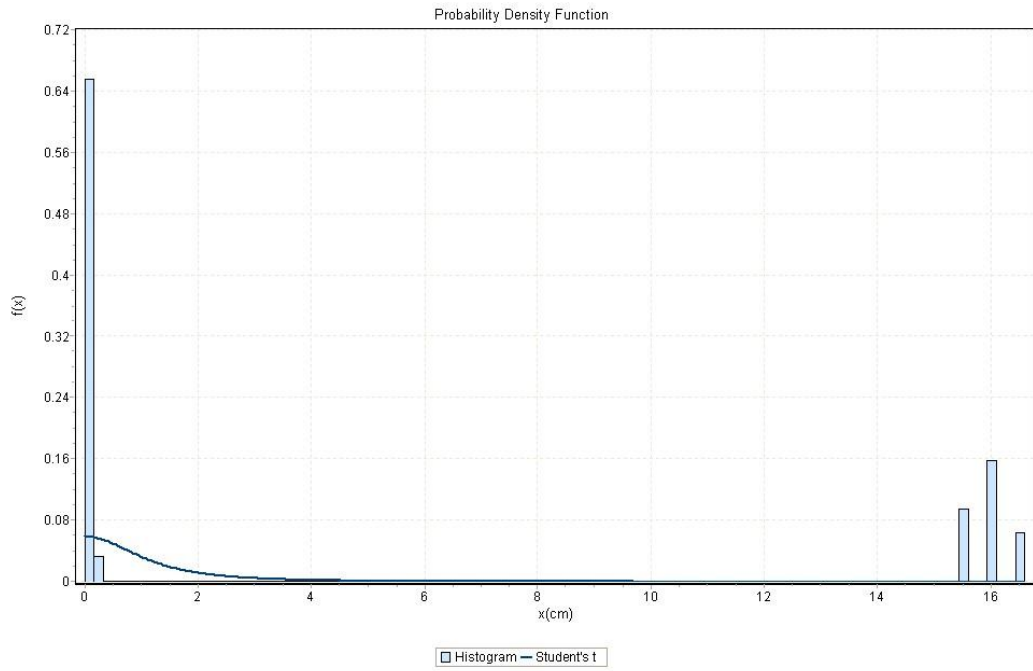


Figure B.6 Student's distribution of shear displacement of discontinuity no. 7

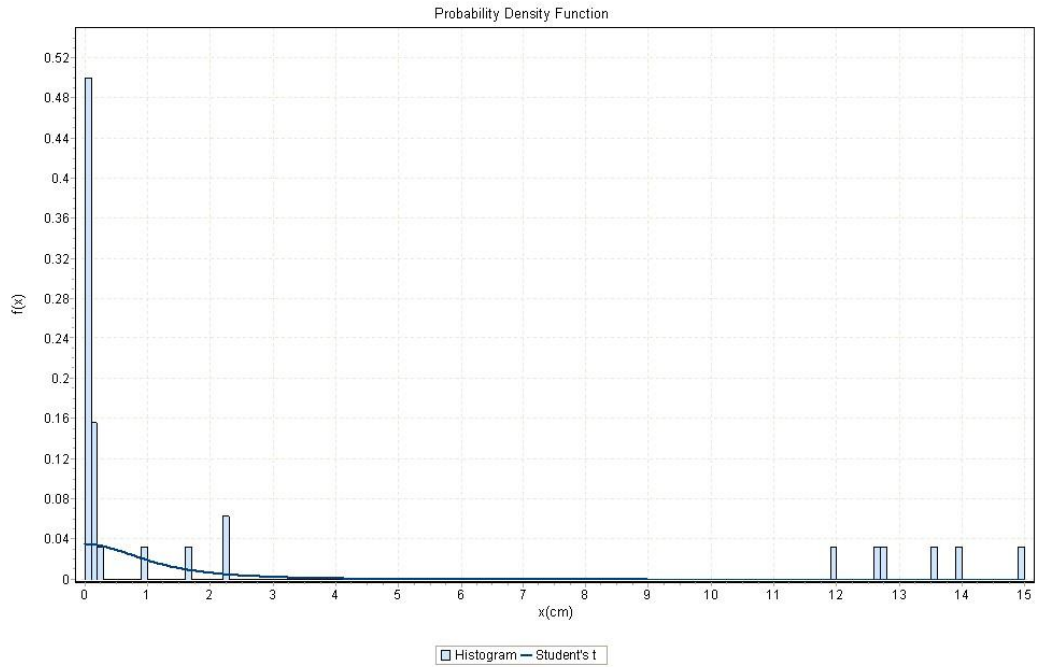


Figure B.7 Student's distribution of shear displacement of discontinuity no. 8

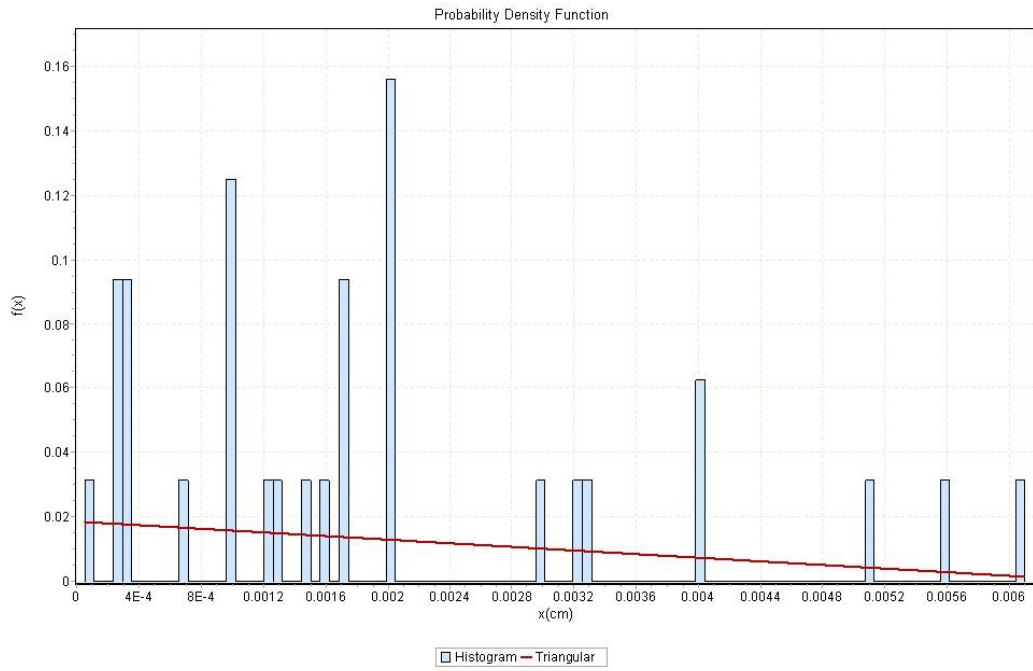


Figure B.8 Triangular distribution of shear displacement of discontinuity no. 9

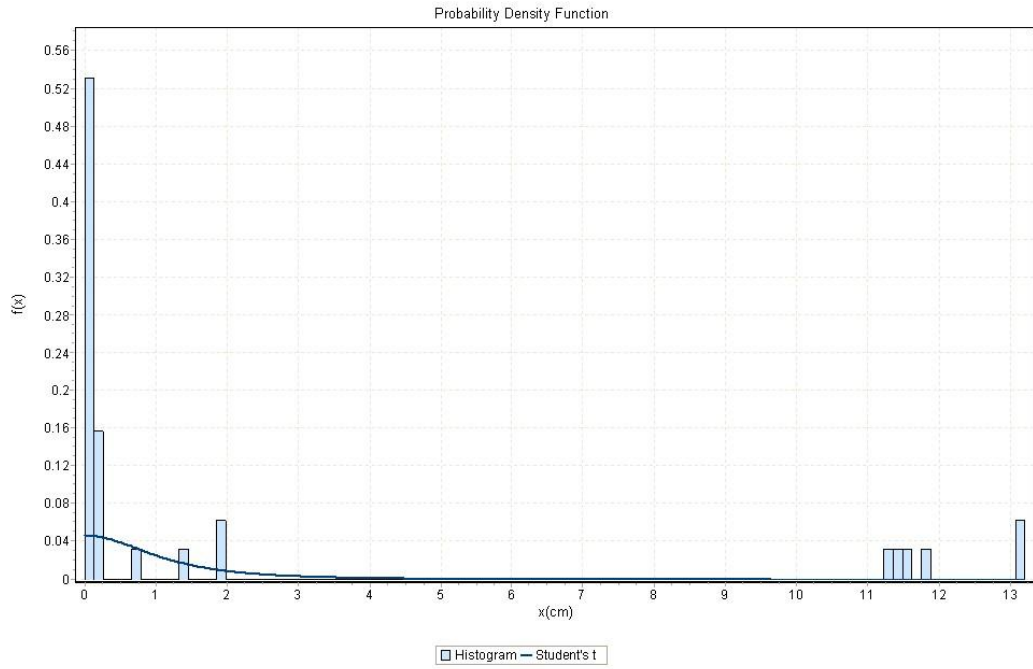


Figure B.9 Student's distribution of shear displacement of discontinuity no. 10

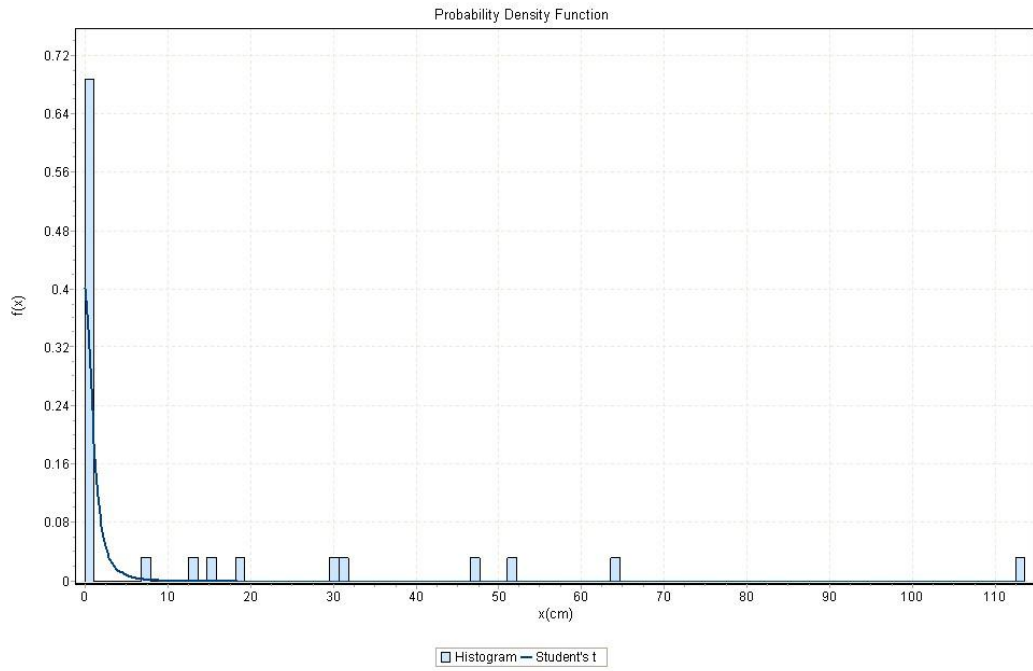


Figure B.10 Student's distribution of shear displacement of discontinuity no. 11

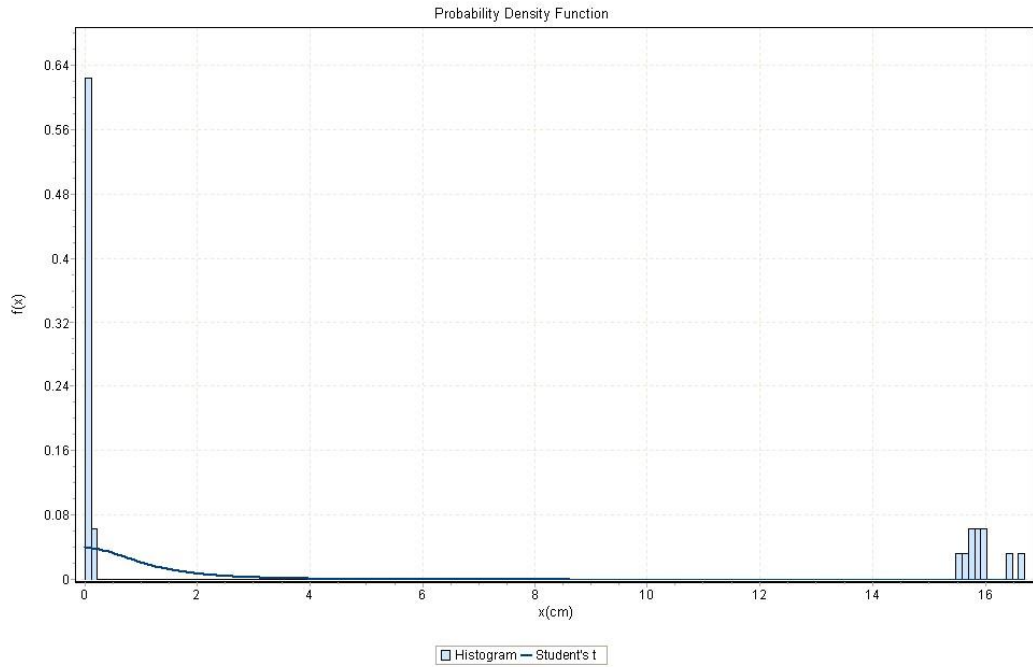


Figure B.11 Student's distribution of shear displacement of discontinuity no. 12

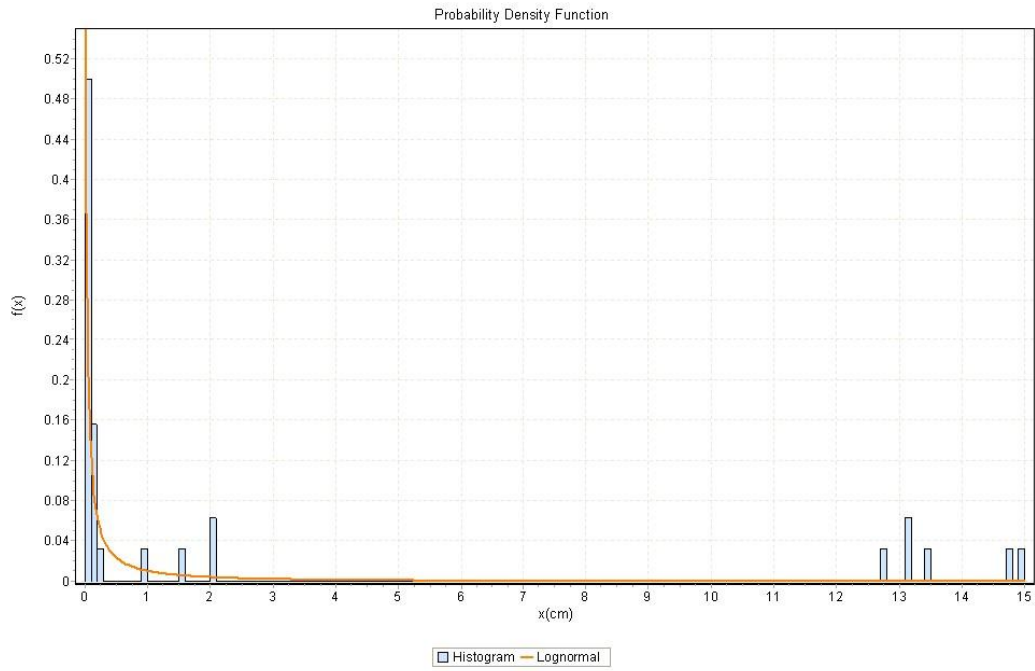


Figure B.12 Lognormal distribution of shear displacement of discontinuity no. 13

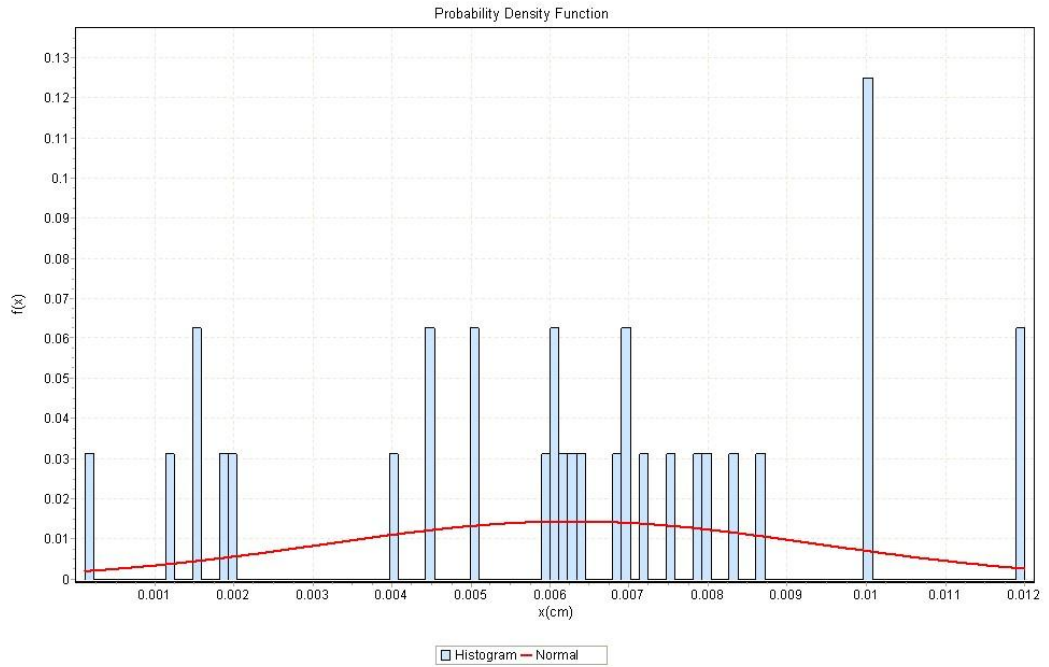


Figure B.13 Normal distribution of shear displacement of discontinuity no. 14

## APPENDIX C:

### WRITTEN CODES IN 3DEC

#### C.1 The master code

new

poly brick 0 67 0 110 0 95

pl bl

jset dip 0 dd 0 org 0 0 20 id 6

hide dip 0 dd 0 org 0 0 20 below

jset dip 90 dd 180 org 0 47 20 id 2

hide dip 90 dd 180 org 0 47 20 above

seek

hide dip 90 dd 180 org 0 47 20 above

hide dip 0 dd 0 org 0 0 40 below

jset dip 87 dd 180 org 0 61 20 id 1

jset dip 75 dd 288 org 14.8 46.9 40 id 8

hide dip 87 dd 180 org 0 61 20 above

hide dip 0 dd 0 org 0 0 40 below

jset dip 75 dd 288 org 53.68 60.85 40 id 9

seek

hide dip 87 dd 180 org 0 61 20 below

hide dip 87 dd 180 org 0 47 20 above

jset dip 0 dd 0 org 0 0 80.4 id 4

seek

del bl 217

seek

del bl 2137

del bl 4353

hide dip 75 dd 288 org 14.8 46.9 40 above

hide dip 0 dd 0 org 0 0 40 below

jset dip 90 dd 197 org 40 47 40 id 11

del bl 5891

jset dip 90 dd 161 org 40 47 40 id 12

del bl 4353

seek

hide dip 0 dd 0 org 0 0 40 below

hide dip 87 dd 180 org 0 61 20 below

hide dip 75 dd 288 org 14.8 46.9 40 below

jset dip 0 dd 0 org 0 0 72.4 id 3

seek

del bl 6693

hide dip 87 dd 180 org 0 61 20 below

hide dip 0 dd 0 org 0 0 40 below

jset dip 55 dd 90 org 65.75 47 40 id 10

del bl 5891

seek

hide dip 0 dd 0 org 0 0 20 below

hide dip 75 dd 288 org 14.8 46.9 40 below

hide dip 87 dd 180 org 0 61 20 below

jset dip 90 dd 196 org 16.5 52.45 40

jset dip 80 dd 240 org 14.976 54 40 id 18

del bl 5891

del bl 4353

del bl 217

seek

hide dip 87 dd 180 org 0 61 20 below

hide dip 0 dd 0 org 0 0 40 below

hide dip 75 dd 288 org 14.8 46.9 40 above

jset dip 70 dd 196 org 40 47 58.4 id 15

del bl 6693

jset dip 70 dd 159 org 40 47 58.4 id 16

del bl 217

seek

hide dip 87 dd 180 org 0 61 20 below

hide dip 0 dd 0 org 0 0 40 below

jset dip 60 dd 288 org 12 62 56 id 19

del bl 2137

seek

hide dip 0 dd 0 org 0 0 20 below

jset dip 80 dd 240 org 14.976 54 40 id 18

del bl 2845

hide dip 87 dd 180 org 0 61 20 above

hide dip 0 dd 0 org 0 0 40 below

jset dip 80 dd 288 org 40.22 65.5 79.2 id 20

seek

hide dip 0 dd 0 org 0 0 20 below

jset dip 55 dd 200 id 17 n 25 org 10.32 62 40 sp 5

seek

del bl 67155

del bl 63281

del bl 5165

del bl 2137

del bl 70311

del bl 217

del bl 68321

del bl 67633

del bl 69669

del bl 3551

del bl 63801

del bl 58903

del bl 2845

del bl 66497

del bl 53811

del bl 59625

del bl 57561

hide dip 87 dd 180 org 0 61 20 below

gen edge 5 range z 20 100

seek

hide dip 87 dd 180 org 0 61 20 above

gen edge 10 range z 20 100

seek

```
gen edge 10 range z 0 20
Prop mat=1 den=0.0026 k=16e4 g=10.0e4
change jcons 7
prop jmat=1 jkn=1e5 jks=5e4
change jmat=1
bound xvel=0 range x -0.1 0.1 y -0.1 110.1 z -0.1 40.1
bound xvel=0 range x 66.6 66.75 y -0.1 110.1 z -0.1 40.1
bound yvel=0 range x -0.1 67 y 109.9 110 z -0.1 95
bound yvel=0 range x -0.1 67 y -0.1 0.1 z -0.1 20
bound zvel=0 range x -0.1 67 y -0.1 110.1 z -0.1 0.1
gravity 0 0 -10
hist unbal
damp auto
his @shea1 @nstav1 @njdisp1 @sheardisp1
his @shea2 @nstav2 @njdisp2 @sheardisp2

his @shea3 @nstav3 @njdisp3 @sheardisp3
his @shea4 @nstav4 @njdisp4 @sheardisp4

his @shea5 @nstav5 @njdisp5 @sheardisp5
his @shea6 @nstav6 @njdisp6 @sheardisp6

his @shea7 @nstav7 @njdisp7 @sheardisp7
his @shea8 @nstav8 @njdisp8 @sheardisp8
his @shea9 @nstav9 @njdisp9 @sheardisp9
his @shea10 @nstav10 @njdisp10 @sheardisp10
```

his @shea11 @nstav11 @njdisp11 @sheardisp11

his @shea12 @nstav12 @njdisp12 @sheardisp12

his @shea13 @nstav13 @njdisp13 @sheardisp13

his @shea15 @nstav15 @njdisp15 @sheardisp15

## **C.2 Code to obtain normal stress and shear displacement for each discontinuity**

```
def av_str1
  whilestepping
    sstav1 = 0
    nstav1 = 0.01
    njdisp1 = 0
    sjdisp1 = 0
    ncono1 = 0
    xsf1=0
    ysf1=0
    zsf1=0
    xsd1=0
    ysd1=0
    zsd1=0
    shear1=0
    sheardisp1=0
    Are1=0
    ic1 = c_near(34.43,57.22,80.4)
    icsub1 = c_cx(ic1)
    Loop while icsub1 # 0
```

```

ncono1 = ncono1 + 1
Are1=Are1 + cx_area(icsub1)
nstav1 = nstav1 +cx_nforce(icsub1)
njdisp1 = njdisp1 + cx_ndis(icsub1)
ssss1 = cx_sforce(icsub1)
ssdisp1 = cx_sdis(icsub1)
xsf1= xsf1+ xcomp(ssss1)
ysf1= ysf1+ ycomp(ssss1)
zsf1= zsf1+ zcomp(ssss1)
xsd1= xsd1+ xcomp(ssdisp1)
ysd1= ysd1+ ycomp(ssdisp1)
zsd1= zsd1+ zcomp(ssdisp1)
icsub1 = cx_next(icsub1)
Endloop
if ncono1 # 0

shea1=sqrt((xsf1)^2+(ysf1)^2+(zsf1)^2)/Are1
sheardisp1 = sqrt((xsd1)^2+(ysd1)^2+(zsd1)^2) / ncono1
nstav1 = nstav1 / Are1
njdisp1 = njdisp1 / ncono1

Endif

end

.....
def av_str2
whilestepping
sstav2 = 0
nstav2 = 0

```

```

njdisp2 = 0
sjdisp2 = 0
ncono2 = 0
xsf2=0
ysf2=0
zsf2=0
  xsd2=0
  ysd2=0
  zsd2=0
    shear2=0
    sheardisp2=0
    Are2=0
ic2 = c_near(40.87,57.2,75.53)
icsub2 = c_cx(ic2)
  Loop while icsub2 # 0
    ncono2 = ncono2 + 1
    Are2=Are2 + cx_area(icsub2)
    nstav2 = nstav2 +cx_nforce(icsub2)
    njdisp2 = njdisp2 + cx_ndis(icsub2)
    ssss2 = cx_sforce(icsub2)
    ssdisp2 = cx_sdis(icsub2)

    xsf2= xsf2+ xcomp(ssss2)
    ysf2= ysf2+ ycomp(ssss2)
    zsf2= zsf2+ zcomp(ssss2)
    xsd2= xsd2+ xcomp(ssdisp2)
    ysd2= ysd2+ ycomp(ssdisp2)

```

```

        zsd2= zsd2+ zcomp(ssdisp2)
        icsub2 = cx_next(icsub2)
    Endloop
    if ncono2 # 0

        shea2=sqrt((xsf2)^2+(ysf2)^2+(zsf2)^2)/Are2
        sheardisp2 = sqrt((xsd2)^2+(ysd2)^2+(zsd2)^2) / ncono2
        nstav2 = nstav2 / Are2
        njdisp2 = njdisp2 / ncono2

    Endif
end
;,,,,,,,,,,,,,,,,,,,,,,,,,,,,,,,,,,,,,

def av_str3
    whilestepping
        sstav3 = 0
        nstav3 = 0
        njdisp3 = 0
        sjdisp3 = 0
        ncono3 = 0
        xsf3=0
        ysf3=0
        zsf3=0
        xsd3=0
        ysd3=0
        zsd3=0
    endwhilestepping
enddef

```

```

shear3=0
sheardisp3=0
Are3=0
ic3 = c_near(46.24,55.64,67.86)
icsub3 = c_cx(ic3)
Loop while icsub3 # 0
    ncono3 = ncono3 + 1
    Are3=Are3 + cx_area(icsub3)
    nstav3 = nstav3 +cx_nforce(icsub3)
    njdisp3 = njdisp3 + cx_ndis(icsub3)
    ssss3 = cx_sforce(icsub3)
    ssdisp3 = cx_sdis(icsub3)
    xsf3= xsf3+ xcomp(ssss3)
    ysf3= ysf3+ ycomp(ssss3)
    zsf3= zsf3+ zcomp(ssss3)
    xsd3= xsd3+ xcomp(ssdisp3)
    ysd3= ysd3+ ycomp(ssdisp3)
    zsd3= zsd3+ zcomp(ssdisp3)
    icsub3 = cx_next(icsub3)
Endloop
if ncono3 # 0
shea3=sqrt((xsf3)^2+(ysf3)^2+(zsf3)^2)/Are3
    sheardisp3 = sqrt((xsd3)^2+(ysd3)^2+(zsd3)^2) / ncono3
    nstav3 = nstav3 / Are3
    njdisp3 = njdisp3 / ncono3

Endif

```

```

end
.....
def av_str4
  whilestepping
    sstav4 = 0
    nstav4 = 0
    njdisp4 = 0
    sjdisp4 = 0
    ncono4 = 0
    xsf4=0
    ysf4=0
    zsf4=0
    xsd4=0
    ysd4=0
    zsd4=0
    shear4=0
    sheardisp4=0
    Are4=0
    ic4 = c_near(36.49,55.85,53.24)
    icsub4 = c_cx(ic4)
    Loop while icsub4 # 0
      ncono4 = ncono4 + 1
      Are4=Are4 + cx_area(icsub4)
      nstav4 = nstav4 +cx_nforce(icsub4)
      njdisp4 = njdisp4 + cx_ndis(icsub4)
      ssss4 = cx_sforce(icsub4)
      ssdisp4 = cx_sdis(icsub4)

```

```

    xsf4= xsf4+ xcomp(ssss4)
    ysf4= ysf4+ ycomp(ssss4)
    zsf4= zsf4+ zcomp(ssss4)
    xsd4= xsd4+ xcomp(ssdisp4)
    ysd4= ysd4+ ycomp(ssdisp4)
    zsd4= zsd4+ zcomp(ssdisp4)
    icsub4 = cx_next(icsub4)

```

Endloop

```

    if ncono4 # 0
        shea4=sqrt((xsf4)^2+(ysf4)^2+(zsf4)^2)/Are4
        sheardisp4 = sqrt((xsd4)^2+(ysd4)^2+(zsd4)^2) / ncono4
        nstav4 = nstav4 / Are4
        njdisp4 = njdisp4 / ncono4

```

Endif

end

.....

```

def av_str5
    whilestepping
        sstav5 = 0
        nstav5 = 0
        njdisp5 = 0
        sjdisp5 = 0
        ncono5 = 0
        xsf5=0
        ysf5=0

```

```

zsf5=0
xsd5=0
ysd5=0
zsd5=0
shear5=0
sheardisp5=0
Are5=0
ic5 = c_near(37.06, 56.05, 45.08)
icsub5 = c_cx(ic5)
Loop while icsub5 # 0
    ncono5 = ncono5 + 1
    Are5=Are5 + cx_area(icsub5)
    nstav5 = nstav5 +cx_nforce(icsub5)
    njdisp5 = njdisp5 + cx_ndis(icsub5)
    ssss5 = cx_sforce(icsub5)
    ssdisp5 = cx_sdis(icsub5)
    xsf5= xsf5+ xcomp(ssss5)
    ysf5= ysf5+ ycomp(ssss5)
    zsf5= zsf5+ zcomp(ssss5)
    xsd5= xsd5+ xcomp(ssdisp5)
    ysd5= ysd5+ ycomp(ssdisp5)
    zsd5= zsd5+ zcomp(ssdisp5)
    icsub5 = cx_next(icsub5)
Endloop
if ncono5 # 0
    shea5=sqrt((xsf5)^2+(ysf5)^2+(zsf5)^2)/Are5
    sheardisp5 = sqrt((xsd5)^2+(ysd5)^2+(zsd5)^2) / ncono5

```

```
nstav5 = nstav5 / Are5
njdisp5 = njdisp5 / ncono5
```

```
Endif
```

```
end
```

```
.....
```

```
def av_str6
```

```
  whilestepping
```

```
    sstav6 = 0
```

```
    nstav6 = 0
```

```
    njdisp6 = 0
```

```
    sjdisp6 = 0
```

```
    ncono6 = 0
```

```
    xsf6=0
```

```
    ysf6=0
```

```
    zsf6=0
```

```
    xsd6=0
```

```
    ysd6=0
```

```
    zsd6=0
```

```
    shear6=0
```

```
    sheardisp6=0
```

```
    Are6=0
```

```
    ic6 = c_near(45.18, 48.78, 41.3)
```

```
    icsub6 = c_cx(ic6)
```

```
  Loop while icsub6 # 0
```

```
    ncono6 = ncono6 + 1
```

```

Are6=Are6 + cx_area(icsub6)
nstav6 = nstav6 +cx_nforce(icsub6)
njdisp6 = njdisp6 + cx_ndis(icsub6)
ssss6 = cx_sforce(icsub6)
ssdisp6 = cx_sdis(icsub6)
xsf6= xsf6+ xcomp(ssss6)
ysf6= ysf6+ ycomp(ssss6)
zsf6= zsf6+ zcomp(ssss6)
xsd6= xsd6+ xcomp(ssdisp6)
ysd6= ysd6+ ycomp(ssdisp6)
zsd6= zsd6+ zcomp(ssdisp6)
icsub6 = cx_next(icsub6)

```

Endloop

```

if ncono6 # 0
shea6=sqrt((xsf6)^2+(ysf6)^2+(zsf6)^2)/Are6
sheardisp6 = sqrt((xsd6)^2+(ysd6)^2+(zsd6)^2) / ncono6
nstav6 = nstav6 / Are6
njdisp6 = njdisp6 / ncono6

```

Endif

end

.....  
,,,,,,,,,,,,,,,,,,,,,

def av\_str7

```

whilestepping
sstav7 = 0
nstav7 = 0

```

```
njdisp7 = 0
sjdisp7 = 0
ncono7 = 0
xsf7=0
ysf7=0
zsf7=0
xsd7=0
ysd7=0
zsd7=0
shear7=0
sheardisp7=0
Are7=0
ic7 = c_near(40.96,69.77,75.72)
icsub7 = c_cx(ic7)
```

Loop while icsub7 # 0

```
ncono7 = ncono7 + 1
Are7=Are7 + cx_area(icsub7)
nstav7 = nstav7 +cx_nforce(icsub7)
njdisp7 = njdisp7 + cx_ndis(icsub7)
ssss7 = cx_sforce(icsub7)
ssdisp7 = cx_sdis(icsub7)
xsf7= xsf7+ xcomp(ssss7)
ysf7= ysf7+ ycomp(ssss7)
zsf7= zsf7+ zcomp(ssss7)
xsd7= xsd7+ xcomp(ssdisp7)
ysd7= ysd7+ ycomp(ssdisp7)
```

```

        zsd7= zsd7+ zcomp(ssdisp7)
        icsub7 = cx_next(icsub7)
Endloop
    if ncono7 # 0
        shea7=sqrt((xsf7)^2+(ysf7)^2+(zsf7)^2)/Are7
        sheardisp7 = sqrt((xsd7)^2+(ysd7)^2+(zsd7)^2) / ncono7
        nstav7 = nstav7 / Are7
        njdisp7 = njdisp7 / ncono7

    Endif
end

;,,,,,,,,,,,,,

def av_str8
    whilestepping
        sstav8 = 0
        nstav8 = 0
        njdisp8 = 0
        sjdisp8 = 0
        ncono8 = 0
        xsf8=0
        ysf8=0
        zsf8=0
        xsd8=0
        ysd8=0
        zsd8=0

```

```

shear8=0
sheardisp8=0
Are8=0
ic8 = c_near(37.74, 75.99, 72.17)
icsub8 = c_cx(ic8)

Loop while icsub8 # 0
    ncono8 = ncono8 + 1
    Are8=Are8 + cx_area(icsub8)
    nstav8 = nstav8 +cx_nforce(icsub8)
    njdisp8 = njdisp8 + cx_ndis(icsub8)
    ssss8 = cx_sforce(icsub8)
    ssdisp8 = cx_sdis(icsub8)
    xsf8= xsf8+ xcomp(ssss8)
    ysf8= ysf8+ ycomp(ssss8)
    zsf8= zsf8+ zcomp(ssss8)
    xsd8= xsd8+ xcomp(ssdisp8)
    ysd8= ysd8+ ycomp(ssdisp8)
    zsd8= zsd8+ zcomp(ssdisp8)
    icsub8 = cx_next(icsub8)

Endloop

if ncono8 # 0
    shea8=sqrt((xsf8)^2+(ysf8)^2+(zsf8)^2)/Are8
    sheardisp8 = sqrt((xsd8)^2+(ysd8)^2+(zsd8)^2) / ncono8
    nstav8 = nstav8 / Are8
    njdisp8 = njdisp8 / ncono8

```

```

        Endif
end

.....
,,,,,,,,,,,,,,,,,,,,,

def av_str9

  whilestepping

    sstav9 = 0

    nstav9 = 0

    njdisp9 = 0

    sjdisp9 = 0

    ncono9 = 0

    xsf9=0

    ysf9=0

    zsf9=0

    xsd9=0

    ysd9=0

    zsd9=0

    shear9=0

    sheardisp9=0

    Are9=0

    ic9 = c_near(55.53,76.17,72.39)

    icsub9 = c_cx(ic9)

    Loop while icsub9 # 0

      ncono9 = ncono9 + 1

```

```

Are9=Are9 + cx_area(icsub9)
nstav9 = nstav9 +cx_nforce(icsub9)
njdisp9 = njdisp9 + cx_ndis(icsub9)
ssss9 = cx_sforce(icsub9)
ssdisp9 = cx_sdis(icsub9)
xsf9= xsf9+ xcomp(ssss9)
ysf9= ysf9+ ycomp(ssss9)
zsf9= zsf9+ zcomp(ssss9)
xsd9= xsd9+ xcomp(ssdisp9)
ysd9= ysd9+ ycomp(ssdisp9)
zsd9= zsd9+ zcomp(ssdisp9)
icsub9 = cx_next(icsub9)

```

Endloop

```

if ncono9 # 0
shea9=sqrt((xsf9)^2+(ysf9)^2+(zsf9)^2)/Are9
sheardisp9 = sqrt((xsd9)^2+(ysd9)^2+(zsd9)^2) / ncono9
nstav9 = nstav9 / Are9
njdisp9 = njdisp9 / ncono9

```

Endif

end

.....  
:.....

def av\_str10

whilestepping

sstav10 = 0

nstav10 = 0

njdisp10 = 0

sjdisp10 = 0

ncono10 = 0

xsf10=0

ysf10=0

zsf10=0

xsd10=0

ysd10=0

zsd10=0

shear10=0

sheardisp10=0

Are10=0

ic10 = c\_near(15.26, 82.87, 70.43)

icsub10 = c\_cx(ic10)

Loop while icsub10 # 0

ncono10 = ncono10 + 1

Are10=Are10 + cx\_area(icsub10)

nstav10 = nstav10 +cx\_nforce(icsub10)

njdisp10 = njdisp10 + cx\_ndis(icsub10)

ssss10 = cx\_sforce(icsub10)

ssdisp10 = cx\_sdis(icsub10)

xsf10= xsf10+ xcomp(ssss10)

ysf10= ysf10+ ycomp(ssss10)

zsf10= zsf10+ zcomp(ssss10)

xsd10= xsd10+ xcomp(ssdisp10)

```
ysd10= ysd10+ ycomp(ssdisp10)
```

```
zsd10= zsd10+ zcomp(ssdisp10)
```

```
icsub10 = cx_next(icsub10)
```

```
Endloop
```

```
if ncono10 # 0
```

```
shea10=sqrt((xsf10)^2+(ysf10)^2+(zsf10)^2)/Are10
```

```
sheardisp10 = sqrt((xsd10)^2+(ysd10)^2+(zsd10)^2) / ncono10
```

```
nstav10 = nstav10 / Are10
```

```
njdisp10 = njdisp10 / ncono10
```

```
Endif
```

```
end
```

```
.....
```

```
def av_str11
```

```
whilestepping
```

```
  sstav11 = 0
```

```
  nstav11 = 0
```

```
  njdisp11 = 0
```

```
  sjdisp11 = 0
```

```
  ncono11 = 0
```

```
  xsf11=0
```

```
  ysf11=0
```

```
  zsf11=0
```

```
  xsd11=0
```

```
  ysd11=0
```

```
  zsd11=0
```

shear11=0

sheardisp11=0

Are11=0

ic11 = c\_near(18.9, 58.57,57.03)

icsub11 = c\_cx(ic11)

Loop while icsub11 # 0

ncono11 = ncono11 + 1

Are11=Are11 + cx\_area(icsub11)

nstav11 = nstav11 +cx\_nforce(icsub11)

njdisp11 = njdisp11 + cx\_ndis(icsub11)

ssss11 = cx\_sforce(icsub11)

ssdisp11 = cx\_sdis(icsub11)

xsf11= xsf11+ xcomp(ssss11)

ysf11= ysf11+ ycomp(ssss11)

zsf11= zsf11+ zcomp(ssss11)

xsd11= xsd11+ xcomp(ssdisp11)

ysd11= ysd11+ ycomp(ssdisp11)

zsd11= zsd11+ zcomp(ssdisp11)

icsub11 = cx\_next(icsub11)

Endloop

if ncono11 # 0

shea11=sqrt((xsf11)^2+(ysf11)^2+(zsf11)^2)/Are11

sheardisp11 = sqrt((xsd11)^2+(ysd11)^2+(zsd11)^2) / ncono11

nstav11 = nstav11 / Are11

njdisp11 = njdisp11 / ncono11

```

        Endif
end

.....
,,,,,,,,,,,,,,,,,,,,,

def av_str12

  whilestepping

    sstav12 = 0

    nstav12 = 0

    njdisp12 = 0

    sjdisp12 = 0

    ncono12 = 0

    xsf12=0

    ysf12=0

    zsf12=0

    xsd12=0

    ysd12=0

    zsd12=0

    shear12=0

    sheardisp12=0

    Are12=0

    ic12 = c_near(17.18, 57.70, 46.29)

    icsub12 = c_cx(ic12)

    Loop while icsub12 # 0

      ncono12 = ncono12 + 1

```

```

Are12=Are12 + cx_area(icsub12)
nstav12 = nstav12 +cx_nforce(icsub12)
njdisp12 = njdisp12 + cx_ndis(icsub12)
ssss12 = cx_sforce(icsub12)
ssdisp12 = cx_sdis(icsub12)
xsf12= xsf12+ xcomp(ssss12)
ysf12= ysf12+ ycomp(ssss12)
zsf12= zsf12+ zcomp(ssss12)
xsd12= xsd12+ xcomp(ssdisp12)
ysd12= ysd12+ ycomp(ssdisp12)
zsd12= zsd12+ zcomp(ssdisp12)
icsub12 = cx_next(icsub12)

```

Endloop

```

if ncono12 # 0
shea12=sqrt((xsf12)^2+(ysf12)^2+(zsf12)^2)/Are12
sheardisp12 = sqrt((xsd12)^2+(ysd12)^2+(zsd12)^2) / ncono12
nstav12 = nstav12 / Are12
njdisp12 = njdisp12 / ncono12

```

Endif

end

```

.....
;
```

def av\_str13

whilestepping

sstav13 = 0

```
nstav13 = 0
njdisp13 = 0
sjdisp13 = 0
ncono13 = 0
xsf13=0
ysf13=0
zsf13=0
xsd13=0
ysd13=0
zsd13=0
shear13=0
sheardisp13=0
Are13=0
ic13 = c_near(14.78, 57.74, 36.46)
icsub13 = c_cx(ic13)
```

```
Loop while icsub13 # 0
```

```
    ncono13 = ncono13 + 1
    Are13=Are13 + cx_area(icsub13)
    nstav13 = nstav13 +cx_nforce(icsub13)
    njdisp13 = njdisp13 + cx_ndis(icsub13)
    ssss13 = cx_sforce(icsub13)
    ssdisp13 = cx_sdis(icsub13)
    xsf13= xsf13+ xcomp(ssss13)
    ysf13= ysf13+ ycomp(ssss13)
    zsf13= zsf13+ zcomp(ssss13)
    xsd13= xsd13+ xcomp(ssdisp13)
```

```
ysd13= ysd13+ ycomp(ssdisp13)
```

```
zsd13= zsd13+ zcomp(ssdisp13)
```

```
icsub13 = cx_next(icsub13)
```

```
Endloop
```

```
if ncono13 # 0
```

```
shea13=sqrt((xsf13)^2+(ysf13)^2+(zsf13)^2)/Are13
```

```
sheardisp13 = sqrt((xsd13)^2+(ysd13)^2+(zsd13)^2) / ncono13
```

```
nstav13 = nstav13 / Are13
```

```
njdisp13 = njdisp13 / ncono13
```

```
Endif
```

```
end
```

```
def av_str15
```

```
whilestepping
```

```
  sstav15 = 0
```

```
  nstav15 = 0
```

```
  njdisp15 = 0
```

```
  sjdisp15 = 0
```

```
  ncono15 = 0
```

```
  xsf15=0
```

```
  ysf15=0
```

```
  zsf15=0
```

```
  xsd15=0
```

```
  ysd15=0
```

```
  zsd15=0
```

```

shear15=0
sheardisp15=0
Are15=0
ic15 = c_near(12.38, 57.78, 26.62)
icsub15 = c_cx(ic15)

Loop while icsub15 # 0
    ncono15 = ncono15 + 1
    Are15=Are15 + cx_area(icsub15)
    nstav15 = nstav15 +cx_nforce(icsub15)
    njdisp15 = njdisp15 + cx_ndis(icsub15)
    ssss15 = cx_sforce(icsub15)
    ssdisp15 = cx_sdis(icsub15)
    xsf15= xsf15+ xcomp(ssss15)
    ysf15= ysf15+ ycomp(ssss15)
    zsf15= zsf15+ zcomp(ssss15)
    xsd15= xsd15+ xcomp(ssdisp15)
    ysd15= ysd15+ ycomp(ssdisp15)
    zsd15= zsd15+ zcomp(ssdisp15)
    icsub15 = cx_next(icsub15)

Endloop

if ncono15 # 0
    shea15=sqrt((xsf15)^2+(ysf15)^2+(zsf15)^2)/Are15
    sheardisp15 = sqrt((xsd15)^2+(ysd15)^2+(zsd15)^2) / ncono15
    nstav15 = nstav15 / Are15
    njdisp15 = njdisp15 / ncono15

```

```

    Endif
end

```

### C.3 Codes to calculate joint material properties and assign the joint material to each discontinuity

```

new
def prop1
  NS11 =0.00378813
  Φ=30
  L1=1.6
  jcs=70
  JRC=15
  fric_14= abs((180/pi)*atan(abs(tan(degrad*(JRC*log(abs(jcs/NS11))+Fi)))-
  degrad*JRC*(1/ln(10))*((tan(degrad*(JRC*log(abs(jcs/NS11))+Fi)))^2+1)))
  coh_14= 0.05+(NS11*abs(tan(degrad*(JRC*log(abs(jcs/NS11))+Fi)))-
  NS11*abs(tan(degrad*fric_1)))
  d_peak1=L1*(JRC/L1)^0.33
  J_kk_14=500*((coh_14)+abs(NS11*tan(degrad*fric_14)))/(L1*(JRC/L1)^0.33)
  ic1=c_near(34.43,57.22,80.4)
  Tp1=m_jcohesion(14)+abs(NS11*tan(degrad*m_jfriction(14)))
end
=====
def prop2
  NS21 = 0.0347388
  jcs=70

```

```

JRC=15
Φ=30
L2=23.9
ic2=c_near(40.87,57.2,75.53)
fric_2= abs((180/pi)*atan(abs(tan(degrad*(JRC*log(abs(jcs/NS21))+Fi)))-
degrad*JRC*(1/ln(10))*((tan(degrad*(JRC*log(abs(jcs/NS21))+Fi))^2+1)))
coh_2= 0.05+(NS21*abs(tan(degrad*(JRC*log(abs(jcs/NS21))+Fi)))-
NS21*abs(tan(degrad*fric_2)))
d_peak2=(L2)*(JRC/L2)^0.33
J_kk_2=500*((coh_2)+abs(NS21*tan(degrad*fric_2)))/d_peak2
end
=====
def prop3
NS31 = 0.0841634
jcs=70
JRC=15
Φ=30
L3=26.4
ic3=c_near(46.24,55.64,67.86)
fric_3= abs((180/pi)*atan(abs(tan(degrad*(JRC*log(abs(jcs/NS31))+Fi)))-
degrad*JRC*(1/ln(10))*((tan(degrad*(JRC*log(abs(jcs/NS31))+Fi))^2+1)))
coh_3= 0.05+ (NS31*abs(tan(degrad*(JRC*log(abs(jcs/NS31))+Fi)))-
NS31*abs(tan(degrad*fric_3)))
d_peak3=(L3)*(JRC)^0.33/(L3)^0.33
J_kk_3=500*((coh_3)+abs(NS31*tan(degrad*fric_3)))/d_peak3
Tp3=m_jcohesion(3)+abs(NS31*tan(degrad*m_jfriction(3)))
end

```

=====

def prop4

NS41 = 0.135121

jcs=70

L4=23

JRC=15

$\Phi=30$

ic4=c\_near(36.49,55.85,53.24)

fric\_4= abs((180/pi)\*atan(abs(tan(degrad\*(JRC\*log(abs(jcs/NS41))+Fi)))-  
degrad\*JRC\*(1/ln(10))\*((tan(degrad\*(JRC\*log(abs(jcs/NS41))+Fi)))^2+1)))

coh\_4= 0.05 + (NS41\*abs(tan(degrad\*(JRC\*log(abs(jcs/NS41))+Fi)))-  
NS41\*abs(tan(degrad\*fric\_4)))

d\_peak4=(L4)\*(JRC)^0.33/(L4)^0.33

J\_kk\_4=500\*(coh\_4+abs(NS41\*tan(degrad\*fric\_4)))/d\_peak4

Tp4=m\_jcohesion(4)+abs(NS41\*tan(degrad\*m\_jfriction(4)))

end

=====

def prop5

NS51 = 0.197149

L5=22.3

jcs=70

JRC=15

$\Phi=30$

fric\_5= abs((180/pi)\*atan(abs(tan(degrad\*(JRC\*log(abs(jcs/NS51))+Fi)))-  
degrad\*JRC\*(1/ln(10))\*((tan(degrad\*(JRC\*log(abs(jcs/NS51))+Fi)))^2+1)))

coh\_5=0.05+ (NS51\*abs(tan(degrad\*(JRC\*log(abs(jcs/NS51))+Fi)))-  
NS51\*abs(tan(degrad\*fric\_5)))

```

d_peak5=(L5)*(JRC/L5)^0.33
J_kk_5=500*(coh_5+abs(NS51*tan(degrad*fric_5)))/d_peak5
Tp5=m_jcohesion(5)+abs(NS51*tan(degrad*m_jfriction(5)))
end

def prop6
  NS61 = 0.270908

  jcs=70

  L6=22.25

  JRC=15

  Φ=30

  ic6=c_near(45.18, 48.78, 41.3)

  fric_6= abs((180/pi)*atan(abs(tan(degrad*(JRC*log(abs(jcs/NS61))+Fi)))-
degrad*JRC*(1/ln(10))*((tan(degrad*(JRC*log(abs(jcs/NS61))+Fi)))^2+1)))
  coh_6= 0.05 + (NS61*abs(tan(degrad*(JRC*log(abs(jcs/NS61))+Fi)))-
NS61*abs(tan(degrad*fric_6)))
  d_peak6=(L6)*(JRC/L6)^0.33
  J_kk_6=500*(coh_6+abs(NS61*tan(degrad*fric_6)))/d_peak6
  Tp6=m_jcohesion(6)+abs(NS61*tan(degrad*m_jfriction(6)))
end

=====

def prop7
  NS71 = 0.0719441

  L7=69

  jcs=70

  JRC=15

  Φ=30

  ic7=c_near(40.96,69.77,75.72)

```

```

fric_7= abs((180/pi)*atan(abs(tan(degrad*(JRC*log(abs(jcs/NS71))+Fi)))-
degrad*JRC*(1/ln(10))*((tan(degrad*(JRC*log(abs(jcs/NS71))+Fi))^2+1)))
coh_7= 0.05 + (NS71*abs(tan(degrad*(JRC*log(abs(jcs/NS71))+Fi)))-
NS71*abs(tan(degrad*fric_7)))
d_peak7=(L7)*(JRC)^0.33/(L7)^0.33
J_kk_7=500*(coh_7+abs(NS71*tan(degrad*fric_7)))/d_peak7
Tp7=m_jcohesion(7)+abs(NS71*tan(degrad*m_jfriction(7)))
end

```

=====

```

def prop8
NS81 = 0.112938
L8=64.8
jcs=70
JRC=15
Φ=30
ic8=c_near(37.74, 75.99, 72.17)
fric_8= abs((180/pi)*atan(abs(tan(degrad*(JRC*log(abs(jcs/NS81))+Fi)))-
degrad*JRC*(1/ln(10))*((tan(degrad*(JRC*log(abs(jcs/NS81))+Fi))^2+1)))
coh_8= 0.05+(NS81*abs(tan(degrad*(JRC*log(abs(jcs/NS81))+Fi)))-
NS81*abs(tan(degrad*fric_8)))
d_peak8=(L8)*(JRC/L8)^0.33
J_kk_8=500*(coh_8+abs(NS81*tan(degrad*fric_8)))/d_peak8
Tp8=m_jcohesion(8)+abs(NS81*tan(degrad*m_jfriction(8)))
end

```

=====

```

def prop9
NS91 = 0.0770756

```

```

L9=54.5
jcs=70
JRC=15
Φ=30
ic9=c_near(55.53,76.17,72.39)
fric_9= abs((180/pi)*atan(abs(tan(degrad*(JRC*log(abs(jcs/NS91))+Fi)))-
degrad*JRC*(1/ln(10))*((tan(degrad*(JRC*log(abs(jcs/NS91))+Fi))^2+1)))
coh_9= 0.05+ (NS91*abs(tan(degrad*(JRC*log(abs(jcs/NS91))+Fi)))-
NS91*abs(tan(degrad*fric_9)))
d_peak9=(L9)*(JRC/L9)^0.33
J_kk_9=500*(coh_9+abs(NS91*tan(degrad*fric_9)))/d_peak9
Tp9=m_jcohesion(9)+abs(NS91*tan(degrad*m_jfriction(9)))

end
=====
def prop10
  NS101= 0.0648886
  jcs=70
  JRC=15
  Φ=30
  L10=17.25
  ic10=c_near(15.26, 82.87, 70.43)
  fric_10= abs((180/pi)*atan(abs(tan(degrad*(JRC*log(abs(jcs/NS101))+Fi)))-
degrad*JRC*(1/ln(10))*((tan(degrad*(JRC*log(abs(jcs/NS101))+Fi))^2+1)))
  coh_10= 0.05+ (NS101*abs(tan(degrad*(JRC*log(abs(jcs/NS101))+Fi)))-
NS101*abs(tan(degrad*fric_10)))
  d_peak10=(L10)*(JRC/L10)^0.33

```

```

J_kk_10=500*(coh_10+abs(NS101*tan(degrad*fric_10)))/d_peak10
Tp10=m_jcohesion(10)+abs(NS101*tan(degrad*m_jfriction(10)))
end
=====
def prop11

NS111 = 0.0708899

L11=15.2

jcs=70

JRC=15

Φ=30

ic11=c_near(18.9, 58.57,57.03)

fric_11= abs((180/pi)*atan(abs(tan(degrad*(JRC*log(abs(jcs/NS111))+Fi)))-
degrad*JRC*(1/ln(10))*((tan(degrad*(JRC*log(abs(jcs/NS111))+Fi))^2+1)))
coh_11= 0.05+ (NS111*abs(tan(degrad*(JRC*log(abs(jcs/NS111))+Fi)))-
NS111*abs(tan(degrad*fric_11)))

d_peak11=(L11)*(JRC/L11)^0.33

J_kk_11=500*(coh_11+abs(NS111*tan(degrad*fric_11)))/d_peak11

Tp11=m_jcohesion(11)+abs(NS111*tan(degrad*m_jfriction(11)))
end
=====
def prop12

NS121 = 0.138155

jcs=70

L12=20.4

JRC=15

Φ=30

```

```

ic12=c_near(17.18, 57.70, 46.29)
fric_12= abs((180/pi)*atan(abs(tan(degrad*(JRC*log(abs(jcs/NS121))+Fi)))-
degrad*JRC*(1/ln(10))*((tan(degrad*(JRC*log(abs(jcs/NS121))+Fi))^2+1)))
coh_12= 0.05+ (NS121*abs(tan(degrad*(JRC*log(abs(jcs/NS121))+Fi)))-
NS121*abs(tan(degrad*fric_12)))
d_peak12=(L12)*(JRC/L12)^0.33
J_kk_12=500*(coh_12+abs(NS121*tan(degrad*fric_12)))/d_peak12
Tp12=m_jcohesion(12)+abs(NS121*tan(degrad*m_jfriction(12)))
End

```

=====

```

def prop13
NS131 = 0.176823
jcs=70
L13=11.7
JRC=15
Φ=30
ic13=c_near(14.78, 57.74, 36.46)
fric_13= abs((180/pi)*atan(abs(tan(degrad*(JRC*log(abs(jcs/NS131))+Fi)))-
degrad*JRC*(1/ln(10))*((tan(degrad*(JRC*log(abs(jcs/NS131))+Fi))^2+1)))
coh_13= 0.05+ (NS131*abs(tan(degrad*(JRC*log(abs(jcs/NS131))+Fi)))-
NS131*abs(tan(degrad*fric_13)))
d_peak13=(L13)*(JRC/L13)^0.33
J_kk_13=500*(coh_13+abs(NS131*tan(degrad*fric_13)))/d_peak13
Tp13=m_jcohesion(13)+abs(NS131*tan(degrad*m_jfriction(13)))
end

```

=====

```

def prop15

```

```

NS151 = 0.285152
jcs=70
L15=11.7
JRC=15
Φ=30
ic15=c_near(12.38, 57.78, 26.62)
fric_15= abs((180/pi)*atan(abs(tan(degrad*(JRC*log(abs(jcs/NS151))+Fi)))-
degrad*JRC*(1/ln(10))*((tan(degrad*(JRC*log(abs(jcs/NS151))+Fi))^2+1)))
coh_15= 0.05+ (NS151*abs(tan(degrad*(JRC*log(abs(jcs/NS151))+Fi)))-
NS151*abs(tan(degrad*fric_15)))
d_peak15=(L15)*(JRC/L15)^0.33
J_kk_15=500*(coh_15+abs(NS151*tan(degrad*fric_15)))/d_peak15
Tp15=m_jcohesion(15)+abs(NS151*tan(degrad*m_jfriction(15)))
end

```

```

hide dip 87 dd 180 org 0 61 20 below
hide dip 75 dd 288 org 14.8 46.9 40 above
hide range z 0 65
change jmat=14
Seek
hide dip 87 dd 180 org 0 61 20 below
hide dip 75 dd 288 org 14.8 46.9 40 above
hide range z 75 85
hide range z 0 58
change jmat=2
Seek
hide dip 87 dd 180 org 0 61 20 below

```

hide dip 75 dd 288 org 14.8 46.9 40 above

hide range z 65 85

hide range z 0 50

change jmat=3

Seek

hide dip 87 dd 180 org 0 61 20 below

hide dip 75 dd 288 org 14.8 46.9 40 above

hide range z 58 85

hide range z 0 42

change jmat=4

Seek

hide dip 87 dd 180 org 0 61 20 below

hide dip 75 dd 288 org 14.8 46.9 40 above

hide range z 50 85

hide range z 0 36

change jmat=5

Seek

hide dip 87 dd 180 org 0 61 20 below

hide dip 75 dd 288 org 14.8 46.9 40 above

hide range z 42 85

hide range z 0 33

change jmat=6

Seek

:: Assigning Jmaterial 7

hide dip 87 dd 180 org 0 61 20 above

hide dip 75 dd 288 org 14.8 46.9 40 above

hide range x 45 67

hide range z 0 68

change jmat=7

Seek

:: Assigning Jmaterial 8

hide dip 87 dd 180 org 0 61 20 above

hide dip 75 dd 288 org 14.8 46.9 40 above

hide range x 45 67

hide range z 0 63

hide range z 78 80

change jmat=8

Seek

hide dip 87 dd 180 org 0 61 20 above

hide dip 75 dd 288 org 14.8 46.9 40 above

hide range x 0 40

hide range z 0 67

change jmat=9

Seek

hide dip 87 dd 180 org 0 61 20 above

hide dip 75 dd 288 org 14.8 46.9 40 below

hide range z 0 67

change jmat=10

Seek

hide dip 87 dd 180 org 0 61 20 below

hide dip 75 dd 288 org 14.8 46.9 40 below

hide range z 45 85

hide range z 0 25

change jmat=13

Seek

hide dip 87 dd 180 org 0 61 20 below

hide dip 75 dd 288 org 14.8 46.9 40 below

hide range z 60 85

hide range z 0 35

change jmat=12

Seek

hide dip 87 dd 180 org 0 61 20 below

hide dip 75 dd 288 org 14.8 46.9 40 below

hide range z 0 50

change jmat=11

Seek

hide dip 87 dd 180 org 0 61 20 below

hide dip 75 dd 288 org 14.8 46.9 40 below

hide range z 36 80

hide range z 0 21

change jmat=15

Seek